

A COMPARATIVE STUDY ON NONLINEAR MODELING OF STRUCTURAL
WALLS

A THESIS SUBMITTED TO
THE GRADUATE SCHOOL OF NATURAL AND APPLIED SCIENCES
OF
MIDDLE EAST TECHNICAL UNIVERSITY

BY

SÜLEYMAN EREN DURSUN

IN PARTIAL FULFILLMENT OF THE REQUIREMENTS
FOR
THE DEGREE OF MASTER OF SCIENCE
IN
CIVIL ENGINEERING

SEPTEMBER 2018

Approval of the thesis:

**A COMPARATIVE STUDY ON NONLINEAR MODELING OF
STRUCTURAL WALLS**

submitted by **SÜLEYMAN EREN DURSUN** in partial fulfillment of the requirements for the degree of **Master of Science in Civil Engineering Department, Middle East Technical University** by,

Prof. Dr. Halil Kalıpçılar
Dean, Graduate School of **Natural and Applied Sciences**

Prof. Dr. İsmail Özgür Yaman
Head of Department, **Civil Engineering**

Prof. Dr. Özgür Kurç
Supervisor, **Civil Engineering, METU**

Prof. Dr. Halûk Sucuoğlu
Co-Supervisor, **Civil Engineering, METU**

Examining Committee Members:

Prof. Dr. Kağan Tuncay
Civil Engineering, METU

Prof. Dr. Özgür Kurç
Civil Engineering, METU

Prof. Dr. Halûk Sucuoğlu
Civil Engineering, METU

Prof. Dr. Tolga Akış
Civil Engineering, Atılım University

Assoc. Prof. Dr. Ozan Cem Çelik
Civil Engineering, METU

Date: 05.09.2018

I hereby declare that all information in this document has been obtained and presented in accordance with academic rules and ethical conduct. I also declare that, as required by these rules and conduct, I have fully cited and referenced all material and results that are not original to this work.

Name, Surname: Süleyman Eren Dursun

Signature:

ABSTRACT

A COMPARATIVE STUDY ON NONLINEAR MODELING OF STRUCTURAL WALLS

Dursun, Süleyman Eren
Master of Science, Civil Engineering
Supervisor: Prof. Dr. Özgür Kurç
Co-Supervisor: Prof. Dr. Halûk Sucuoğlu

September 2018, 157 pages

The need for tall buildings increases day by day because of many reasons such as increase in population. Representing the behavior of tall buildings under seismic loads is a complicated problem. Thus, in structural engineering, performance based analysis and design approach is generally used for tall buildings which may require nonlinear analysis of buildings. In such an analysis, however, modeling of structural walls has several challenges especially for the ones with irregular cross sections. Therefore, this study mainly focuses on the comparison of different nonlinear modeling approaches for the structural walls. First, a calibration study was conducted. For this purpose, typical wall layouts were modeled with different modeling approaches and elastic linear analysis results were compared with the theoretical solutions. Results showed that finite element modeling approach is good enough for the elastic analysis of structural walls. Then, walls were modeled as distributed inelasticity (fiber) model with Perform3D and ETABS and also continuum model were created utilizing DIANA FEA. The analyses results were compared with experimental results for rectangular and T-shaped walls. Results indicated that both modeling approaches can capture the behavior of planar walls under cyclic loading but fiber model overestimate the capacity of the flanged walls. As a final step, 4 (squat wall) and 15

(slender wall) story buildings having a core wall were modeled elastically with ETABS and designed according to ASCE7-10 and ACI-318. These buildings were modeled nonlinearly with both Perform3D and DIANA FEA. Behavior of the buildings was compared according to pushover and time history analyses. With this comparison it was seen that fiber modeling approach cannot capture the effect of shear cracks in concrete. Moreover, fiber model cannot correctly calculate the behavior of wall flanges under tension.

Keywords: Tall Buildings, Reinforced Concrete Structures, Slender Structural Walls, Squat Structural Walls

ÖZ

YAPISAL DUVARLARIN DOĞRUSAL OLMAYAN MODELLEMESİ ÜZERİNE KARŞILAŞTIRMALI ÇALIŞMA

Dursun, Süleyman Eren
Yüksek Lisans, İnşaat Mühendisliği
Tez Danışmanı: Prof. Dr. Özgür Kurç
Ortak Tez Danışmanı: Prof. Dr. Halûk Sucuoğlu

Eylül 2018, 157 sayfa

Yüksek binalara olan ihtiyaç, nüfus artışı gibi birçok nedenden dolayı günbegün artmaktadır. Yüksek binaların deprem yüklerinin altındaki davranışının hesabı karmaşık bir problemdir. Bu yüzden, performans dayalı analiz ve tasarım yaklaşımı genellikle yüksek binalar için kullanılmaktadır. Bu yaklaşım kimi zaman, doğrusal olmayan modelleme yapmayı gerektirmektedir. Ancak, özellikle dikdörtgen keside sahip olmayan duvarların modellenmesi hala çözülememiş bir sorundur. Bu nedenle, bu çalışmada yapısal duvarlar için farklı doğrusal olmayan modelleme yaklaşımlarının karşılaştırılmasına odaklanılmıştır. İlk olarak, bir kalibrasyon çalışması yapılmış, duvarlar için geliştirilmiş olan farklı modelleme yaklaşımları ile tipik duvar düzenleri modellenmiş ve elde edilen doğrusal sonuçlar ile teorik çözümler karşılaştırılmıştır. Sonuçlar, sonlu eleman modelleme yaklaşımının yapısal duvarların doğrusal analizi için yeterince iyi olduğunu göstermiştir. Daha sonra, duvarlar için Perform3D ve ETABS ile yayılı fiber modeli ve ayrıca DIANA FEA ile süreklilik modeli oluşturulmuş ve analizler yapılmıştır. Elde edilen sonuçlar, dikdörtgen ve T-şekilli duvarlar için deney sonuçları ile karşılaştırılmıştır. Sonuçlar, her iki modelleme yaklaşımının, tersinir yükleme altında dikdörtgen duvarların davranışını yakalayabildiğini, fakat fiber modelinin, düzensiz duvarların kapasitesini fazla

hesapladığını göstermiştir. Son olarak, bir çekirdek duvarına sahip 4 (bodur duvar) ve 15 katlı binalar ETABS ile elastik olarak modellenip, ASCE7-10 ve ACI-318 e göre tasarlanmıştır. Bu binalar, hem Perform3D hem de DIANA FEA ile doğrusal olmayan şekilde modellenmiştir. Binaların davranışları, itme ve zaman alanında doğrusal olmayan analiz sonuçlarına göre karşılaştırılmıştır. Bu karşılaştırmada fiber modelleme yaklaşımının kesme ve eğilme kaynaklı çatlama davranışını doğru hesaplayamadığı, çekme kuvveti altında duvar flanş bölgesinin davranışını da hatalı bir şekilde hesapladığı görülmüştür.

Anahtar Kelimeler: Yüksek Binalar, Betonarme Yapılar, Narin Yapısal Duvarlar, Kısa ve Kalın Yapısal Duvarlar

To my family

ACKNOWLEDGMENTS

I would like to thank to my supervisor Prof. Dr. Özgür Kurç for his continuous guidance and constructive criticism that he has provided throughout the preparation of the thesis. Working with him was an honor.

I would also like to express my sincere thanks to Prof. Dr. Haluk Sucuoğlu for his suggestion and contributions.

I would like to thank Assoc. Prof. Dr. Yalın Arıcı for giving me the opportunity to use his computer and to answer all my questions.

I would like to give special thanks to B. Feyza Soysal Albostan. It was not possible to finish this thesis without her continuous help and support. I would like to thank to her once again for responding to all my questions via e-mail when I am working outside the campus. Moreover, I would also like to express my thanks to Utku Albostan for solving all the problems I experienced about computers.

I would like to express my gratitude to Raşit Emre Çakır. Thanks to the code that he wrote, I got rid of the big trouble of reading the results. Without his code I lost lots of time.

Finally, my deepest gratitude goes to my family, my mother, father and sister. I am deeply grateful to them. Whatever I will say about my mother and father is not enough to explain my feelings about them. Only thing that I can say is that without their endless love, this dissertation would not have been completed.

TABLE OF CONTENTS

ABSTRACT	v
ÖZ	vii
ACKNOWLEDGMENTS	x
TABLE OF CONTENTS	xi
LIST OF TABLES	xiii
LIST OF FIGURES	xvi
1. INTRODUCTION	1
1.1. Importance of Modeling of Reinforced Concrete Structural Walls	1
1.2. Literature Review	3
1.3. Objectives and Scope	9
2. ELASTIC CALIBRATION STUDIES	11
2.1. Torsional Behavior of Box and C-Shaped Section	11
2.1.1. Torsional Behavior of Box Shaped Section.....	11
2.1.2. Torsional Behavior of C-Shaped Section	17
2.1.3. Mid-Column Method	23
2.1.3.1. Mid-Column Method for Box Section	24
2.1.3.2. Mid-Column Method for C-Shaped Section	26
2.2. Behavior of Box Section and C-Shaped Section Under Pure Bending	28
2.2.1. Behavior of Box Section Under Pure Bending	28
2.2.2. Behavior of C-Shaped Section Under Pure Bending.....	29
2.2.3. Mid-Colum Method for Bending.....	32
2.2.3.1. Mid-Column Method for Box Section	32

2.2.3.2. Mid-Column Method for C-Shaped Section.....	33
2.3. Discussion of Results	33
3. MODELING FOR NONLINEAR BEHAVIOR.....	35
3.1. Modeling of RW2 Specimen.....	36
3.1.1. Modeling of RW2 Specimen with the Fiber Model	40
3.1.2. Modeling of RW2 Specimen with the Continuum Model	46
3.2. Modeling of TW2 Specimen.....	51
3.2.1. Modeling of TW2 Specimen with the Fiber Model	54
3.2.2. Modeling of TW2 Specimen with the Continuum Model.....	59
3.3. Discussion of Results	63
4. CASE STUDIES	65
4.1. Pushover Analysis of E-Shaped Structural Wall	68
4.2. Pushover Analysis.....	72
4.2.1. Pushover Analysis of 4-Storey Structure	72
4.2.2. Pushover Analysis of 15-Storey Structure	89
4.3. Time-History Analysis.....	102
4.3.1. Time-History Analysis of 4-Storey Structures.....	103
4.3.2. Time-History Analysis of 15-Storey Structures.....	110
4.4. Discussion of the Results	119
5. SUMMARY AND CONCLUSION.....	121
REFERENCES.....	127
APPENDIX A	131
APPENDIX B.....	151

LIST OF TABLES

TABLES

Table 2-1. Section properties and parameters that used in analysis.....	12
Table 2-2 ETABS results for angle of twist values of box shaped cantilever wall ..	15
Table 2-3 DIANA results for angle of twist values of box shaped cantilever wall ...	15
Table 2-4 ETABS results for angle of twist values of 35 meter length structure	16
Table 2-5 Analysis Parameters.....	17
Table 2-6 ETABS results for C-Shaped Cantilever Wall	22
Table 2-7 DIANA results for C-Shaped Cantilever Wall	22
Table 2-8 Analysis results of different methods for box shaped structural wall	25
Table 2-9 Comparison of different methods for box shaped cantilever wall.....	26
Table 2-10 Analysis results of different methods for C-shaped cantilever wall.....	27
Table 2-11 ETABS results for displacement values of box shaped cantilever wall ..	28
Table 2-12 DIANA results for displacement values of box shaped cantilever wall ..	29
Table 2-13 ETABS results for displacement values of C-shaped cantilever wall	30
Table 2-14 DIANA Results for displacement values of C-shaped cantilever wall....	31
Table 2-15 Analysis results of different methods for box shaped cantilever wall.....	33
Table 2-16 Analysis results of different methods for C-shaped cantilever wall.....	33
Table 3-1 Calibrated material properties for concrete in tension.....	39
Table 3-2 Calibrated material properties for concrete in confined zone.....	39
Table 3-3 Calibrated compression properties for concrete unconfined zone.....	39
Table 3-4 Calibrated material properties for #3 rebar in compression	39
Table 3-5 Calibrated material properties for #2 rebar in compression	39
Table 3-6 Calibrated material properties for #3 rebar in tension	39
Table 3-7 Calibrated material properties for #2 rebar in tension	40
Table 3-8 Calibrated material properties for concrete in tension.....	52
Table 3-9 Calibrated material properties for concrete in confined zone of flange section	52

Table 3-10 Calibrated compression properties for concrete in unconfined zone of flange and web section.....	52
Table 3-11 Calibrated compression properties for concrete in confined zone of flange-web intersection.....	53
Table 3-12 Calibrated compression properties for concrete in confined zone of web section.....	53
Table 3-13 Calibrated material properties for #3 rebar in compression.....	53
Table 3-14 Calibrated material properties for #2 rebar in compression.....	53
Table 3-15 Calibrated tension properties for #3 rebar in confined zone of flange section.....	53
Table 3-16 Calibrated tension properties for #3 rebar in confined zone of flange-web intersection.....	53
Table 3-17 Calibrated tension properties for #3 rebar in confined zone of web section	54
Table 3-18 Calibrated tension properties for #2 rebar in unconfined zone of flange section.....	54
Table 3-19 Calibrated tension properties for #2 rebar in unconfined zone of web section.....	54
Table 4-1 Decreased moment of inertia values	67
Table 4-2 Time history analysis results of 4-storey symmetric structure in Y direction	105
Table 4-3 Time history analysis results of 4-storey symmetric structure in X direction	105
Table 4-4 Time history analysis results of 4-storey asymmetric structure in Y direction	108
Table 4-5 Time history analysis results of 4-storey asymmetric structure in X direction	108
Table 4-6 Time history analysis results of 15-storey symmetric structure in Y direction	112

Table 4-7 Time history analysis results of 15-storey symmetric structure in X direction	113
Table 4-8 Time history analysis results of 15-storey asymmetric structure in Y direction	116
Table 4-9 Time history analysis results of 15-storey asymmetric structure in X direction	117

LIST OF FIGURES

FIGURES

Figure 1-1 Diagram of the buildings that were called tallest building at one time (CTBUH, 2009)	1
Figure 1-2 Typical MVLEM element and wall model (Orakcal, 2004)	5
Figure 1-3 Nonlinear modeling approaches (PEER and ATC72-1, 2010)	7
Figure 2-1 Sectional Properties of Box Section	12
Figure 2-2. Models used in ETABS	14
Figure 2-3 Angle of twist values of box shaped cantilever wall for different mesh size	16
Figure 2-4 C-shaped cross section	17
Figure 2-5 Determination of the torsional stiffness (Young & Budynas, 2002)	18
Figure 2-6 Models that are used in ETABS for C-shaped wall	19
Figure 2-7 Parameters that are used for the calculation of torsional stiffness	21
Figure 2-8 Angle of twist values of C-shaped cantilever wall for different mesh size	23
Figure 2-9 Modeling of box section with frame elements	24
Figure 2-10 Modeling of C-shaped section with frame elements	27
Figure 2-11 Lateral displacement values of box shaped cantilever wall for different mesh size	29
Figure 2-12 Lateral displacement values of C-shaped cantilever wall in x direction for different mesh size	31
Figure 2-13 Lateral displacement values of C-shaped cantilever wall in y direction for different mesh size	32
Figure 3-1 Geometry of RW2 (Thomsen, 1995)	36
Figure 3-2 Cross section of RW2 (Thomsen, 1995)	37
Figure 3-3 Reinforcement placement of RW2 (Thomsen, 1995)	37
Figure 3-4 Test specimen (Thomsen, 1995)	38
Figure 3-5 Elevation view of RW2	41

Figure 3-6 Applied displacement time history function to RW2	42
Figure 3-7 Applied vertical load (KN) and horizontal displacement (mm)	42
Figure 3-8 Example of definition of material properties for concrete and steel	42
Figure 3-9 Definition of wall cross section in terms of nonlinear hinges (Alendar & Milicevic, 2015)	43
Figure 3-10 Fibers used in model	43
Figure 3-11 Analysis results of RW2 with fiber modeling approach	44
Figure 3-12 Hognestad material model for concrete	45
Figure 3-13 Modeling parameters for steel	45
Figure 3-14 Analysis results of RW2 according to design material parameters	46
Figure 3-15 Compressive and Tensile Behavior of Concrete (DIANA FEA User's Manual - Release 9.5, n.d.)	47
Figure 3-16 Finite element model of RW2 with embedded reinforcements	48
Figure 3-17 Analysis results of RW2 with continuum model	49
Figure 3-18 Comparison of different modeling techniques for RW2	49
Figure 3-19 Analysis results of RW2 according to design material parameters	50
Figure 3-20 Comparison of different modeling techniques for RW2 according to design material parameters	50
Figure 3-21 Geometry of TW2 (Thomsen, 1995)	51
Figure 3-22 Cross section and reinforcement placement of TW2 (Thomsen, 1995) ..	52
Figure 3-23 Elevation view of TW2	55
Figure 3-24 Applied displacement according to time (in mm)	55
Figure 3-25 Applied horizontal displacements (mm) and vertical loads (kN)	56
Figure 3-26 Definition of wall cross section in terms of nonlinear hinges (Alendar & Milicevic, 2015)	56
Figure 3-27 Properties of fibers for flange section of TW2	57
Figure 3-28 Properties of fiber for web section of TW2	57
Figure 3-29 Analysis results of TW2 with fiber model	58
Figure 3-30 Analysis results of TW2 according to design material parameters	59
Figure 3-31 Finite element model of TW2 with embedded reinforcements	60

Figure 3-32 Analysis results of TW2 with continuum model	61
Figure 3-33 Analysis results of TW2 according to design material parameters.....	62
Figure 3-34 Analysis results of computer programs for RW2	63
Figure 3-35 Analysis results of computer programs for TW2.....	63
Figure 4-1 Floor plan of the buildings (in meters)	66
Figure 4-2 Section properties of E-Shaped wall (in meters)	66
Figure 4-3 Load deformation curve of E-shaped wall in Y direction.....	68
Figure 4-4 Load deformation curve of E-shaped wall in X direction.....	69
Figure 4-5 Comparison of pushover and cyclic analysis results of E-shaped wall in Y direction	70
Figure 4-6 Comparison of pushover and cyclic analysis results of E-shaped wall in X direction	71
Figure 4-7 Comparison of pushover and cyclic analysis results of E-shaped wall in Y direction	71
Figure 4-8 Analysis models of the building in DIANA and PERFORM3D	72
Figure 4-9 Lateral and longitudinal reinforcements of the building.....	73
Figure 4-10 Application of forces.....	74
Figure 4-11 Comparison of base shear results for Y direction	74
Figure 4-12 Comparison of base shear results for X direction	75
Figure 4-13 Coloring of wall section according to limit strain value.....	77
Figure 4-14 Flexural cracking strains at 3 mm top displacements (0.024% Drift ratio, point A).....	78
Figure 4-15 Flexural cracking strains at 10 mm top displacement (0.08% Drift ratio, point B)	79
Figure 4-16 Cracked wall sections at 0.07% drift ratio	79
Figure 4-17 Shear cracks at 20 mm top displacement (0.17% Drift ratio, point C)..	80
Figure 4-18 Wall sections passing the limit strain value at 0.24% drift ratio	80
Figure 4-19 Crack strains at the end of the analysis (1.5% Drift ratio, point D).....	81
Figure 4-20 Wall sections passing the limit strain value at 1.5% drift ratio	81
Figure 4-21 Yielding of longitudinal reinforcement at 1.5% drift ratio in DIANA ..	82

Figure 4-22 Yielding of longitudinal reinforcement at 1.5% drift ratio in Perform3D	82
Figure 4-23 Flexural cracking strains at 3 mm top displacement (0.025% drift ratio)	83
Figure 4-24 Flexural cracking strains at 7.5 mm top displacement (0.0625% Drift ratio)	84
Figure 4-25 Wall strain at 0.06% drift ratio	84
Figure 4-26 Flexural cracking strains at 30 mm top displacement (0.25% Drift ratio, Point C)	85
Figure 4-27 Wall sections passing the limit strain value at 0.17% drift ratio	85
Figure 4-28 Flexural cracking strains at 0.5% drift ratio (Point D)	86
Figure 4-29 Wall sections passing the limit strain value at 0.5% drift ratio	86
Figure 4-30 Yielding of longitudinal reinforcements in DIANA at 0.5% drift ratio	88
Figure 4-31 Yielding of longitudinal reinforcements in Perform3D at 0.5% drift ratio	88
Figure 4-32 Analysis models of the tall building in DIANA and Perform3D	90
Figure 4-33 Lateral and longitudinal reinforcements of the building	91
Figure 4-34 Application of forces	92
Figure 4-35 Comparison of pushover analysis results in Y direction	92
Figure 4-36 Comparison of pushover analysis results in X direction	93
Figure 4-37 Initiation of flexural cracks (0.11% Drift ratio, point A)	94
Figure 4-38 Shear cracking strains at 57.5 mm top displacement (0.13% Drift ratio, point B)	95
Figure 4-39 Strain value of the walls at 0.18% drift ratio	95
Figure 4-40 Flexural cracking strains at the end of the analysis (1.8% Drift ratio, Point C)	96
Figure 4-41 Strain value of the walls at 1.8% drift ratio	96
Figure 4-42 Yielding of longitudinal reinforcements in DIANA at 1.8% drift ratio	97
Figure 4-43 Yielding of longitudinal reinforcements in Perform3D at 1.8% drift ratio	97

Figure 4-44 Initiation of cracks at 30 mm top displacement (0.067% Drift ratio, point A)	98
Figure 4-45 Flexural cracking strains at 92.8 mm top displacement (0.21% Drift ratio, point B)	99
Figure 4-46 Wall sections that pass the limit strain value at 0.25% drift ratio.....	99
Figure 4-47 Flexural cracking strains at the end of the analysis (2.2% Drift ratio, point C)	100
Figure 4-48 Wall sections that have strain values more than the limit value at 2.2% drift ratio	100
Figure 4-49 Yielding of longitudinal reinforcement in DIANA at 2.2% drift ratio	101
Figure 4-50 Yielding of longitudinal reinforcements in Perform3D at 2.2% drift ratio	101
Figure 4-51 Floor plan of the asymmetric buildings (in meters).....	103
Figure 4-52 Time history analysis results of 4-storey symmetric structure in Y direction	104
Figure 4-53 Time history analysis results of 4-storey symmetric structure in X direction	104
Figure 4-54 Comparison of drift ratios in Y direction for 4-storey symmetric structure	106
Figure 4-55 Comparison of drift ratios in X direction for 4-storey symmetric structure	106
Figure 4-56 Time history analysis results of 4-storey asymmetric structure in Y direction	107
Figure 4-57 Time history analysis results of 4-storey asymmetric structure in X direction	108
Figure 4-58 Comparison of drift ratios in Y direction for 4-storey asymmetric structure	109
Figure 4-59 Comparison of drift ratios in X direction for 4-storey asymmetric structure	109

Figure 4-60 Time history analysis results of 15-storey symmetric structure in Y direction	110
Figure 4-61 Time history analysis results of 15-storey symmetric structure in X direction	111
Figure 4-62 Comparison of drift ratios in Y direction for 15-storey symmetric structure	114
Figure 4-63 Comparison of drift ratios in X direction for 15-storey symmetric structure	114
Figure 4-64 Time history analysis results of 15-storey asymmetric structure in Y direction	115
Figure 4-65 Time history analysis results of 15-storey asymmetric structure in X direction	116
Figure 4-66 Comparison of drift ratios in Y direction for 15-storey asymmetric structure.....	118
Figure 4-67 Comparison of drift ratios in X direction for 15-storey asymmetric structure.....	118

CHAPTER 1

INTRODUCTION

1.1. Importance of Modeling of Reinforced Concrete Structural Walls

Over the centuries, people have constructed high towers for many reasons such as to show off their cities. From a historical perspective, tall structures imply the great rulers, empires, and religions such as Athos monasteries that were constructed to top of mountains in order to being closer to the heaven (Gerometta, 2009). However, these historical structures are overshadowed by today's skyscrapers. Construction of skyscrapers started nearly 150 years ago (Gerometta, 2009). Generally, Home Insurance Building that was designed by William Le Baron Jenney is accepted as the first skyscraper and it was also the first structure in order to claim the title of “World’s Tallest Building” at 55m (180ft) (Gerometta, 2009). Next, World Building that was constructed in New York in 1890 claimed that title. Height of the structures has increased steadily as technology has improved. Figure 1-1 shows the world’s tallest building according to their construction time.

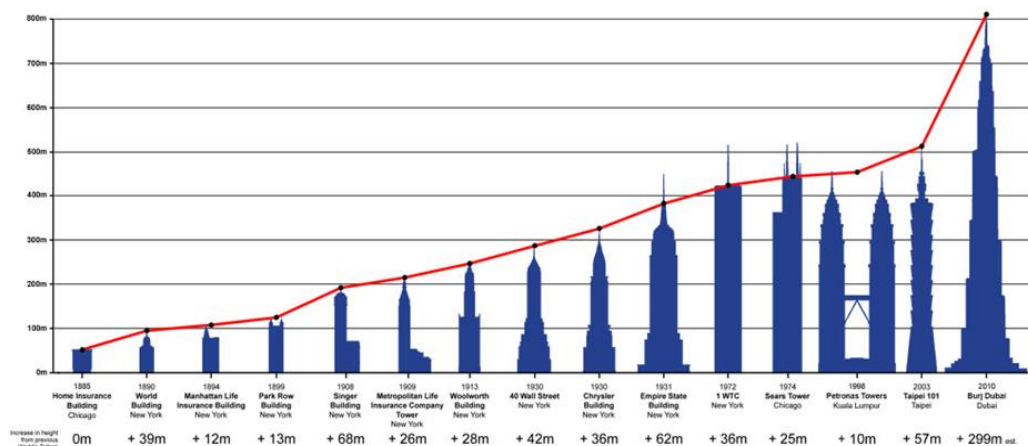


Figure 1-1 Diagram of the buildings that were called tallest building at one time (CTBUH, 2009)

Changes in urban life encourages the cities to build taller structures. Population of cities and their economies are increasing continually day by day. Because of this, the land prices of cities are rising excessively, thus the need for new living regions has been needed. These problems led people to build tall buildings. Moreover, with the help of developments in material science, constructing new life spaces by towards vertical direction instead of horizontal direction became possible. Taking all these facts into account, the need for tall building are increasing gradually day by day.

There are some architectural limitations for high rise buildings. Generally, beams are not preferred because they are not suitable for aesthetics. Moreover, some buildings (diagrid structures) also do not have columns to create space. Slabs, columns and structural walls are mainly utilized as a load resisting elements in reinforced concrete buildings. Columns and slabs are used to carry the vertical loads such as dead load, live load and superimposed dead load. On the other hand, structural walls are the main structural elements that are utilized to resist lateral loads such as earthquake and wind loads.

Design of tall buildings according to earthquake load is a sophisticated process. Therefore, performance based analysis and design approach is generally preferred for tall buildings but modeling of structural walls has some important complexities in the performance based analysis. For instance, accurate modeling of structural walls having irregular cross sections is still being studied. There are several modeling approaches and tools which can be utilized to model structural walls. All these approaches, however, are based on some simplifications and assumptions. Even though, they give acceptable results for a certain type of walls, their accuracy at an actual building with irregular shaped structural walls is still questionable. Therefore, this study focuses on comparison of different nonlinear modeling approaches for structural walls that are being utilized by structural engineers. This way, the structural engineers will have some guidelines and some results that they can use while designing an actual building.

1.2. Literature Review

Reinforced concrete structural walls in tall buildings are one of the most important structural members that resist lateral loads caused by wind or earthquake loadings. They are expected to provide sufficient stiffness and deformation capacity to satisfy the demand of strong earthquakes. Using core walls with slab/column to resist lateral loads is one of the most commonly used structural systems in tall buildings (Wallace, 2007).

Flat slab/column frame systems are usually used to resist the gravity loads. Actually, they are just designed to resist the gravity loads but their capability to resist the gravity loads under the lateral deformations caused from the lateral forces must be checked. The aim of this check is to prevent punching failures at the service level (Wallace, 2007).

As the height of the building increases, structural walls behave like a slender member i.e. they resist loads by bending rather than shear deformation. In order to model such behavior, usually, force-based fiber elements are preferred instead of the 3D continuum model because of their simplicity and low memory requirement (Vasquez et al., 2016). However, if fiber elements are used for modeling the structural walls, interaction between axial, bending and shear components must be considered which is not a straightforward process. Special formulations must be used in order to make response more accurate (Vasquez et al., 2016). In order to combining shear and flexural behavior in fiber elements, a softened membrane model was utilized by Mallapudi and Ayoub (2009). In this model, equilibrium equations are imposed in transverse direction also. This approach, however, increases the run time. When the results of the model are compared with the experimental results, it is seen that for critical elements shear response can be successfully captured. The main disadvantage of this model is the assumption of plane sections remain plane and uniform shear strain distribution (Mullapudi and Ayoub, 2009). The other challenge in modeling the nonlinear behavior of structural walls is associated with the damage localization.

When any material shows softening, damage localization is observed (Coleman and Spacone, 2001). As a solution of this localization problem usage of modified constitutive curves for concrete and steel fibers is proposed (Vasquez et al., 2016). Instead of peak stress of each fiber, global strength should be used. But in order to capture the global cyclic behavior, shear deformation, buckling of reinforcements, bar fracture and, pullout strength should be defined in the model (Vasquez et al., 2016).

The most common modeling method for a reinforced concrete structural wall are either the finite element method or the fiber element method. The first one is rarely used by practicing engineers since it is computationally very demanding. Fiber models, on the other hand, have the capability to capture the flexure and axial behavior of reinforced concrete structures and therefore they are commonly used but they are not completely reliable since they cannot capture shear with flexure and axial behavior (Petrangeli, 1999).

Multiple Vertical Line Element Model (MVLEM) is the first well-known macroscopic model that was proposed by Vulcano (Vulcano, 1988). Figure 1-2 shows the MVLEM model. In this model, horizontal spring is used at the center of rotation to simulate the shear behavior. This model cannot couple the flexural and shear behavior of the structural wall. MVLEM uses the plane sections remain plane assumption in calculations of strain level of wall element. In MVLEM, stress-strain behavior of reinforcements is represented with relationship of Menegotto and Pinto (1973) and in order to represent the behavior of concrete, constitutive relation of Chang and Mander (1994) is used. MVLEM is an effective model to capture the important nonlinear behavior of reinforced concrete structural walls. More recently, a new constitutive model was proposed by Orakcal (2004) by using the MVLEM's formulation. However, with these macroscopic models structural walls are represented as nonlinear translational and/or rotational springs that are connected by using rigid links. In order to prevent the complicated analysis, hysteretic representations of these springs should be selected as much as simple. These models cannot properly represent the hysteretic behavior of reinforced concrete structures, particularly in the case of shear behavior.

Moreover, these models do not have the capability to represent the strength degradation under reversal loading (Orakcal, 2004).

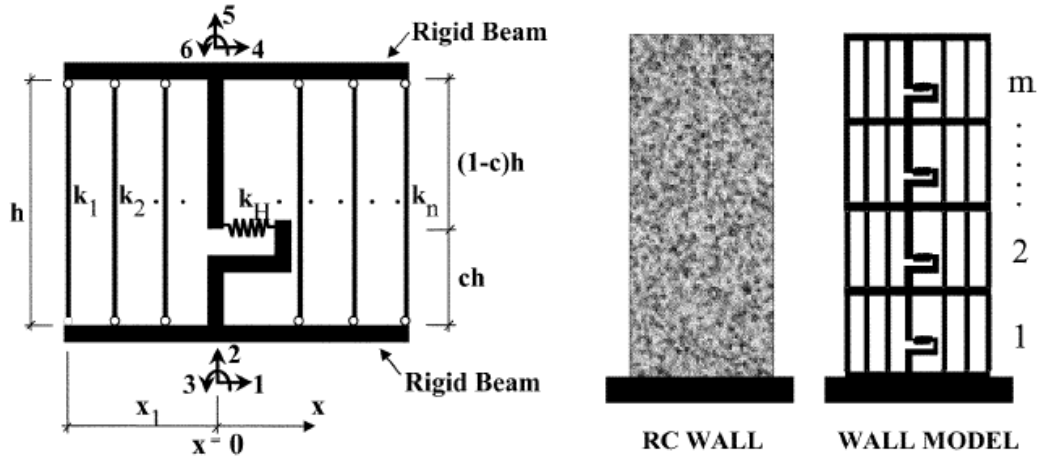


Figure 1-2 Typical MVLEM element and wall model (Orakcal, 2004)

In order to analyze the reinforced concrete structures under seismic loads, realistic analytical models that are capable of predicting the stiffness (as a function of damage) and ductility characteristics of members under reversal loading are required (Oosterle, 1979). Experimental studies show that shear deformations can be quite important locally although the behavior of the structure is generally governed by flexure (Oosterle, 1979). Inelastic shear deformations are especially distinct for structural walls since flexural yielding triggers the shear yielding even though the structure is designed with large shear capacity (Saatcioglu, 1988). These studies state that elastic shear behavior cannot be ensured by providing larger shear capacity compared to flexural capacity.

Cyclic behavior of slender (flexural) elements can be dominated by shear deformations also. It can be said that almost all cyclic failures are caused by shear failures (Petrangeli, 1999). Because of cyclic loading, shear capacity of the structure decreases under axial load.

Strain distribution of planar sections shows nearly linear distribution along the wall section. On the other hand, for flanged sections, when the flange of the section is under tension, tensile strains of both concrete and steel show a nonlinear distribution along the width of the flange (Orakcal et al., 2006). Therefore, modeling approaches that used the assumption of plane sections remain plane, cannot correctly calculate the nonlinear behavior of flanged sections. This assumption provides a uniform tensile strain distribution for flange section and causes the overestimation of the capacity of the section when the flange is under tension (Orakcal et al., 2006).

Deformation limits generally determine the performance of structural walls. For the deformation limit, a comprehensive study was conducted on rectangular structural walls by Kazaz (2012). Effect of design parameters, such as shear stress, change in axial load, length of the wall, reinforcement ratio of web and boundary elements and shear span to length ratio on deformation limits were studied. Reinforcement of boundary element and length of the wall are the most crucial parameters on the yielding deformation (Kazaz et al., 2012). Other parameters, such as shear span to length ratio, reinforcement of web elements, and length of wall affect the ultimate deformation capacity (Kazaz et al., 2012).

Performance of reinforced concrete structures can be estimated from the limit states (Kazaz et al., 2012). These limit states are represented in terms of drift ratios and plastic hinge rotations. Most analysis approaches use plane sections remain plane assumption, thus calculated plastic hinge rotations do not represent the actual rotations. On the other hand, drift ratios and member end rotations are the best structural deformation measurements since they simulate the integration along deformed section (Kazaz et al., 2012).

Inelastic models can be differentiated according to modeling assumptions (PEER and ATC72-1, 2010). Figure 1-3 shows three idealized nonlinear models for simulating the nonlinear behavior of structural walls. Continuum model consists of finite elements that represent the concrete, transverse and longitudinal reinforcement in

which associated with cracking, crushing of concrete, yielding of steel, buckling and fracture of reinforcement and bond between reinforcement and concrete. In continuum models predefined section behavior is not required. Moreover, while creating a continuum model, defining member strength, stiffness, deformation capacity is not required since all these effects are inherently captured by the model through material properties.

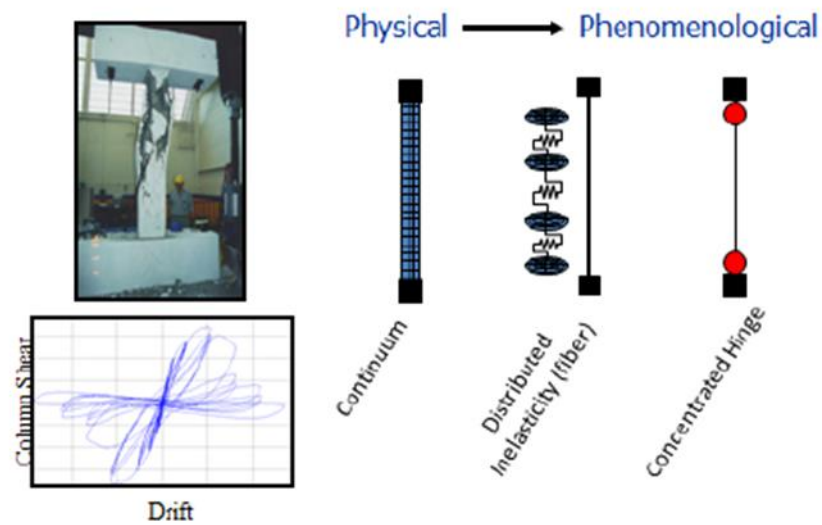


Figure 1-3 Nonlinear modeling approaches (PEER and ATC72-1, 2010)

The other type of nonlinear modeling approach is the concentrated hinge (lumped plasticity) model (PEER and ATC72-1, 2010). These models are defined by the overall force deformation response of the component of the structure. Lumped plasticity models have some shortcomings. First, during loading and unloading these models do not have the ability to account for the movement of the neutral axis of the wall section. Secondly, these models cannot take into account the interaction between connecting members such as slabs and beams and effects of variation of axial load level of the structural wall and stiffness (PEER and ATC72-1, 2010). Moreover, modeling non planar walls such as T-shaped cross section using this method may overestimate the capacity of the wall (PEER and ATC72-1, 2010). Because in this method sections are represented with frame elements and connecting flange web

sections problems for modeling. On the other hand, lumped plasticity models with hinges at member ends are relatively easy to use and also computationally effective. Assigning stiffness parameters and hinge rotations are straight forward. Required parameters for modeling structural walls with this method are values of effective stiffness for flexure and shear ($E_c I_{eff}$, $G_c A$), yield strengths (M_y and V_y), deformation capacities, residual strength and post yield stiffness. All of these parameters can be defined by the help of codes or experimental results. Since this method cannot take into account the variation in axial load on the wall strength, flexural strength can be modeled by assuming an average axial load (PEER and ATC72-1, 2010).

Fiber (distributed inelasticity) models are in between the continuum modeling and concentrated hinge modeling approaches. Fiber models are mainly used in practice and on the basis of beam/column element formulation. In this beam/column element formulation, the wall cross section is discretized using a number of steel and concrete fibers. Fiber models have the capacity to capture the nonlinear behavior of flexure controlled (slender) structural walls acceptably well in terms of global responses such as load-deformation behavior. On the other hand, this method generally cannot predict the local responses such as rotations and strains of the structural walls because of the assumptions that are used in model development such as the assumption of plane sections remain plane (PEER and ATC72-1, 2010).

Moreover, most of the models that are used in practice do not have the capacity to capture the experimentally known interaction between flexure and shear for structural walls with moderate aspect ratios such as between 1.0 and 3.0. Experiments show that for walls with moderate aspect ratios both nonlinear shear deformation and flexural yielding occur simultaneously and according to researches, shear deformations can form up to 30% to 50% of total lateral wall displacements and so shear deformations can reduce wall stiffness, strength and deformation capacity. Fiber models that are used in practice cannot consider coupling between the shear and flexural deformations. Because of this reason, shear deformation cannot completely capture the mechanism of structural walls under lateral loading and this deficiency causes the

overestimation of lateral load carrying capacity of structural walls with moderate aspect ratios and underestimation of compressive strains for slender structural walls that are controlled by flexure (PEER and ATC72-1, 2010).

Continuum and fiber models more accurately capture the behavior of structural walls such as yielding of reinforcement and cracking of concrete but their ability to capture strength degradation such as bond slip, shear failure and buckling of reinforcement are limited. On the other hand, concentrated hinge models have the ability to capture the strength degradation in an empirical manner (PEER and ATC72-1, 2010).

1.3. Objectives and Scope

Different nonlinear modelling approaches for performance based analysis of structural walls are compared in this study as a main purpose. This study is selected because construction of tall buildings increases gradually day by day and in the performance based analysis of tall buildings, modeling of structural walls always be a complicated process and thus this study is restricted with the modeling of walls.

First, a calibration study for elastic analysis was performed. Typical wall cross-sections such as closed section (box section) and open section (C-shaped cross-section) were used. These sections were analyzed under pure torsion and pure bending scenarios by using the finite element method and the mid-column method and results were compared with the available theoretical solutions. This comparison implied that the finite element method is good enough for the analysis of structural walls that are under pure torsion and pure bending.

As a second step, structural walls were modeled with the distributed inelasticity (fiber) model by using Perform3D and ETABS, and the continuum model by using DIANA FEA (DIANA). Analyses were performed for rectangular and T-shaped cross sections and results were compared with the experimental results. According to the results, although fiber modeling approach overestimates the initial stiffness of the wall, it can be said that both computer programs have the capability to capture the nonlinear behavior of planar structural walls. Moreover, this calculation implies that fiber

modeling approach cannot correctly calculate the capacity of flanged structural walls. In the fiber model, the capacity of the flange is over-estimated under tension loading. Finally, behavior of squat and slender walls were compared. In order to represent squat wall and slender wall, 4-storey and 15-storey structures were selected, respectively. Design of these buildings were performed according to ASCE 7-10 and ACI-318R-08. Nonlinear pushover and nonlinear time history analyses are performed for these structures. In order to perform these analyses, structures were modeled with the fiber method and the continuum method in Perform3D and DIANA, respectively. Comparison of the results showed that, effect of shear cannot be captured by the fiber model. On the other hand, continuum approach can couple the shear and flexure. In addition, for flange sections, the capacity cannot be captured correctly by the fiber model. In addition, asymmetric 4-storey and 15-storey structures were modeled and their behavior were compared with symmetric ones in order to see the effect of torsion.

CHAPTER 2

ELASTIC CALIBRATION STUDIES

Structural engineers generally perform linear elastic analysis for the design of buildings. While modeling the structural wall of buildings, some modeling approaches such as mid-column method and finite element method are usually used. When finite element method is used, wall sections are modeled with shell elements, whereas, in the mid-column method, wall cross sections are modeled with frame elements and these frame elements are connected each other with rigid links. Generally, structural engineers prefer to use mid-column method due to its simplicity in post-processing the analysis results. On the other hand, mid-column approach may give inaccurate results when the wall sections are different than rectangles (Akış, 2004). Because of this reason, the accuracy of another method, which is the modified version of mid-column method, was also tested together with aforementioned elastic modeling methods in this chapter.

Test cases consisted of wall cross sections with box sections and C-shaped sections in order to check the analysis results for the open and closed section behaviors. Loads were applied in such a way that they create pure torsion and pure bending on the wall sections. Then analyses were performed for these two cases and the results were compared with analytical solutions.

2.1. Torsional Behavior of Box and C-Shaped Section

2.1.1. Torsional Behavior of Box Shaped Section

For a given box section with uniform thickness, presented in Figure 2-1, the angle of twist due to torsional load can be determined by Equation 2.1 (Timoshenko and Goodier, 1951).

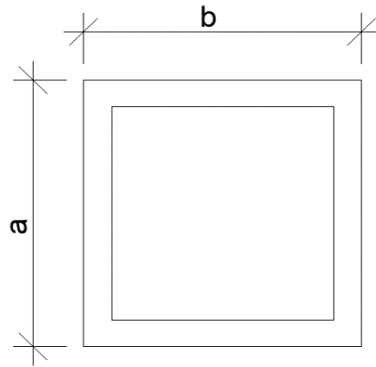


Figure 2-1 Sectional Properties of Box Section

$$\phi = \frac{M_t \times L \times s}{4 \times A^2 \times G \times \gamma} \quad (2.1)$$

Table 2-1. Section properties and parameters that used in analysis

Parameter	Value	Explanation	Unit
M_t	10	Applied torsion	kN.m
L	3.5	Length of the structure	m
s	3.6	Length of the centerline of the section	m
A	0.81	Areas enclosed by the outer and the inner boundaries of the section	m ²
G	13750	Shear modulus	MPa
γ	0.1	Uniform thickness	m
a	1	Side length of the section	m
b	1	Side length of the section	m

For a cantilever column having a length of 3.5 m under a 10 kN.m tip torsional moment, the angle of twist value was calculated as 3.492×10^{-5} rad with Equation 2.1. it should be noted that, the solution obtained with Equation 2.1 is approximate solution based on membrane analogy assumption. In this approach, rectangular section is assumed as cylindrical section with neglecting the effect of sides. The same problem

was also solved with 6 different models having different number of finite elements (Figure 2-2). Two different analysis software were utilized for this purpose, ETABS and DIANA. In these models, bottom of the structure was restrained against translation. Rigid diaphragm was assigned at the top of the structure in ETABS (Rigid diaphragm cannot be used in DIANA. Therefore, loads were applied to the points in such a way to create the torsion at the middle of the section). Force pairs were applied at the end points of the section to create desired torsion at the center of the section.

The angle of twist results obtained from each model with ETABS and DIANA are presented in Table 2-2 and Table 2-3, respectively. In these tables percent difference was calculated with Equation 2.2.

$$\text{Percent Difference} = \frac{\text{Analysis Result} - \text{Approximation}}{\text{Approximation}} \quad (2.2)$$

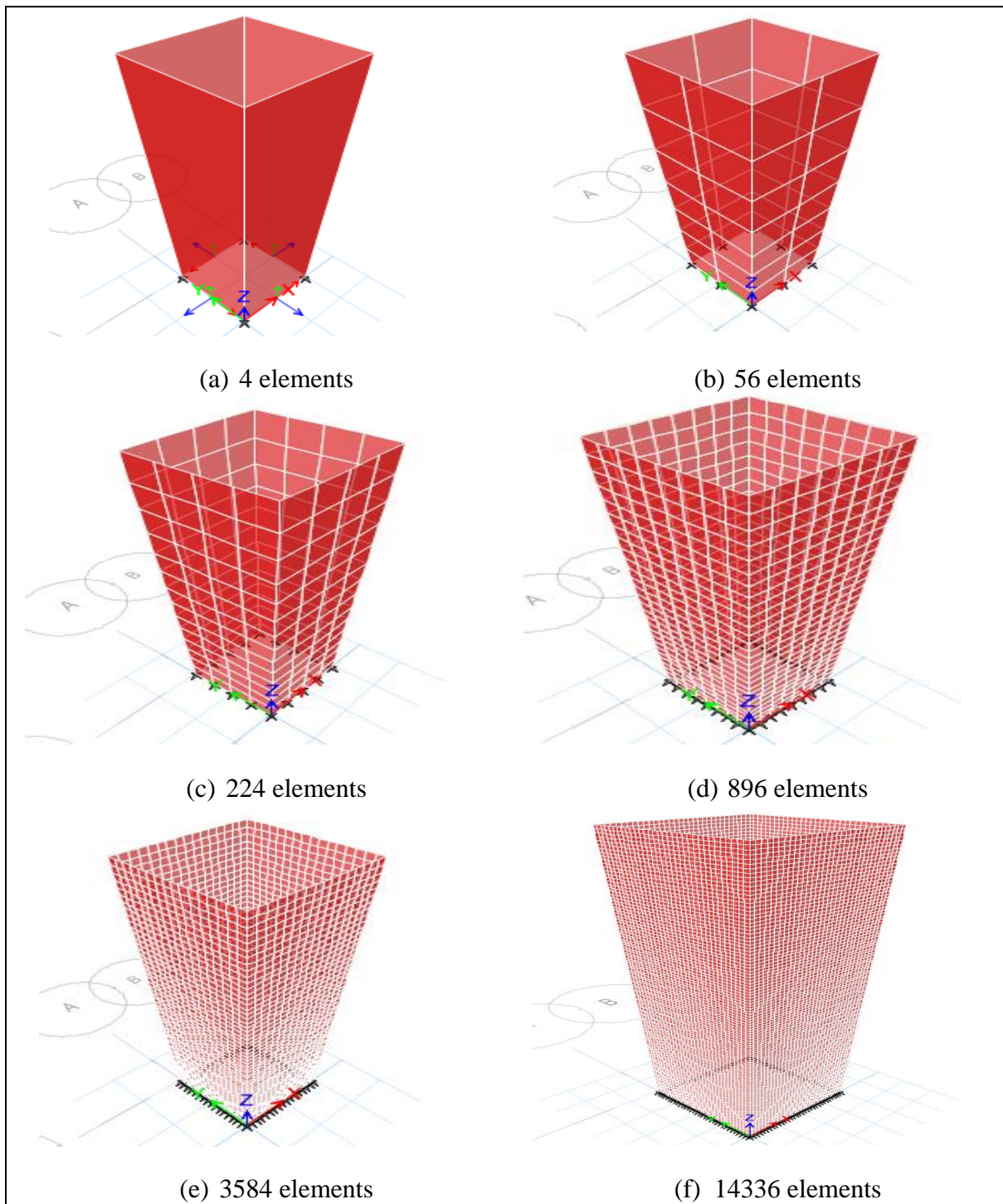


Figure 2-2. Models used in ETABS

Table 2-2 ETABS results for angle of twist values of box shaped cantilever wall

Number of Elements	Angle of Twist (rad)	Percent Difference(%)
4	3.435×10^{-5}	1.63
56	3.412×10^{-5}	2.29
224	3.408×10^{-5}	2.41
896	3.412×10^{-5}	2.29
3584	3.421×10^{-5}	2.03
14336	3.428×10^{-5}	1.83
Analytical Result	3.492×10^{-5}	

Table 2-3 DIANA results for angle of twist values of box shaped cantilever wall

Number of Elements	Angle of Twist (rad)	Percent Difference(%)
4	3.600×10^{-5}	3.09
56	3.578×10^{-5}	2.46
224	3.600×10^{-5}	3.09
896	3.600×10^{-5}	3.09
3584	3.600×10^{-5}	3.09
14336	3.600×10^{-5}	3.09
Analytical Result	3.492×10^{-5}	

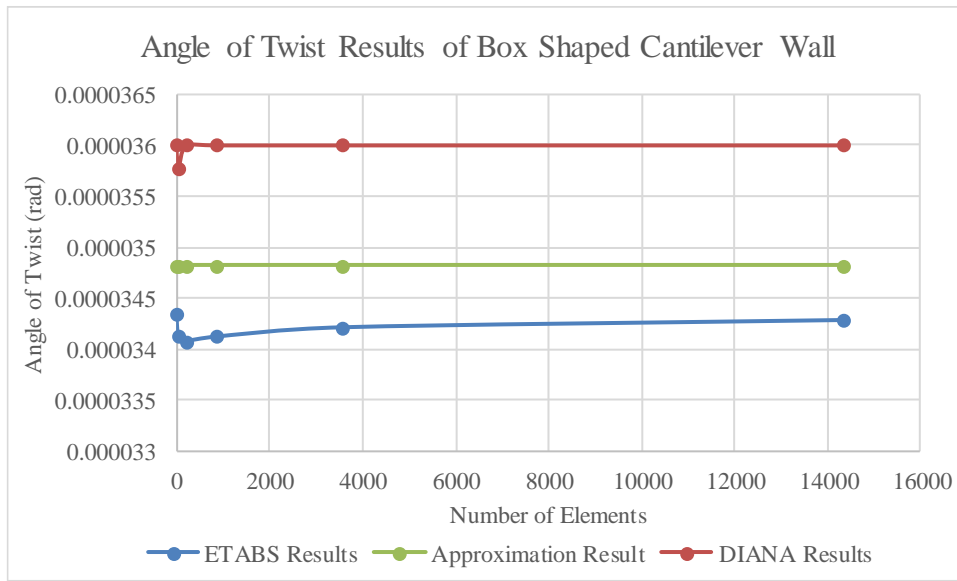


Figure 2-3 Angle of twist values of box shaped cantilever wall for different mesh size

The results indicate that the finite element method is capable of computing torsional behavior of closed box sections under pure torsion. There is a small difference between ETABS and DIANA results. This may be due to the difference in finite element formulations. Also, there is 3% difference between analytical results and numerical results. This is mainly due to the assumptions of the Equation 2.1. In order to examine another case, same cantilever model with 35 m length was analyzed in a similar manner. The results of this case is given in Table 2-4. For long cantilevers, the accuracy of the results has a similar tendency with the short cantilever.

Table 2-4 ETABS results for angle of twist values of 35 meter length structure

Number of Elements	Angle of Twist (rad)	Percent Difference(%)
40	3.435×10^{-4}	1.63
560	3.412×10^{-4}	2.29
2240	3.408×10^{-4}	2.41
8960	3.412×10^{-4}	2.29
Approximation Result	3.492×10^{-5}	

2.1.2. Torsional Behavior of C-Shaped Section

Analytical results for angle of twist under torsion of C-shaped sections can be determined by a rough approximation by assuming that the torsional rigidity of C-shaped section is equal to the sum of the torsional rigidities of the three rectangles (Timoshenko and Goodier, 1951). In order to test the accuracy of finite element modeling approach for such a section, the channel shape presented in Figure 2-4 and Table 2-5 was analytically solved and the result was compared with the results of the finite element analysis with ETABS and DIANA.

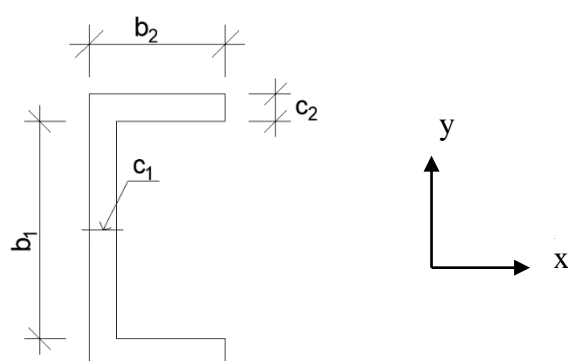


Figure 2-4 C-shaped cross section

Table 2-5 Analysis Parameters

Parameter	Value	Explanation	Unit
M_t	10	Applied torsion	kN.m
L	3.5	Length of the structure	m
s	3.6	Length of the centerline of the section	m
A	0.81	Areas enclosed by the outer and the inner boundaries of the section	m^2
G	13750	Shear modulus	MPa
γ	0.1	Uniform thickness	m

$$\phi = \frac{3 \times M_t \times L}{(b_1 \times c_1^3 + 2 \times b_2 \times c_2^3) \times G} \quad (2.3)$$

At the top ($L=3.5$ m), the angle of twist was calculated as 4.242×10^{-3} rad by using Equation 2.3. On the other hand, angle of twist for C-shaped section can also be determined from the Equation 2.4 (Young and Budynas, 2002). In this case, the angle of twist was calculated as 4.74×10^{-3} rad.

$$\theta = \frac{T \times L}{K \times G} \quad (2.4)$$


<p>L-section; $b \geq d$. For definitions of r and D, see case 26.</p>	$K = K_1 + K_2 + \alpha D^4$ <p>where $K_1 = ab^3 \left[\frac{1}{3} - 0.21 \frac{b}{a} \left(1 - \frac{b^4}{12a^4} \right) \right]$</p> $K_2 = cd^3 \left[\frac{1}{3} - 0.105 \frac{d}{c} \left(1 - \frac{d^4}{192c^4} \right) \right]$ $\alpha = \frac{d}{b} \left(0.07 + 0.076 \frac{r}{b} \right)$ $D = 2[d + b + 3r - \sqrt{2(2r + b)(2r + d)}]$ <p>for $b < 2(d + r)$</p>
<p>U- or Z-section</p> 	<p>K = sum of K's of constituent L-sections computed</p>

Figure 2-5 Determination of the torsional stiffness (Young & Budynas, 2002)

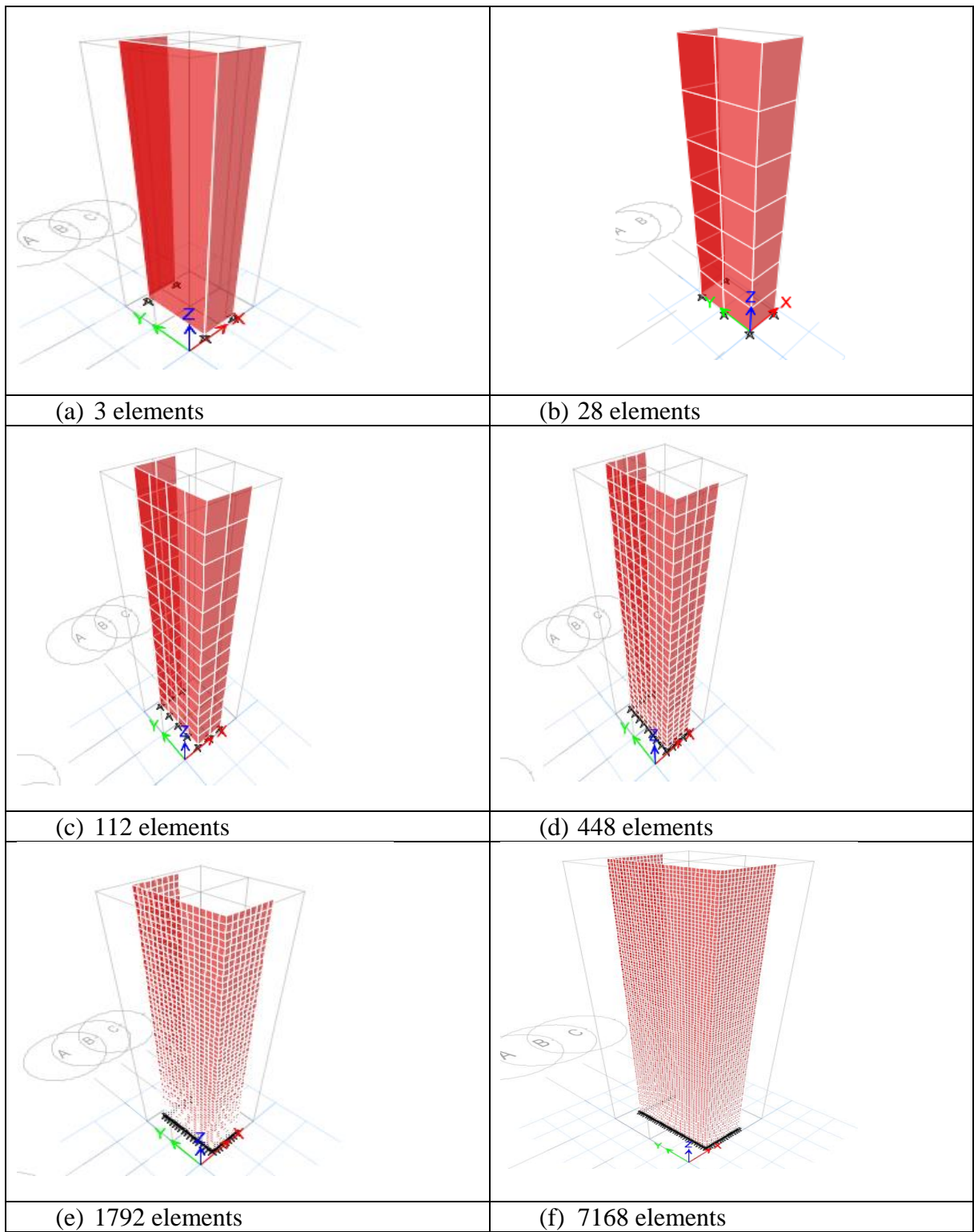


Figure 2-6 Models that are used in ETABS for C-shaped wall

Figure 2-6 shows the finite element analysis models with ETABS. In these models, bottom of the structure was restrained against translation as in the box-section case. Rigid diaphragm was assigned at the top of the structure. Force pairs were applied at the end points of the section to create desired torsion at the center of the section.

For C-shaped section effect of warping is ignored in Equations 2.3 and 2.4. If the bending of the flanges is restrained against in-plane deformation, the member resist to torsion with warping also. Since in the finite element models, the member is modeled as one end is fixed and the other end is free this restraint would cause warping deformation in addition to torsional deformation. For such a case, the total non-uniform torsion T_n can be calculated by Equation 2.5 (Mc Guire, 1968).

$$T_n = T_{sv} + T_w \quad (2.5)$$

In this equation T_w represents the warping torsion and T_{sv} represents the St. Venant's torsion. The differential equation for non-uniform torsional resistance $T_n(z)$ can be determined as the sum of these two effects.

$$T_n = G \times J \times \frac{d\theta}{dz} - E \times C_w \times \frac{d^3\theta}{dz^3} \quad (2.6)$$

In Equation 2.6, GJ and EC_w represent the St. Venant's torsional stiffness and warping rigidity, respectively. C_w is the warping constant for the cross-section and can be found by the help of Equation 2.7. Parameters used in Equation 2.7 and Equation 2.8 are presented in Figure 2-7.

$$C_w = d^2 \times b^3 \times t \times \left| \frac{1 - 3\alpha}{6} + \frac{\alpha^2}{2} \times \left(1 + \frac{d \times w}{6 \times b \times t} \right) \right| \quad (2.7)$$

$$\alpha = \frac{1}{2 + d \times w / 3 \times b \times t} \quad (2.8)$$

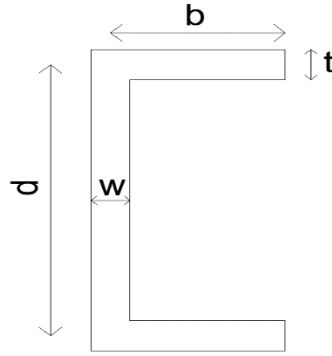


Figure 2-7 Parameters that are used for the calculation of torsional stiffness

If following boundary conditions are used (Equations 2.9 and 2.10), Equation 2.6 can be simplified as shown in Equation 2.11.

- @ $z = 0$ $\frac{d\theta}{dz} = 0$ (2.9)

- @ $z = L$ $\frac{d^3\theta}{dz^3} = 0$ (2.10)

$$\frac{d\theta}{dz} = \frac{T}{G \times J} \times \left[1 - \frac{\cosh \frac{L-z}{a}}{\cosh \frac{L}{a}} \right] \quad (2.11)$$

where

$$a^2 = \frac{E \times C_w}{G \times J} \quad (2.12)$$

In order to calculate the angle of twist, Equation 2.11 is integrated.

$$\theta = \frac{T}{G \times J} \times \left[z + \frac{a \times \sinh \frac{L-z}{a}}{\cosh \frac{L}{a}} - a \times \tanh \frac{L}{a} \right] \quad (2.13)$$

At $z=L$

$$\theta = \frac{T}{G \times J} \times \left[L - a \times \tanh \frac{L}{a} \right] \quad (2.14)$$

Thus, when the warping effect was considered, the angle of twist value for the C-shaped section was determined as 2.49×10^{-3} rad according to Equation 2.14. The following tables, Table 2-6 and Table 2-7 show the results of the finite element analysis with ETABS and DIANA, respectively.

Table 2-6 ETABS results for C-Shaped Cantilever Wall

Number of Elements	Angle of Twist (rad)	Percent Difference(%)
3	2.476×10^{-3}	0.59
28	2.514×10^{-3}	0.96
112	2.522×10^{-3}	1.29
448	2.526×10^{-3}	1.45
1792	2.528×10^{-3}	1.53
7168	2.528×10^{-3}	1.53
Analytical Result	2.49×10^{-3}	

Table 2-7 DIANA results for C-Shaped Cantilever Wall

Number of Elements	Angle of Twist (rad)	Percent Difference(%)
3	2.606×10^{-3}	4.65
28	2.562×10^{-3}	2.89
112	2.673×10^{-3}	7.35
448	2.673×10^{-3}	7.35
1792	2.673×10^{-3}	7.35
7168	2.673×10^{-3}	7.35
Analytical Result	2.49×10^{-3}	

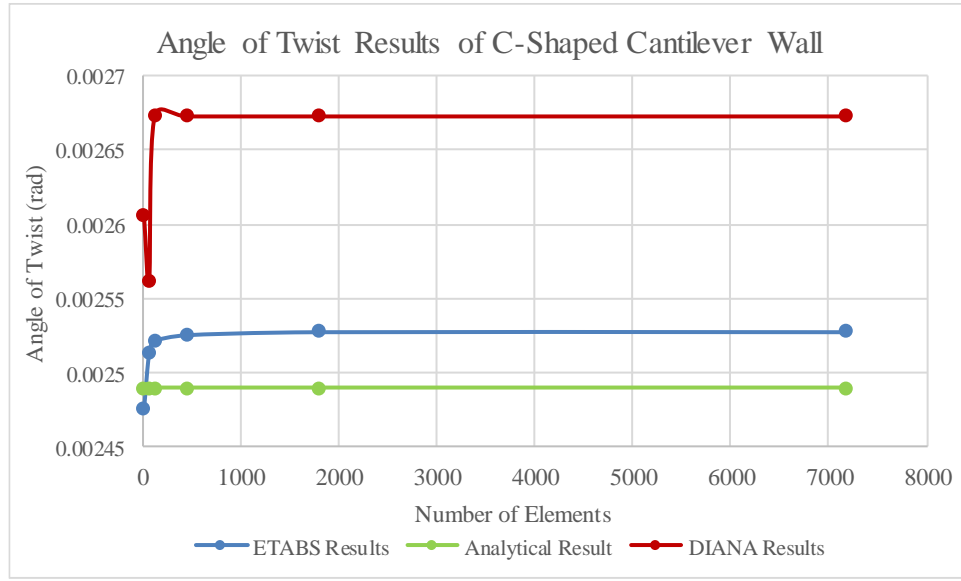


Figure 2-8 Angle of twist values of C-shaped cantilever wall for different mesh size

The results state that, the finite element method has the capability to predict torsional behavior of C-shaped sections under pure torsion. There is a small difference between computer programs and this may be caused from the difference in finite element formulations. Also, there is 2% difference between analytical results and numerical results. This is mainly due to the assumptions of Equation 2.14.

Moreover, for long sections that L/a ratio yields to infinite and $\tanh(L/a)$ values approach to 1. So Equation 2.14 turns to Equation 2.15 for long structures.

$$\theta = \frac{T}{G \times J} \times \left[L - a \times \tanh \frac{L}{a} \right] \quad (2.15)$$

Equation 2.15 states that as the ratio of L/a increases, effect of warping decreases.

2.1.3. Mid-Column Method

Up to this point both box section and C-shaped section were modelled by finite element method. Then a widely used method which is called as mid-column method was utilized and same analyses were performed to check the validity of this method for torsional behavior of closed and open sections.

2.1.3.1. Mid-Column Method for Box Section

In this method four side of the box section was modelled with frame elements which have sectional dimensions 0.1 m x 1 m and 0.1 m x 0.8 m. These frames were connected each other by rigid links as presented in Figure 2-9.

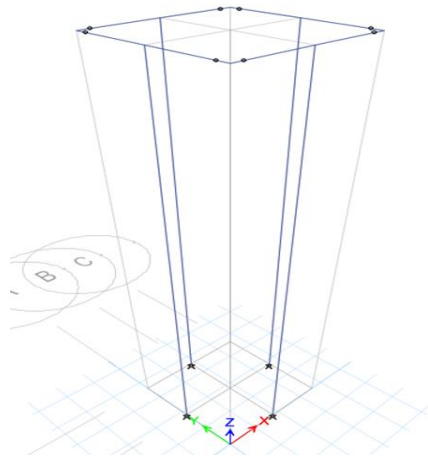


Figure 2-9 Modeling of box section with frame elements

For pure torsion, it is observed that rigid beams behave independently from the columns. The main reason of this is that torsional stiffness of this structural system is smaller than the torsional stiffness of the actual system. As Smith and Girgis (1986) stated, the closed section structural walls modelled by mid-column method became much stiffer than the one with the finite element method (Smith and Girgis, 1986). In order to solve this problem torsional releases are assigned to the rigid frames.

For rigid links, massless material was used. Modulus of elasticity of this material was selected as 330000 MPa. Sectional property of rigid element was selected as 4 m x 4 m. Table 2-8 shows the analysis results of the mid-column method. For this analysis, it was observed that increasing the modulus of elasticity of the massless material does not change the result.

Table 2-8 Analysis results of different methods for box shaped structural wall

	Angle of Twist (rad)	Percent Difference (%)
Mid-Column Method without Torsional Release	6.9×10^{-4}	1875
Mid-Column Method with Torsional Release	6.4×10^{-4}	1732
Analytical Result	3.492×10^{-5}	

As it is understood from the results, this method does not give accurate results for the box section. In order to obtain better results with this modeling approach, Akış (Akış, 2004) proposed an approach. The proposed model adjusts the torsional constant of the columns so that the total torsional stiffness developed by mid-columns are equal to the torsional stiffness of the actual wall section. This method has three steps.

- i. Calculation of J_c : the torsional constant of the closed section
- ii. Calculation of J_i : the torsional constant of the columns
- iii. Calculation of the modified torsional constant of columns

Modified torsional constant of columns can be determined by the help of Equation 2.16.

$$\bar{J}_l = \frac{J_c}{\sum_{k=1}^n J_k} \times J_i \times B_i \quad (2.16)$$

In this formulation;

- B_i is the constant related with the horizontal distance between the centroid of the closed section and centroid of the section. The value of B_i is 1 for square structural wall.
- n is the number of columns

J_c (torsional constant) of a square closed section can be determined by the help of Equation 2.17.

$$J_c = 0.1406 \times b^4 \quad (2.17)$$

In this analyses in order to catch the actual geometry of the structure two type of columns which have different section dimensions were used. Section dimensions of columns were selected as 0.1 m x 1 m and 0.1 m x 0.8 m. Modified torsional constant of columns were calculated as 0.0256 m⁴ and 0.0205 m⁴ respectively. After adjusting the torsional constant of the columns according to these results, the structure was reanalyzed and this time angle of twist was determined as 2.7x10⁻⁵ rad. Table 2-9 shows the comparisons of all the solutions.

Table 2-9 Comparison of different methods for box shaped cantilever wall

	Angle of Twist (rad)	Percent Difference (%)
Mid-Column Method without Torsional Release	6.9x10 ⁻⁴	1875
Mid-Column Method with Torsional Release	6.4x10 ⁻⁴	1732
Modified-Mid Column Method	2.7x10 ⁻⁵	22.7
Finite Element Method	3.435x10 ⁻⁵	1.63
Analytical Result	3.492x10 ⁻⁵	

According to the results presented in Table 2-9, the results of the mid-column method with and without torsional release is unacceptable. Although modified mid-column method improves the torsional behavior significantly and reduces the difference from the analytical solution to 22.7%, it still does not provide as accurate as the finite element method.

2.1.3.2. Mid-Column Method for C-Shaped Section

The accuracy of the mid-column method was also tested for the torsional behavior of C-shaped walls. In this case, the C-shaped wall was modeled with three columns that connected by rigid links as shown in the Figure 2-10. Section dimensions of columns were selected as 0.1 m x 1 m and 0.1 m x 0.4 m.

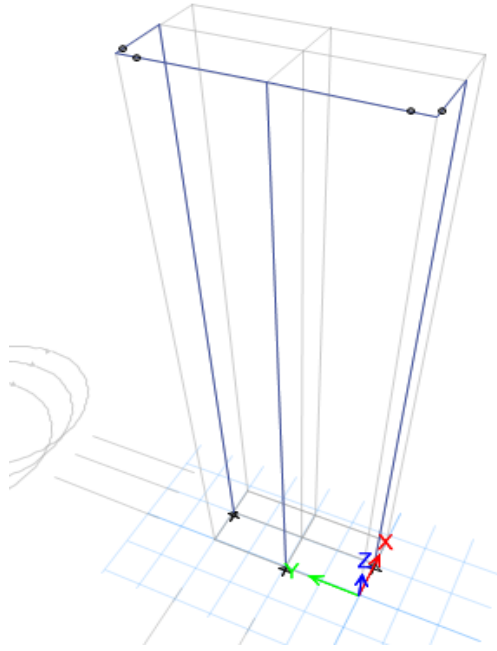


Figure 2-10 Modeling of C-shaped section with frame elements

Similar to the box section, torsional releases were defined at the ends of the rigid links. The material and sectional properties of the rigid links were taken similar to the previous case.

Table 2-10 Analysis results of different methods for C-shaped cantilever wall

	Angle of Twist (rad)	Percent Difference (%)
Mid-Column Method without Torsional Release	4.74×10^{-3}	90.4
Mid-Column Method with Torsional Release	3.66×10^{-3}	47
Analytical Result	2.49×10^{-3}	

When the results that are presented in Table 2-9 and Table 2-10 are studied, it is seen that mid-column method provides more reasonable results for the C-shaped walls when compared with the box section. But, still finite element method provides much more accurate results for the torsional behavior of the open sections.

2.2. Behavior of Box Section and C-Shaped Section Under Pure Bending

2.2.1. Behavior of Box Section Under Pure Bending

For a cantilever, the translational tip displacement can be calculated with Equation 2.18.

$$F = K \times U \quad (2.18)$$

In this formulation, F represents the applied point load, K is the translational stiffness of the cantilever and U is the tip displacement. While computing the translational stiffness only bending deformation was considered, shear deformation was ignored. The same models presented in Figure 2-2 were analyzed with both ETABS and DIANA and the tip displacements were compared with the analytical results. In these models, rigid diaphragms were used in ETABS (in DIANA, loads were applied in such a way to create bending force at the shear center of the section) and in order to prevent rotation lateral force was applied at shear center. In this study, the elastic modulus was taken as equal to 33000 MPa. Under the effect of 100 kN applied tip point load, lateral displacement of the cantilever was calculated as 1.013×10^{-3} m. Analysis results are presented in Table 2-11 and Table 2-12.

Table 2-11 ETABS results for displacement values of box shaped cantilever wall

Number of Elements	Lateral Displacement (m)	Percent Difference (%)
4	7.795×10^{-4}	23
56	1.038×10^{-3}	2.47
224	1.042×10^{-3}	2.86
896	1.045×10^{-3}	3.16
3584	1.046×10^{-3}	3.26
14336	1.047×10^{-3}	3.36
Analytical Result	1.013×10^{-3}	

Table 2-12 DIANA results for displacement values of box shaped cantilever wall

Number of Elements	Lateral Displacement (m)	Percent Difference(%)
4	1.03×10^{-3}	1.68
56	1.05×10^{-3}	3.65
224	1.05×10^{-3}	3.65
896	1.05×10^{-3}	3.65
3584	1.05×10^{-3}	3.65
14336	1.05×10^{-3}	3.65
Analytical Result	1.013×10^{-3}	

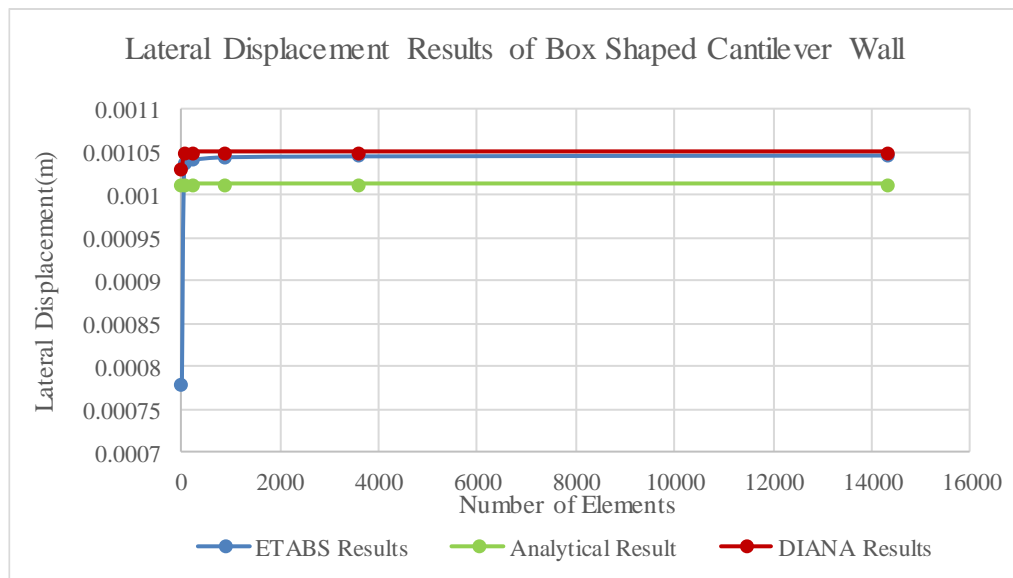


Figure 2-11 Lateral displacement values of box shaped cantilever wall for different mesh size

According to the results presented in Table 2-11 and Table 2-12, finite element method is capable of calculating the flexural behavior of box sections under pure bending with acceptable error limits when more than 4 elements are utilized.

2.2.2. Behavior of C-Shaped Section Under Pure Bending

The C-shaped wall whose cross sectional properties that are given in Table 2-5, was analyzed for pure bending. The lateral displacement values were calculated as 2.0261

mm and 11.3 mm in x and y directions, respectively. In this analysis elastic modulus was also taken as 33000 MPa. Likewise, rigid diaphragm was defined at the top of the wall and lateral force was applied at shear center of the section to prevent torsion. The same wall was also modeled with finite elements having different mesh sizes as shown in Figure 2-6 and analyzed with ETABS and DIANA. The lateral displacements and their comparison with the analytical results are presented in Table 2-13 and Table 2-14.

Table 2-13 ETABS results for displacement values of C-shaped cantilever wall

Number of Elements	Lateral Displacement (m)		Percent Difference (%)	
			X Direction	Y Direction
3	1.571×10^{-3}	0.00855	22.46	24.34
56	2.052×10^{-3}	0.0114	1.28	0.8
112	2.072×10^{-3}	0.0115	2.27	1.77
448	2.078×10^{-3}	0.0115	2.56	1.77
1792	2.08×10^{-3}	0.0116	2.66	2.3
7168	2.08×10^{-3}	0.0116	2.57	2.39
Analytical Result	2.03×10^{-3}	0.0113		

Table 2-14 DIANA Results for displacement values of C-shaped cantilever wall

Number of Elements	Lateral Displacement (m)		Percent Difference (%)	
	U_x	U_y	X Direction	Y Direction
3	2.1×10^{-3}	0.0113	3.65	0
56	2.06×10^{-3}	0.0115	1.68	1.78
112	2.1×10^{-3}	0.0116	3.65	2.65
448	2.05×10^{-3}	0.0116	1.18	2.65
1792	2.1×10^{-3}	0.0116	3.5	2.65
7168	2.1×10^{-3}	0.0116	3.5	2.65
Analytical Result	2.03×10^{-3}	0.0113		

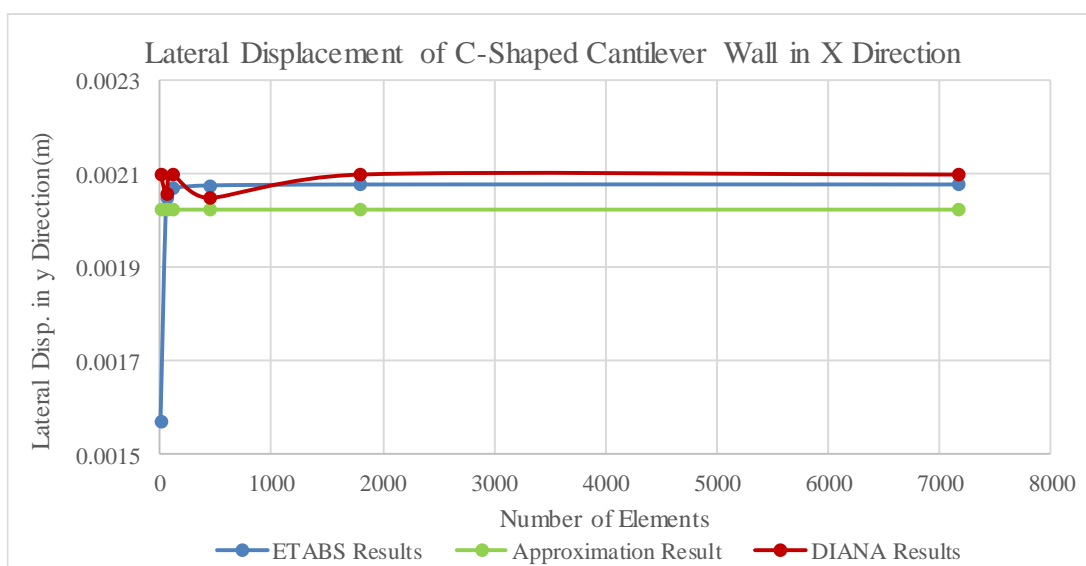


Figure 2-12 Lateral displacement values of C-shaped cantilever wall in x direction for different mesh size

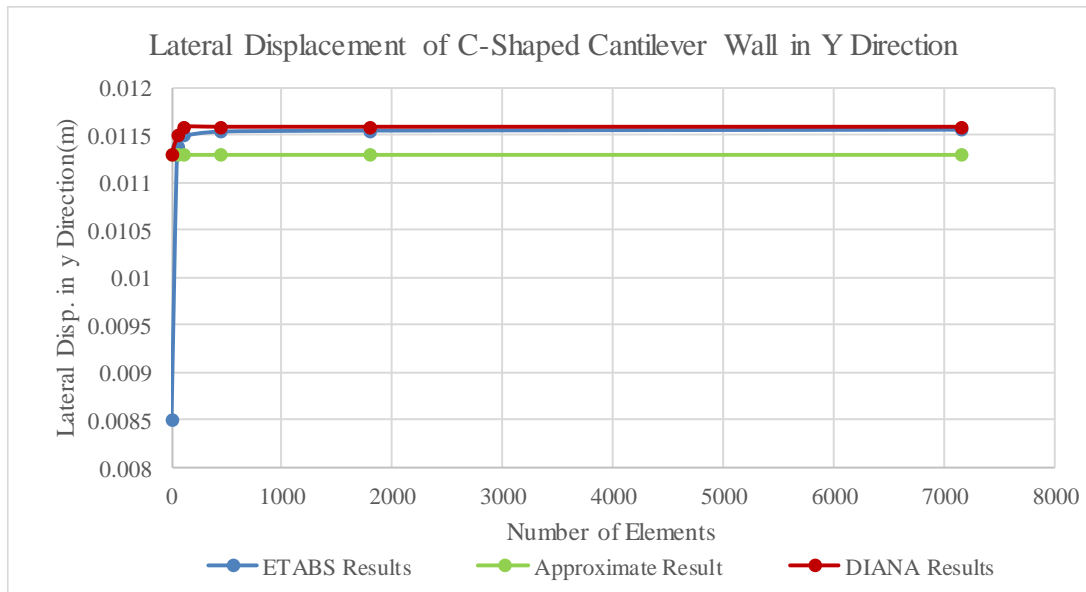


Figure 2-13 Lateral displacement values of C-shaped cantilever wall in y direction for different mesh size

When the analysis results that are presented in Table 2-13 and Table 2-14 are studied, it is seen that finite element method of computer programs can capture the elastic behavior of C-shaped walls under pure bending within acceptable accuracy.

2.2.3. Mid-Column Method for Bending

Up to this point both box and C-shaped sections were analyzed with finite element method utilizing ETABS and DIANA under bending. The same structures are now analyzed with mid-column method to check its accuracy for bending behavior.

2.2.3.1. Mid-Column Method for Box Section

Mid column method was used for the bending analysis of the same box section whose sectional properties are presented in Table 2-1. The obtained results were compared with both the results of finite element analysis with ETABS and the analytical solution.

Table 2-15 Analysis results of different methods for box shaped cantilever wall

	Lateral Displacement (m)	Percent Error (%)
Mid-Column Method	1.9×10^{-3}	87.59
Finite Element Method	1.04×10^{-3}	2.47
Approximation Result	1.013×10^{-3}	

When the results are studied, it is seen that mid-column method over-estimates the stiffness of the box. The difference in the displacement from the analytical results is unacceptable.

2.2.3.2. Mid-Column Method for C-Shaped Section

Same sectional properties and structural models that were used in torsion analysis of C-shaped wall were also used for bending analysis. Analysis results with mid-column method and finite element analysis results with ETABS are presented in Table 2-16. Similar to the box section case, mid-column method over-estimates the stiffness of the C-shaped wall.

Table 2-16 Analysis results of different methods for C-shaped cantilever wall

	Lateral Displacement (m)	Percent Error (%)
Mid-Column Method	1.9×10^{-3}	87.59
Finite Element Method	1.04×10^{-3}	2.47
Approximation Result	1.013×10^{-3}	

2.3. Discussion of Results

In this chapter linear elastic analysis was performed for structural walls having a box and C-shaped cross section under pure torsion and pure bending. Aim of this study is compare the modeling approximations. In this way, the accuracy of the following modeling approaches was questioned.

- Finite Element Method with ETABS and DIANA

- Mid-Column Method
- Modified Mid-Column Method

Mid-column method gives acceptable results for open sections under pure torsion by arranging the stiffness of the rigid links. This method ignores the warping effect and calculates the results with 60% error when warping is significant. Also, mid column method calculates the bending displacements with 90% error for box section. For this reason, modified mid column method can be suggested for box sections since it reduces the error for torsional displacement but not decrease to enough values. If we compare the results, finite element method with fine mesh is the best method to determine the torsional and bending deformations for both box and C-shaped sections.

CHAPTER 3

MODELING FOR NONLINEAR BEHAVIOR

In order to resist the earthquake, using reinforced concrete structural walls is common. Thus, estimation of the inelastic response of the structural walls and wall systems need effective modeling and analysis programs that can combine nonlinear material characteristics and behavioral response of the structure such as confinement, gap opening and closure and so on. Nonlinear analysis is considered as one of the best ways to estimate these main characteristics of structural walls (PEER and ATC72-1, 2010). As the main aim of this chapter, detailed comparisons between different nonlinear modelling approaches are investigated and nonlinear modeling approaches are tested using experimental results for further detailed studies.

Nonlinear response of planar and flanged reinforced concrete structural walls can be defined by using fiber beam-column (distributed inelasticity) models and detailed finite element (continuum) model (PEER and ATC72-1, 2010). All of these models have some advantages and disadvantages. For example, lumped plasticity model cannot account the neutral axis migration along the wall cross section under cyclic loading. Moreover, interaction with connecting members such as slab and girders cannot be captured. In addition, stiffness and strength of the walls are calculated independent from the axial load. Advantages of this model is ease of use and efficiency in computation. Limits of hinge rotations and stiffness parameters are easily defined (PEER and ATC72-1, 2010). Distributed inelasticity model can solve the many disadvantages of lumped plasticity method. Contrary to the lumped plasticity model, stiffness of the wall section is calculated from the defined material properties and depend to axial load in distributed inelasticity model (PEER and ATC72-1, 2010). The most complicated modeling type is continuum model. In this model, yielding of

horizontal and vertical direction can be calculated. Modeling of concrete element and reinforcement is possible with this method (PEER and ATC72-1, 2010).

In this part of the study, planar and flanged structural walls were modelled with distributed inelasticity model with ETABS and Perform3D and continuum model with DIANA. Firstly, rectangular cross section (RW2) and T-shaped cross section (TW2) that were tested experimentally by Thomsen et al., 1995 were modelled with fiber model and continuum model.

3.1. Modeling of RW2 Specimen

The rectangular structural wall (RW2) that was tested by Thomsen et al., 1995 was modelled with continuum model of DIANA and fiber model of ETABS and Perform3D. Figure 3-1 shows the geometry of the tested rectangular wall, named as RW2. The wall has a cross section of 1.22 m x 0.102 m and height of 3.66 m. Aspect ratio of the wall equals to 3.

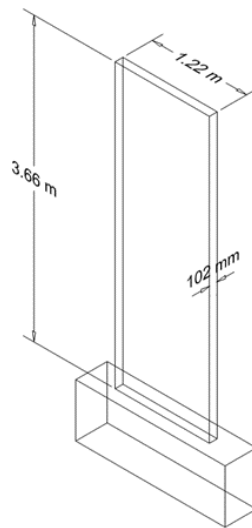


Figure 3-1 Geometry of RW2 (Thomsen, 1995)

Figure 3-2 and Figure 3-3 show the reinforcement of RW2. Using the displacement based approach proposed by Wallace (1994), boundary elements were placed at the end of walls to provide confinement at the wall edges. For longitudinal reinforcement

of the confinement zones 8 - #3 bars were used. On the hand, 2- #2 bars were used for lateral and longitudinal web reinforcement.

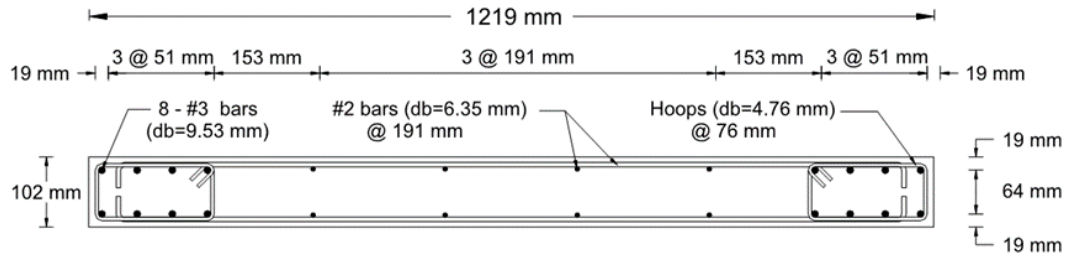


Figure 3-2 Cross section of RW2 (Thomsen, 1995)

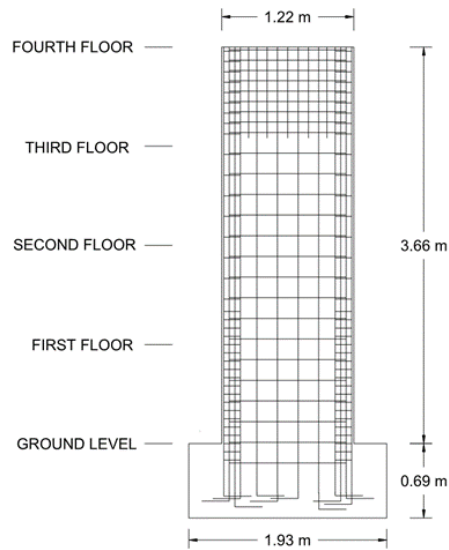
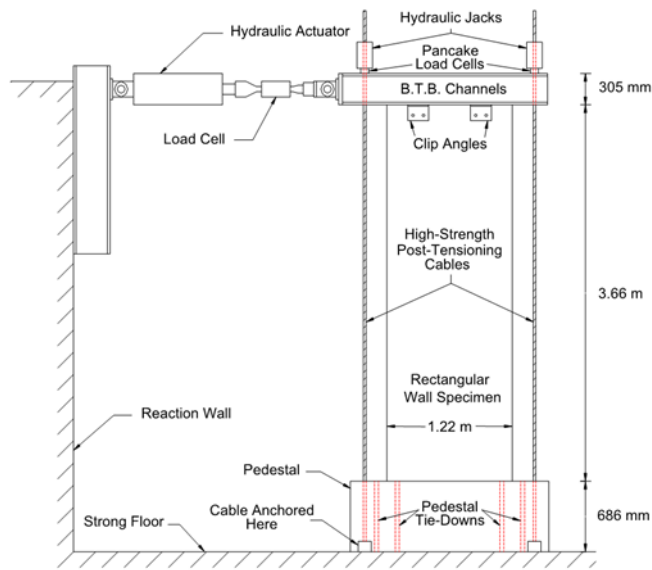


Figure 3-3 Reinforcement placement of RW2 (Thomsen, 1995)

Figure 3-4 shows the test set-up for RW2. Displacements were applied by hydraulic jacks at the top of the wall. Cyclic load was applied to the top of the wall.



calibrated according to the empirical relations that introduced by Mander (1988). Tables 3-1 to 3-7 present the calibrated material properties.

Table 3-1 Calibrated material properties for concrete in tension

f_t (MPa)	ϵ_t	E_c (GPa)	ϵ_{cr}	r
2.03	0.00008	31.03	∞	1.2

Table 3-2 Calibrated material properties for concrete in confined zone

f_c (MPa)	ϵ_c	E_c (GPa)	ϵ_{cr}	r
47.6	0.0033	31.03	0.0037	1.9

Table 3-3 Calibrated compression properties for concrete unconfined zone

f_c (MPa)	ϵ_c	E_c (GPa)	ϵ_{cr}	r
42.8	0.0021	31.03	0.0022	7

Table 3-4 Calibrated material properties for #3 rebar in compression

σ_y (MPa)	E_0 (GPa)	b
434	200	0.02

Table 3-5 Calibrated material properties for #2 rebar in compression

σ_y (MPa)	E_0 (GPa)	b
448	200	0.02

Table 3-6 Calibrated material properties for #3 rebar in tension

σ_y (MPa)	E_0 (GPa)	b
395	200	0.02

Table 3-7 Calibrated material properties for #2 rebar in tension

σ_y (MPa)	E_0 (GPa)	b
336	200	0.035

3.1.1. Modeling of RW2 Specimen with the Fiber Model

At this part, RW2 specimen was modelled with the fiber model element of ETABS. In this method, the cross section is described with steel and concrete fibers individually. Along the cross section sufficient number of fibers should be used to capture the strain gradient.

Nonlinear time history analysis of the 2D model of RW2 was first performed. The ETABS model is presented in Figure 3-5. The model was divided into four stories with 0.915 m storey height where fiber plastic hinge was defined at the first storey. Elastic material properties were defined for the upper three stories.

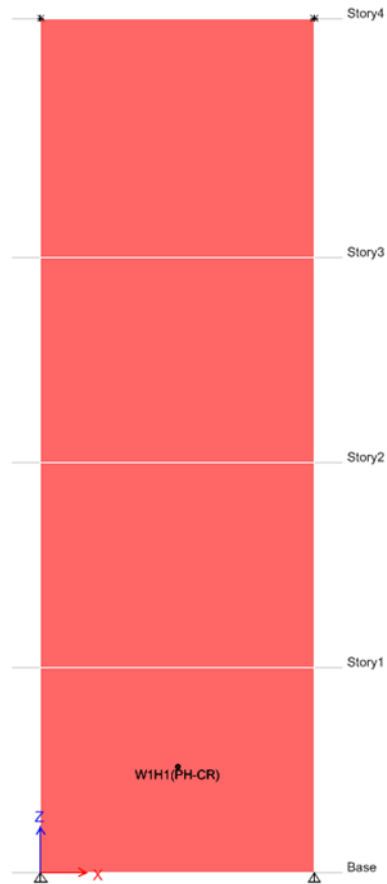


Figure 3-5 Elevation view of RW2

Loading history was defined as displacement time history function. In the analysis part first, compressive gravity forces were applied to the wall as point loads and then nonlinear displacement time history analysis was performed. Figure 3-6 shows the displacement time history and Figure 3-7 shows the applied loads to the system.

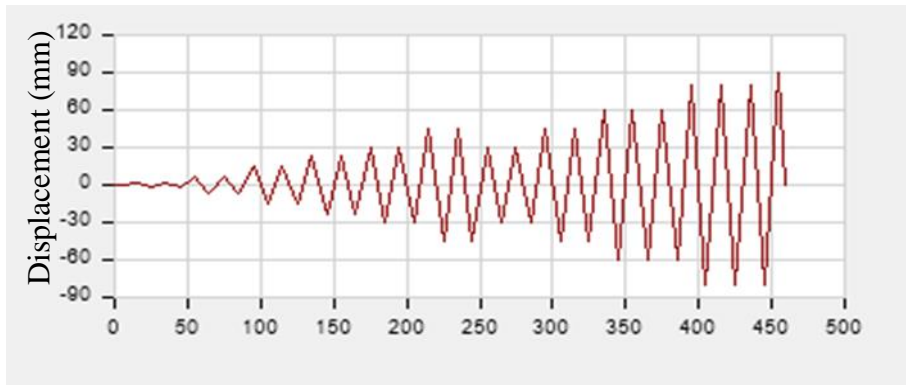


Figure 3-6 Applied displacement time history function to RW2

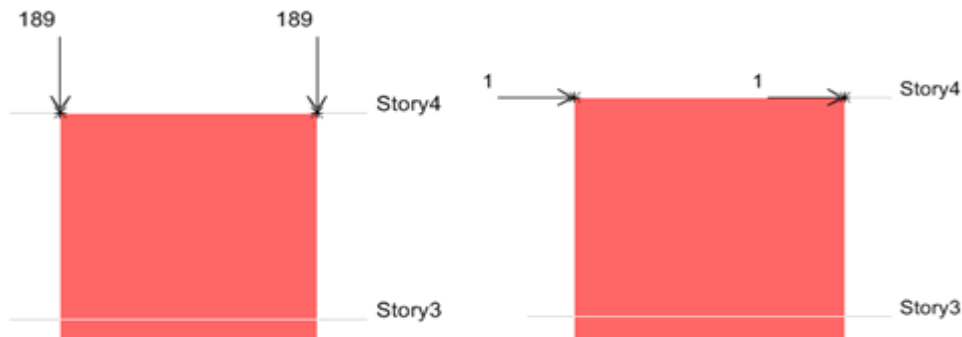


Figure 3-7 Applied vertical load (KN) and horizontal displacement (mm)

Simplified material relations were used in this analysis. For reinforcement bilinear material model with strain hardening was used and for concrete, trilinear material model with linear loading, plateau region and linear degradation was used as shown in Figure 3-8.

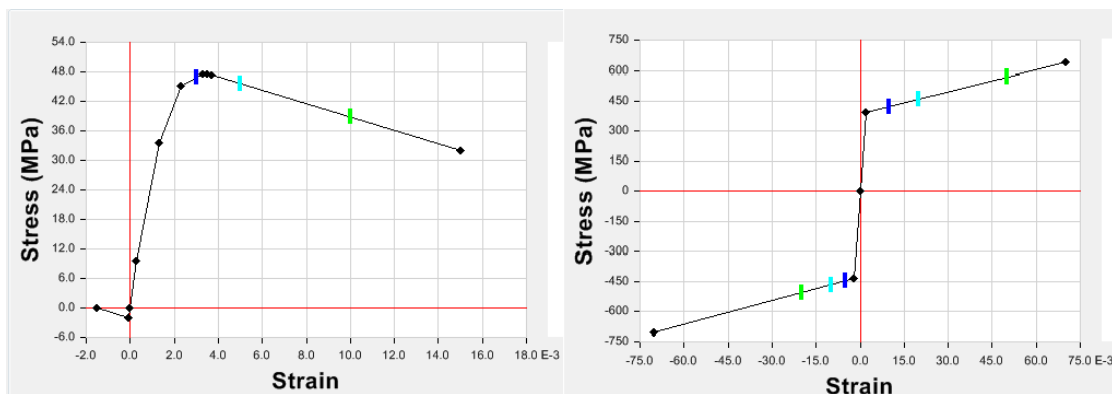


Figure 3-8 Example of definition of material properties for concrete and steel

As it was mentioned, in this approach cross section is defined with steel and concrete fibers. Figure 3-9 shows the idealization of the cross section and Figure 3-10 shows the material properties of fibers. Calibrated material properties that are given in Tables 3-1 to 3-7 were used for the analysis.

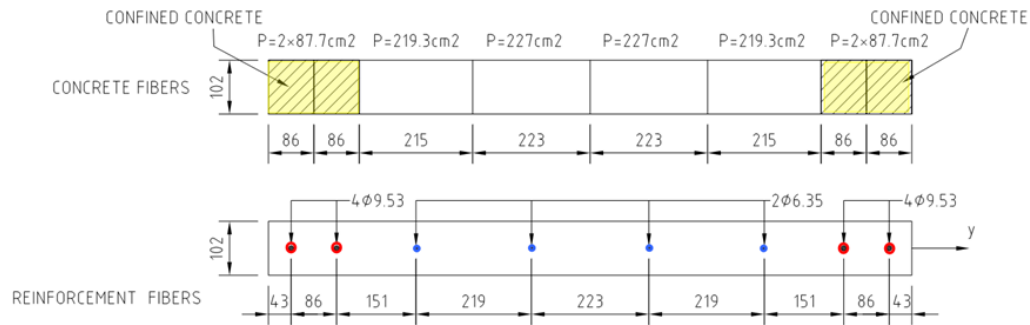


Figure 3-9 Definition of wall cross section in terms of nonlinear hinges (Alendar & Milicevic, 2015)

Fiber Definition Data			
Fiber	Area cm²	Coord2 mm	Material
1	2.9	-566.5	R400 #3
2	87.7	-566.5	ConcConf fc'=47.6
3	87.7	-480.5	ConcConf fc'=47.6
4	2.9	-480.5	R400 #3
5	219.3	-330	ConcNormal fc'=42.8MPa
6	0.6	-330	R400 #2
7	0.6	-111.3	R400 #2
8	227	-111.3	ConcNormal fc'=42.8MPa
9	227	111.3	ConcNormal fc'=42.8MPa
10	0.6	111.3	R400 #2

Figure 3-10 Fibers used in model

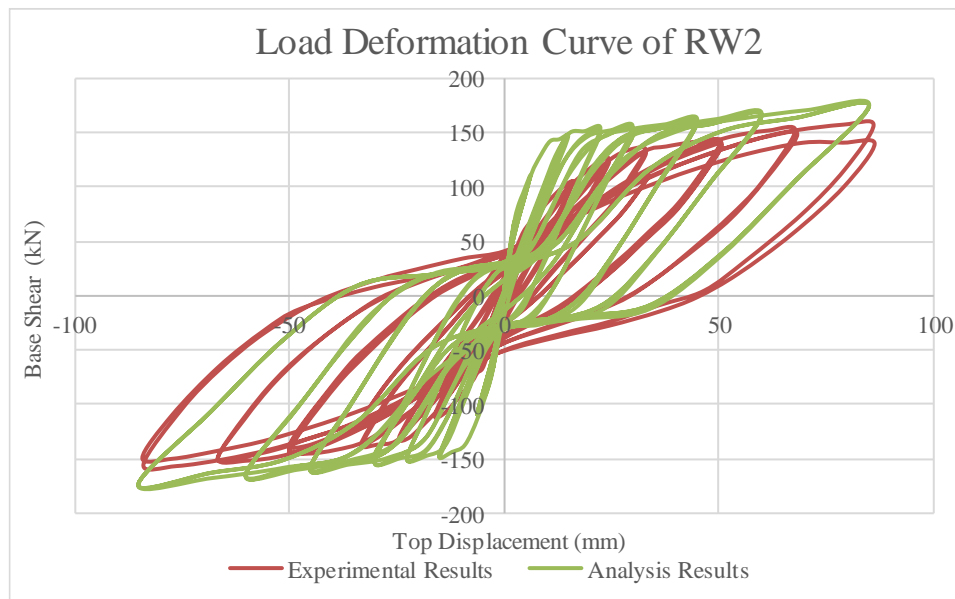


Figure 3-11 Analysis results of RW2 with fiber modeling approach

Figure 3-11 presents the analysis and experimental results for RW2. In this analysis material properties both for reinforcement and concrete were defined according to calibrated material properties that are provided in Tables 3-1 to 3-7. When the analysis results are studied, it is seen that fiber model cannot capture the initial stiffness of the wall. In the fiber model, wall reaches the shear capacity nearly at the beginning of the analysis. Moreover, fiber model over-estimates the capacity of the wall with 10% difference at the end of the analysis. Same analysis was then performed with design material properties: Grade 60 steel and concrete that have 27.6 MPa compressive strength. For concrete, in order to determine the nonlinear compression stress strain parameters, Hognestad model was used. Figure 3-12 and Figure 3-13 summarize the modeling properties of concrete and steel.

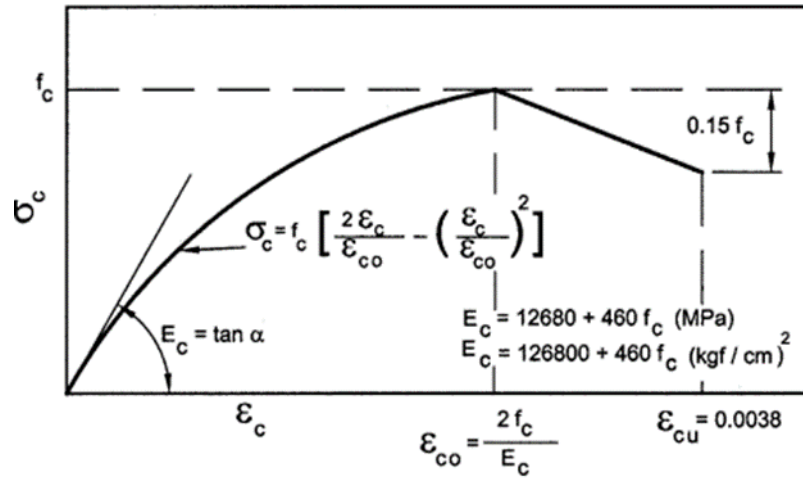


Figure 3-12 Hognestad material model for concrete

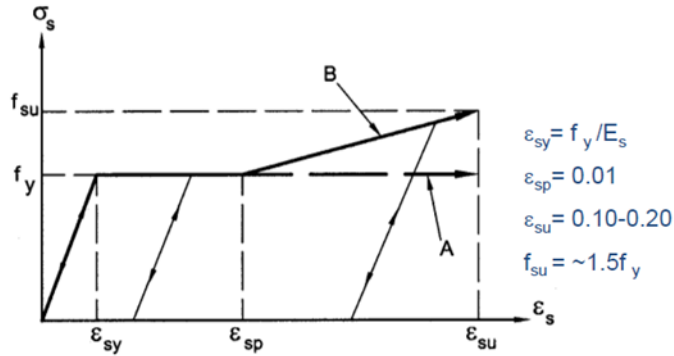


Figure 3-13 Modeling parameters for steel

Analysis results with design material parameters is provided in Figure 3-14. When the results that are presented in Figure 3-11 and Figure 3-14 are compared, it is seen that there is not an important difference. The convenience between the results can be explained with strength of the reinforcement. Reinforcement strength of calibrated material properties and design material properties are nearly same. Therefore, results of the analyses are similar. But, analysis results of design material parameters provide better match with experimental results when compared to the calibrated material parameters.

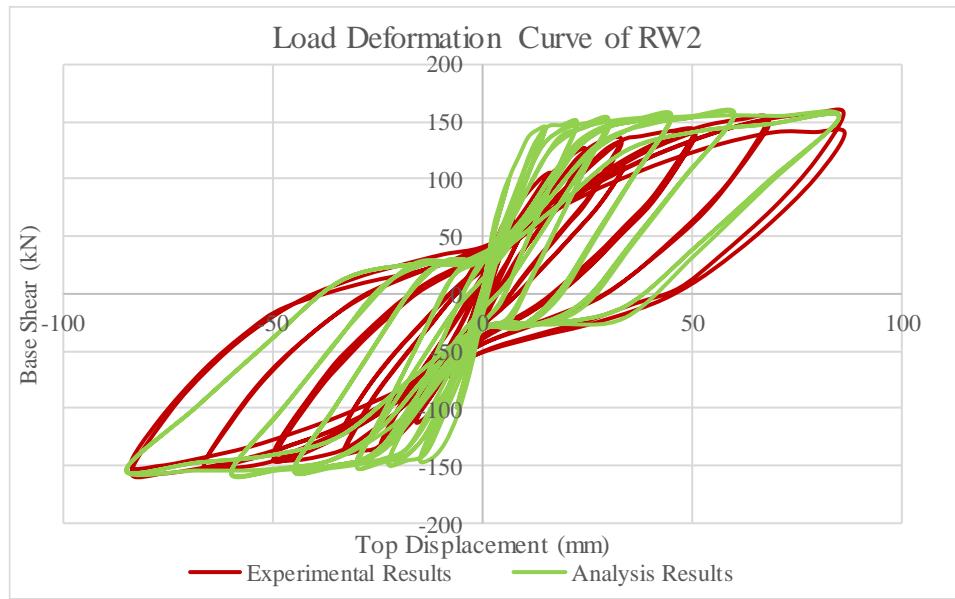


Figure 3-14 Analysis results of RW2 according to design material parameters

3.1.2. Modeling of RW2 Specimen with the Continuum Model

After modeling RW2 specimen with the fiber method, the specimen was modelled with the continuum model with DIANA. In DIANA, 2D nonlinear time history analysis was performed with CQ16M element. This element is an 8 node quadrilateral isoparametric plane stress element and it is based on Gauss integration and quadratic interpolation. Detailed information about this element type is presented in APPENDIX A. In DIANA, cracking model of concrete was modelled as total strain rotating crack models that introduced by Rashid (1968) and developed further by Vecchio (1986).

In DIANA reinforcements were modelled as embedded reinforcements that do not have degrees of freedom of their own but add its stiffness to the system. For standard reinforcements strains of the reinforcement are calculated from the displacement field of the structural elements that reinforcements are embedded in. This assumes perfect bond between concrete and reinforcement. Nonlinear compression behavior of concrete was defined as a parabolic function of stress and strain that is based on a multilinear approach and tensile behavior of concrete was defined by elastic brittle

stress-strain function that based on the tensile strength as shown in Figure 3-15. Unloading and reloading behavior was modelled by using the secant approach.

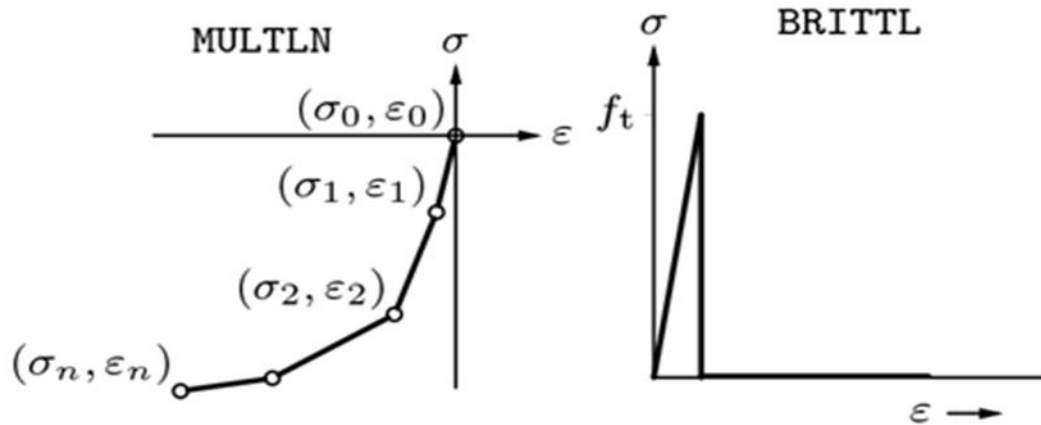


Figure 3-15 Compressive and Tensile Behavior of Concrete (DIANA FEA User's Manual - Release 9.5, n.d.)

For reinforcement, compressive and tensile stress strain behavior were described by using von Mises yield criterion (isotropic plasticity). In order to determine the behavior of reinforcement after yielding, strain hardening was employed by using the ultimate and yield strength values that are obtained from material tests.

After the geometry of the wall is defined, meshing process was performed and as a result of the meshing of the geometry, the model has 839 nodes and 252 plane-stress elements. Geometry and the alignment of the reinforcement are shown in Figure 3-16.

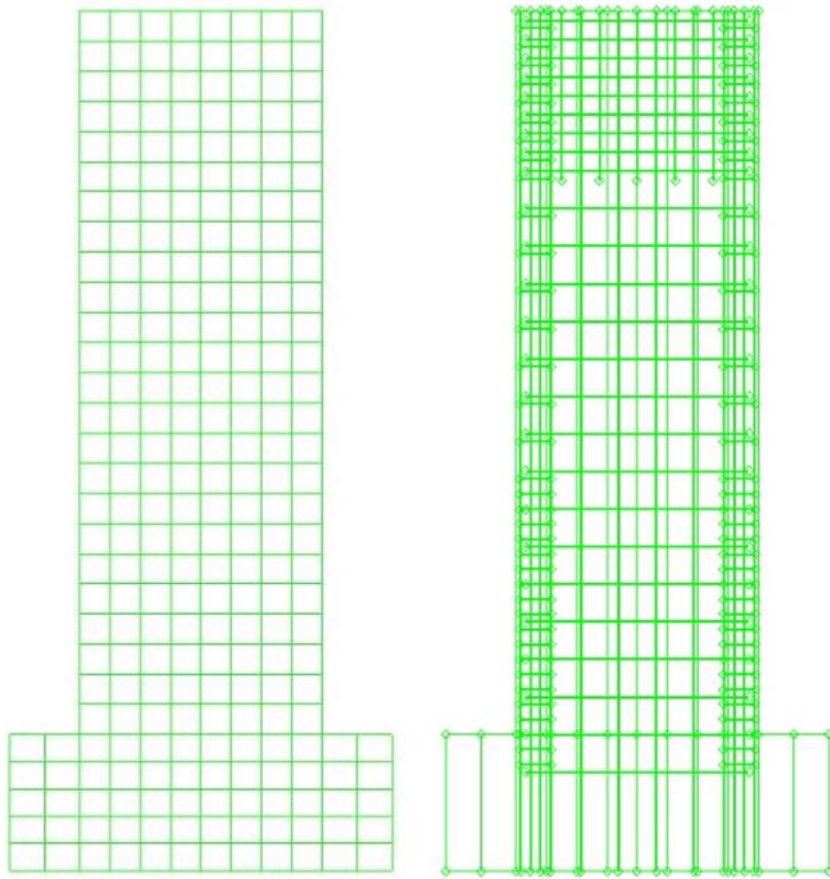


Figure 3-16 Finite element model of RW2 with embedded reinforcements

Figure 3-17 shows the comparison of experimental results and computational results for RW2 specimen and Figure 3-18 shows the comparison of continuum model and fiber model with experimental results. As these figures are studied, it can be said that continuum model better estimates the initial stiffness of the wall section. Although continuum model correctly calculates the capacity of the wall at the end of the analysis, back bone curve obtained from continuum model show a more hysteretic damping compared to the experimental results.

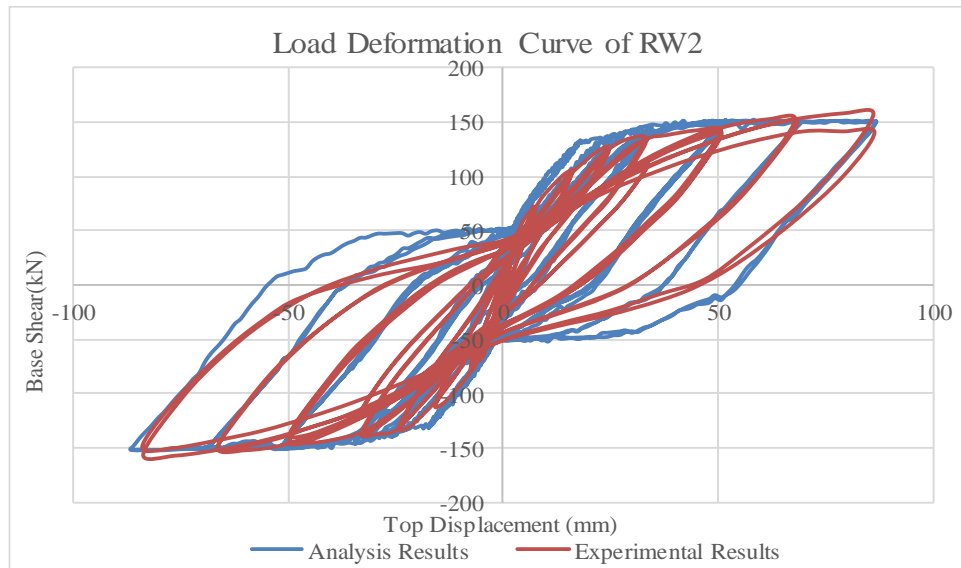


Figure 3-17 Analysis results of RW2 with continuum model

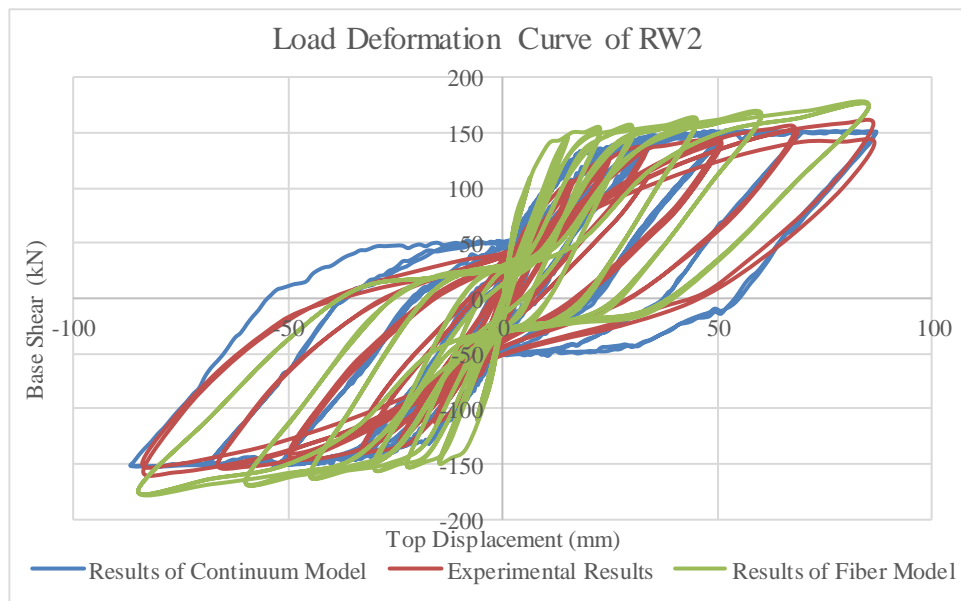


Figure 3-18 Comparison of different modeling techniques for RW2

Same analysis was repeated with the design material. Figure 3-19 shows the comparison of experimental results and analytical results of continuum model for RW2 specimen and Figure 3-20 shows the comparison of continuum model and fiber model with experimental results. As these figures are studied, it can be said that results of continuum model are in well agreement with the experimental results. Moreover,

continuum model gives a better match when compared with the results of the fiber model.

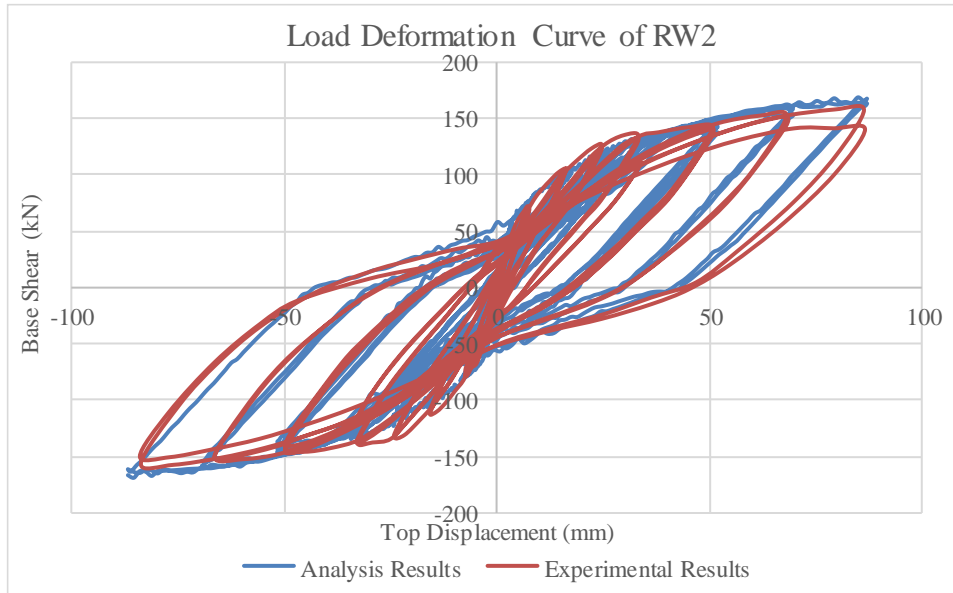


Figure 3-19 Analysis results of RW2 according to design material parameters

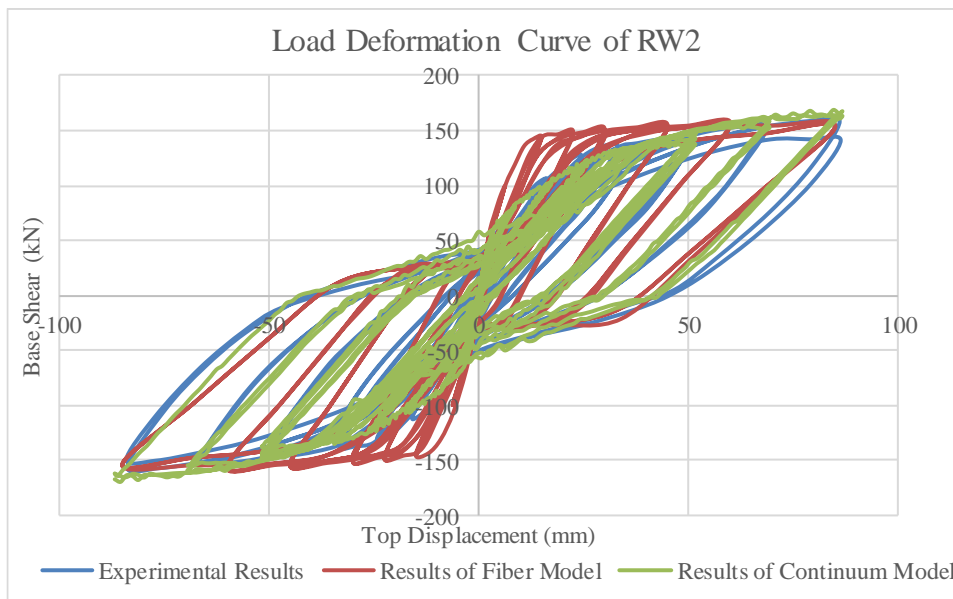


Figure 3-20 Comparison of different modeling techniques for RW2 according to design material parameters

3.2. Modeling of TW2 Specimen

In this part of the study, T-shaped structural wall that has a cross section of 1.12 m x 0.102 m with 1.22 m x 0.102 m flange section and height of 3.66 m was analyzed by using the fiber method (ETABS and Perform3D) and the continuum method (DIANA). Figure 3-21 shows the geometric properties of TW2. Thickness of the wall is equal to 102 mm and length of the wall is equal to 3.66 m. Figure 3-22 shows the cross section and reinforcement placement of TW2. Confinement zones were used at the end of the wall and intersection between web and flange. Material properties were again calibrated in same ways with RW2 and these material properties are presented in Tables 3-8 to 3-19.

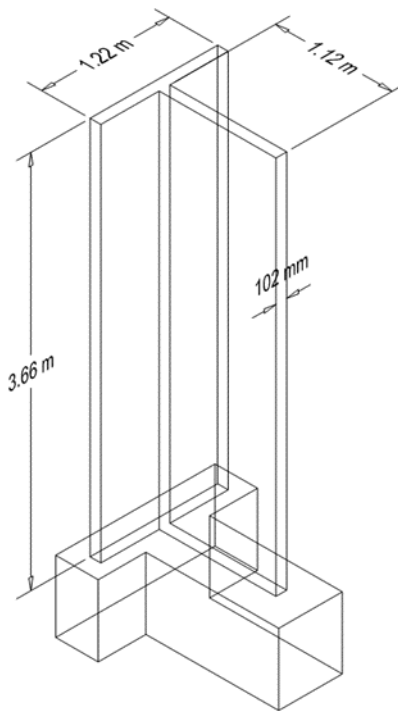


Figure 3-21 Geometry of TW2 (Thomsen, 1995)

Table 3-11 Calibrated compression properties for concrete in confined zone of flange-web intersection

f_c (MPa)	ϵ_c	E_c (GPa)	ϵ_{cr}	r
43.9	0.0024	31.03	0.0025	3.8

Table 3-12 Calibrated compression properties for concrete in confined zone of web section

f_c (MPa)	ϵ_c	E_c (GPa)	ϵ_{cr}	r
43.9	0.0024	31.03	0.0025	3.8

Table 3-13 Calibrated material properties for #3 rebar in compression

σ_y (MPa)	E_0 (GPa)	b
434	200	0.02

Table 3-14 Calibrated material properties for #2 rebar in compression

σ_y (MPa)	E_0 (GPa)	b
448	200	0.02

Table 3-15 Calibrated tension properties for #3 rebar in confined zone of flange section

σ_y (MPa)	E_0 (GPa)	b
395	200	0.0185

Table 3-16 Calibrated tension properties for #3 rebar in confined zone of flange-web intersection

σ_y (MPa)	E_0 (GPa)	b
395	200	0.0185

Table 3-17 Calibrated tension properties for #3 rebar in confined zone of web section

σ_y (MPa)	E_0 (GPa)	b
387	200	0.02

Table 3-18 Calibrated tension properties for #2 rebar in unconfined zone of flange section

σ_y (MPa)	E_0 (GPa)	b
336	200	0.035

Table 3-19 Calibrated tension properties for #2 rebar in unconfined zone of web section

σ_y (MPa)	E_0 (GPa)	b
356	200	0.0295

3.2.1. Modeling of TW2 Specimen with the Fiber Model

The fiber method was also used for the analysis of TW2 specimen. In ETABS four storey structural wall was modeled. Plastic hinges were just assigned at the first storey by considering the run time and the rest of the structure was defined as an elastic section as shown in Figure 3-23. Loading history was defined as displacement time history function as shown in Figure 3-24. In the analysis part first, compressive force applied by the hydraulic jacks was applied to the wall as point loads and then nonlinear displacement time history analysis was performed. Load application is presented in Figure 3-25.

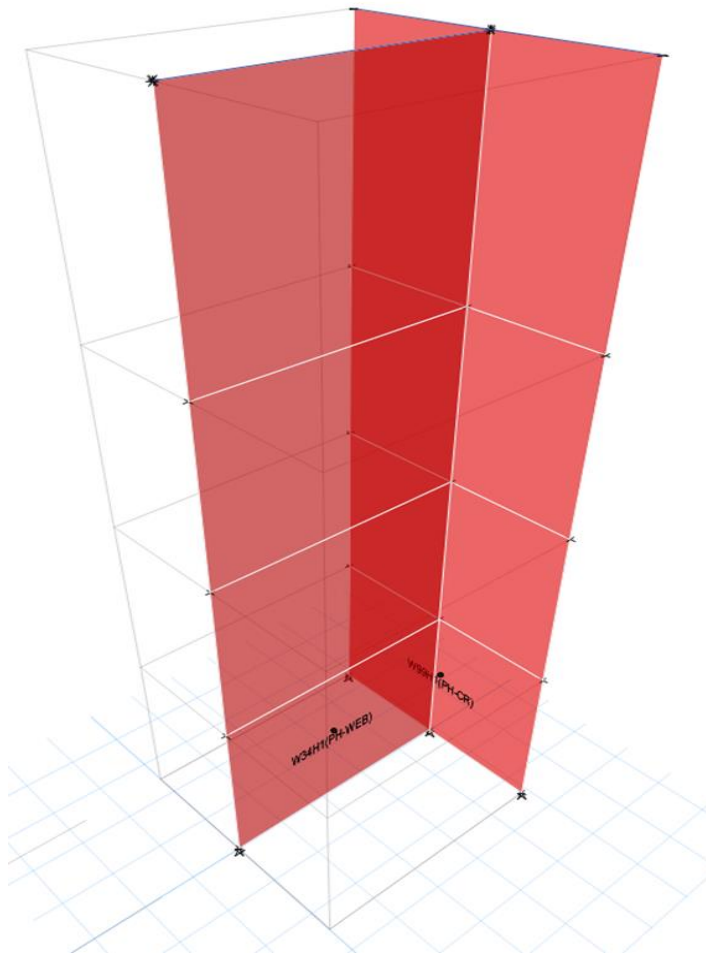


Figure 3-23 Elevation view of TW2

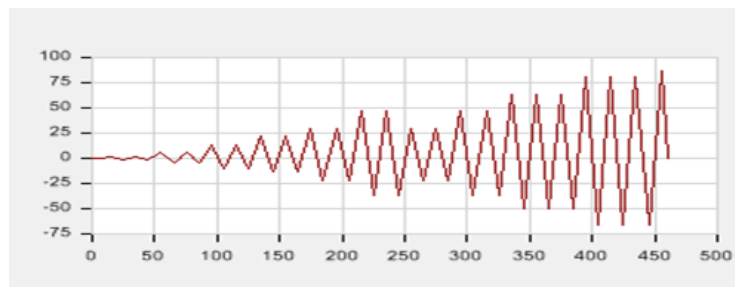
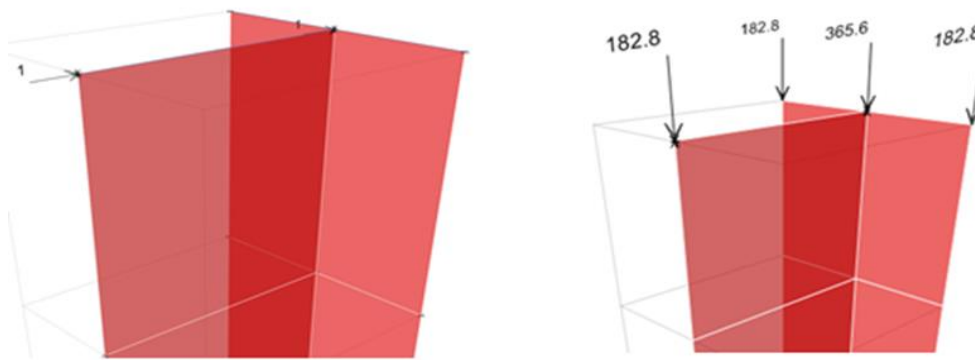


Figure 3-24 Applied displacement according to time (in mm)



Fiber	Area cm ²	Coord2 mm	Material
1	2.9	-566.5	RFT #3 - Flange
2	87.7	-566.5	Conc fc'=43.9 MPa Confined Flange
3	87.7	-480.5	Conc fc'=43.9 MPa Confined Flange
4	2.9	-480.5	RFT #3 - Flange
5	219.3	-330	Conc Fc'=42.8MPa Unconfined
6	0.6	-330	RFT #2 - Flange
7	0.6	-111.3	RFT #2 - Flange
8	227	-111.3	Conc Fc'=42.8MPa Unconfined
9	227	111.3	Conc Fc'=42.8MPa Unconfined
10	0.6	111.3	RFT #2 - Flange

Figure 3-27 Properties of fibers for flange section of TW2

Fiber	Area cm ²	Coord2 mm	Material
1	2.9	568.5	RFT #3- Web
2	2.9	482.5	RFT #3- Web
3	0.6	353.5	RFT #2 - Web
4	0.6	197.5	RFT #2 - Web
5	0.6	57.5	RFT #2 - Web
6	0.6	-73	RFT #2 - Web
7	0.6	-184.5	RFT #2 - Web
8	2.9	-337.5	RFT #3- Web
9	2.9	-525.5	RFT #3- Web
10	87.7	568.5	Conc fc'=57.1MPa Confined Web

Figure 3-28 Properties of fiber for web section of TW2

Figure 3-29 shows the comparison of analysis and experimental results. In this analysis, calibrated material properties were used. According to the results at Figure 3-29, significant differences between analysis results and experimental results are observed. First of all, the analysis results over-estimate the initial stiffness and the capacity of the wall. The capacity of the wall when the flange is in tension is overestimated by nearly 30%. In the previous section, it is shown that the fiber model can accurately present the behavior of a rectangular wall. When the wall has a flange, the fiber model cannot accurately present the flange behavior under tensile forces and this deficiency causes an artificial increase in the wall capacity.

The same analysis was repeated with design material properties and the results are presented in Figure 3-30. When the results that are presented in Figure 3-29 and Figure 3-30 are examined, it is seen that there is not an important difference. This shows that the wall behavior is mainly influenced by the tensile reinforcement behavior for wall under flexural deformation.

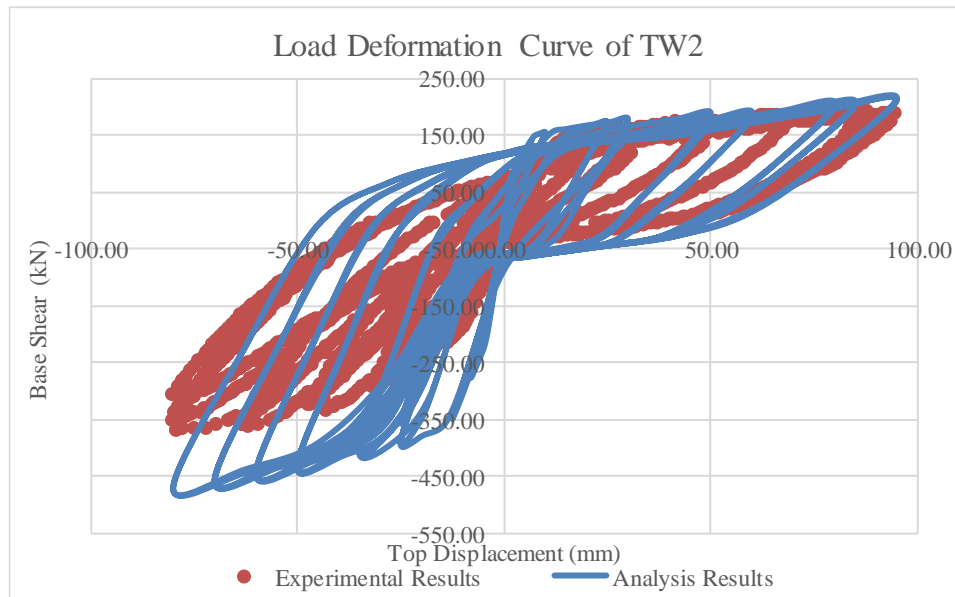


Figure 3-29 Analysis results of TW2 with fiber model

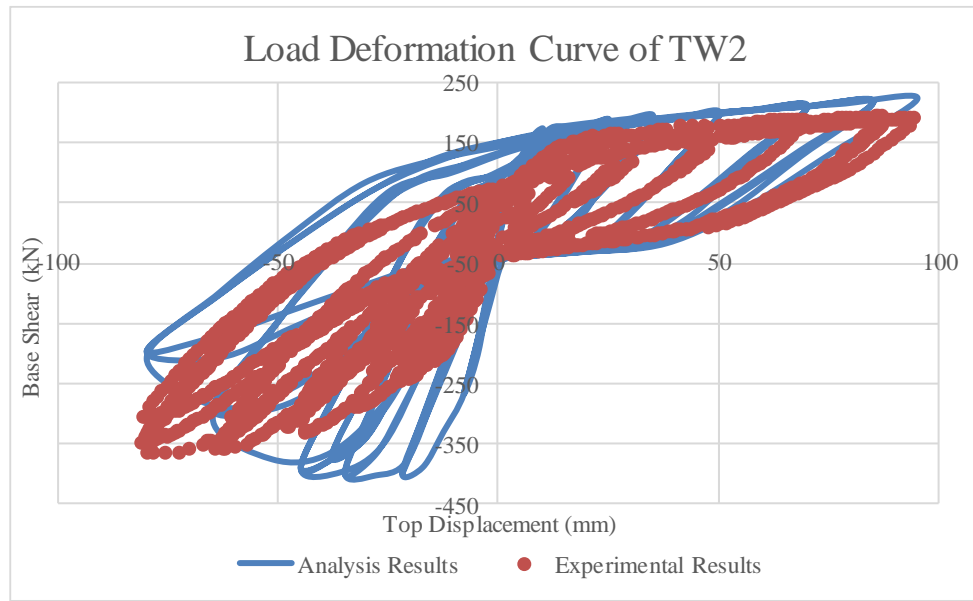


Figure 3-30 Analysis results of TW2 according to design material parameters

3.2.2. Modeling of TW2 Specimen with the Continuum Model

TW2 specimen was also modeled with the continuum model by using DIANA. 3D nonlinear time history analysis was performed. In DIANA 3D structural analysis, the CQ16M element type cannot be used thus, CQ40S element type was utilized instead which is a quadrilateral isoperimetric curved shell element with 8 nodes and based on Gauss integration and quadratic interpolation was used. Detailed information about this element type is presented in APPENDIX A.

In DIANA, cracking model of concrete for TW2 was modelled as Total Strain Rotating Crack Models. Reinforcements were modelled as embedded reinforcements and for reinforcements, compressive and tensile stress strain behavior were described by using von Mises yield criterion (isotropic plasticity). In order to determine the behavior of reinforcement after yielding, strain hardening was employed by using the ultimate and yield strength values that were obtained from material tests.

The final model has 1585 nodes and 494 shell elements. Geometry and the alignment of the reinforcement are presented in Figure 3-31.

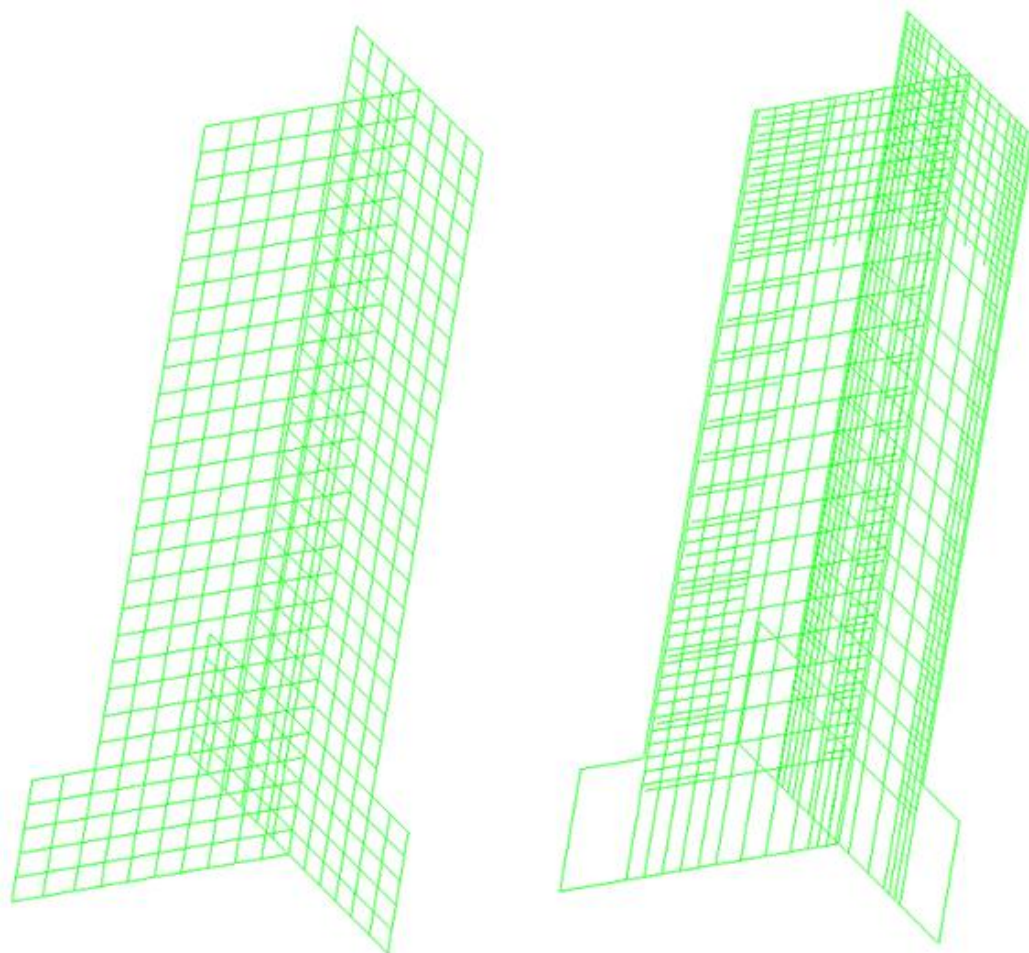


Figure 3-31 Finite element model of TW2 with embedded reinforcements

Figure 3-32 presents the analysis results of TW2 specimen with the continuum model. When the results are studied, it can be said that capacity of the wall correctly calculated when the flange section is under compression. Moreover, in the continuum model, yielding point of the wall can be predicted but this point cannot be predicted by the fiber model.

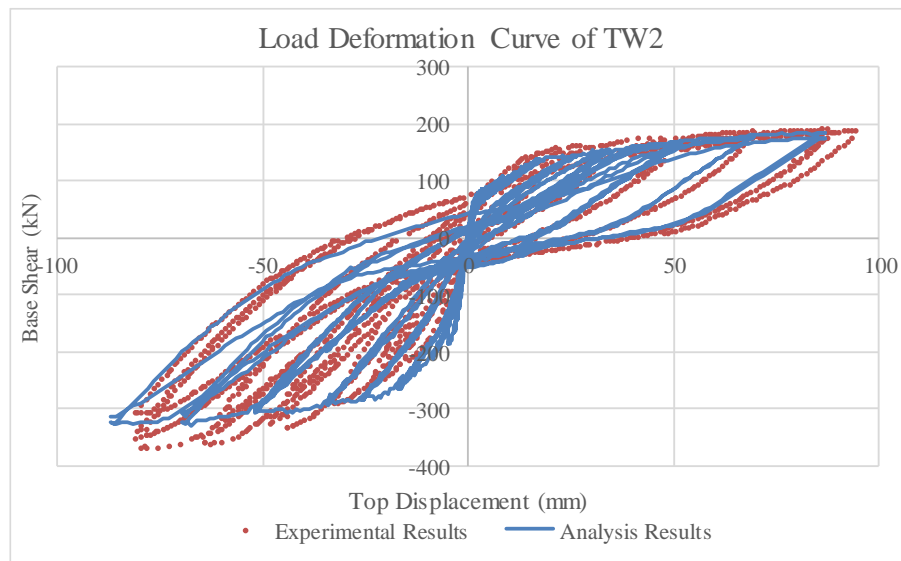


Figure 3-32 Analysis results of TW2 with continuum model

Figure 3-33 shows the comparison of analysis results and experimental results of TW2 specimen according to design material parameters. When the results are studied, initial stiffness and yielding point of the wall can be correctly captured. In addition, when the flange section is under compression capacity of the wall can be calculated correctly. But, when the flange section is under tension, capacity is over-estimated by approximately 14%.

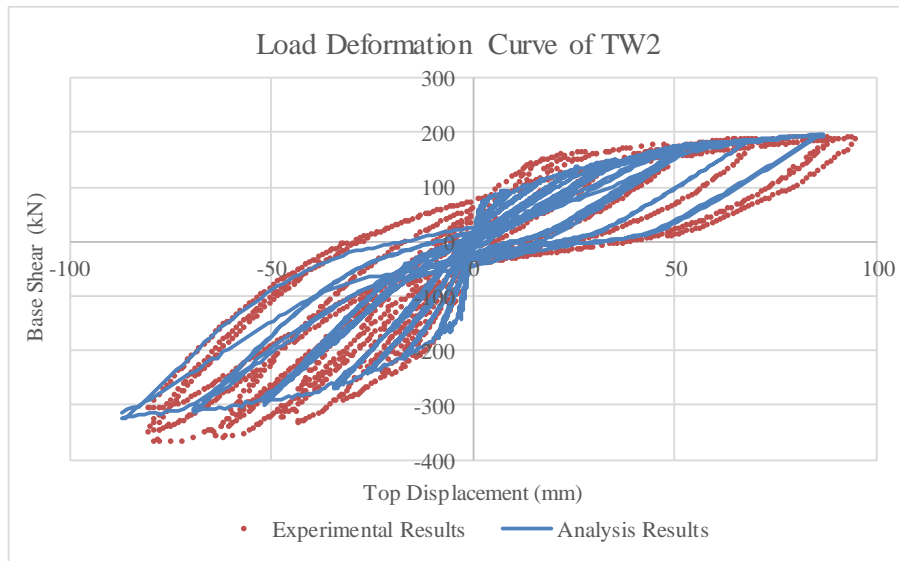


Figure 3-33 Analysis results of TW2 according to design material parameters

As a final step, both RW2 and TW2 specimens were modeled with Perform3D that has a special wall element based on fiber modeling approach. The material properties were defined in a similar way as ETABS. Figure 3-34 and Figure 3-35 shows the comparison of analysis results with Perform3D, DIANA and experimental results for RW2 and TW2 specimens, respectively. When these results are studied, although, Perform3D overestimates initial stiffness, it can capture the nonlinear behavior of planar reinforced concrete structures. On the other hand, when the flange section is under tension, the fiber modeling approach of Perform3D calculate it as all flange section resists the tension and thus, capacity of the wall is overestimated by nearly 30%.

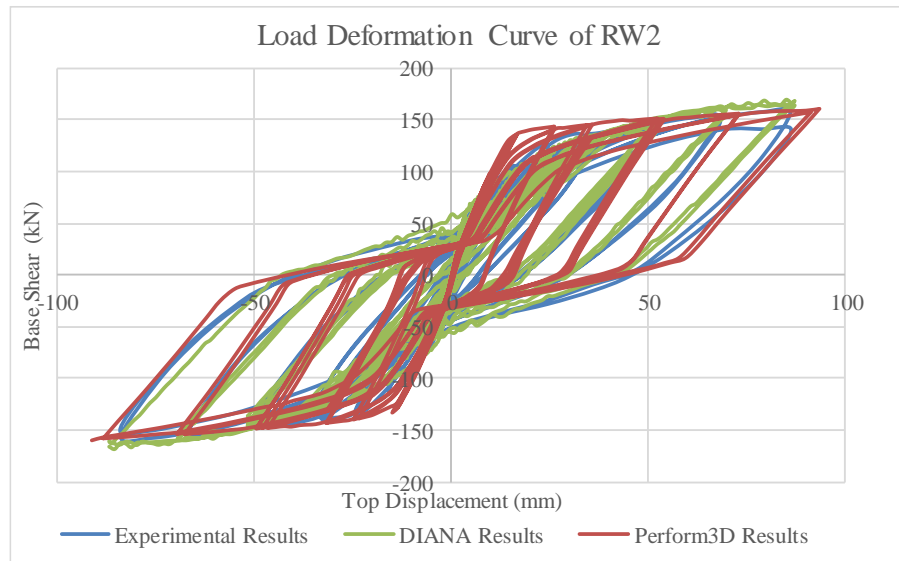


Figure 3-34 Analysis results of computer programs for RW2

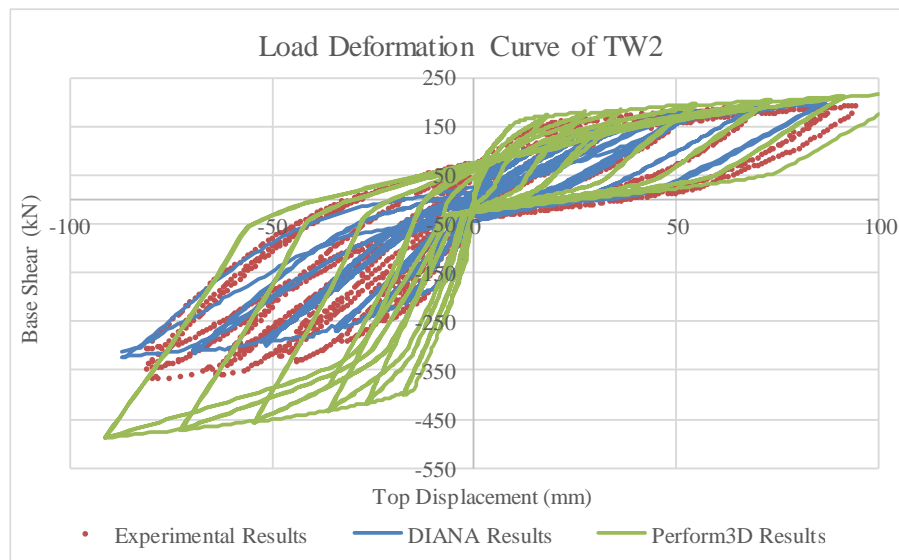


Figure 3-35 Analysis results of computer programs for TW2

3.3. Discussion of Results

When the results of RW2 and TW2 specimens that are presented in Figure 3-11, Figure 3-14, Figure 3-17, Figure 3-19, Figure 3-29, Figure 3-30, Figure 3-32, Figure 3-33 are considered it can be concluded that all of the methods have some advantages and disadvantages to capture the behavior of structural walls. When the fiber model results

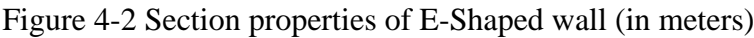
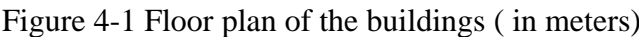
for RW2 are studied, it is seen that the fiber model overestimate the initial stiffness of the wall. Also, at the end of the experiment it was measured degradation in the capacity and stiffness of the wall in the positive direction because of the buckling of longitudinal reinforcement and this behavior cannot be captured by this model since this method does not take into account bar buckling. Generally, by looking at the results, it can be said that the fiber model can capture the nonlinear behavior of rectangular structural walls reasonably well. When we look at the results of TW2 with the fiber model, it can be said that, this method over-estimates the initial stiffness of the structure in both directions. When flange of the specimen is under compression, fiber model can reasonably capture the capacity of the flanged structural walls. On the other hand, when the flange is under completely tension, the fiber model overestimates the capacity of the wall. The reason of the difference between the experimental results and analysis results can be explained with the nonlinear tensile strain distribution of the flange. When the experiment results are studied, tensile strain along the width of the flange follow a nonlinear distribution that cannot be captured by the analytical model.

As it is mentioned above, the continuum model is a complete model that include all the properties of the structural component. When the results of the continuum model are studied for RW2 and TW2 specimens, it can be said that continuum model capture the nonlinear behavior of structural walls reasonably well except stiffness degradation because the current model did not consider the bar buckling.

CHAPTER 4

CASE STUDIES

Linear elastic and nonlinear analyses were performed up to this point to compare the modeling approaches. According to these analyses, it is observed that flexural behavior of structural walls can be predicted by both modeling approaches. During these analyses, shear behavior was not considered. As a final step of this study, modeling approaches were compared according to their capability to capture the shear behavior. Therefore, squat and slender structural walls were modeled with these modeling approaches. In order to present the squat walls, a 4-storey building (short building) with 3 meter storey height was selected and for slender wall 15-storey building (tall building) with a height of 45 m was selected. Floor plan of the buildings are presented in Figure 4-1. Dimensions of the floor sections were selected as 24 m x 18 m and 18 columns with 60 cm x 60 cm were used for the structures. Thickness of the slab was taken as 25 cm. E shaped structural walls with 45 cm wall thickness was selected. Dimensions of structural walls are provided in Figure 4-2. It was assumed that structures are located in the first seismic zone and response spectrum was selected according to ASCE 7-10. Information about the design of the structures is presented in APPENDIX B.



Linear elastic analyses were performed with ETABS to design the walls. In order to determine the reinforcement of structural walls ASCE 7-10 (ASCE 7-10, 2010) and ACI 318 (ACI, 2008) were used. Analyses were performed by just taking in to account four load cases; dead load, superimposed dead load, live load and earthquake loads. Superimposed dead load and live load were taken as 2 kN/m² and 4.79 kN/m², respectively. In elastic analysis, effective inertia of structural members is utilized according to ACI-318 section 10.10.4.1 (ACI, 2008). Table 4-1 shows the effective moment of inertia values used in the elastic model. In this table I_g means the moment of inertia of gross section.

Table 4-1 Decreased moment of inertia values

Structural Member	Moment of Inertia
Columns	$0.7I_g$
Walls	$0.7I_g$
Slabs	$0.25I_g$

According to the analysis results, first mode period of the structures was calculated as 0.134 seconds and 1.047 seconds for short and tall buildings, respectively. Also, base shear values of short building and tall building were determined about 1700 kN and 3300 kN, respectively. According to the analysis results, reinforcement of the structural wall of the short building was selected as $2\phi 18/30^{cm}$ in longitudinal direction and $2\phi 16/30^{cm}$ in lateral direction. These reinforcements are determined according to the minimum reinforcement requirement of ACI 318-10. For the short building, boundary regions were not required. Basically the same uniform reinforcement is utilized at every storey in the short building. On the other hand, the longitudinal reinforcement requirements changes from storey to storey in the tall building. Moreover, boundary regions are formed at the ends of the walls. The reinforcement details for the tall building are presented in APPENDIX B.

4.1. Pushover Analysis of E-Shaped Structural Wall

As a starting point, instead of performing the nonlinear analysis of the 4-storey structure, first nonlinear analysis of a single 12 m high E-shaped structural wall was analyzed under cyclic loads with both ETABS and DIANA. Figure 4-3 and Figure 4-4 show the force deformation relationship of E-shaped structural wall in y and x directions.

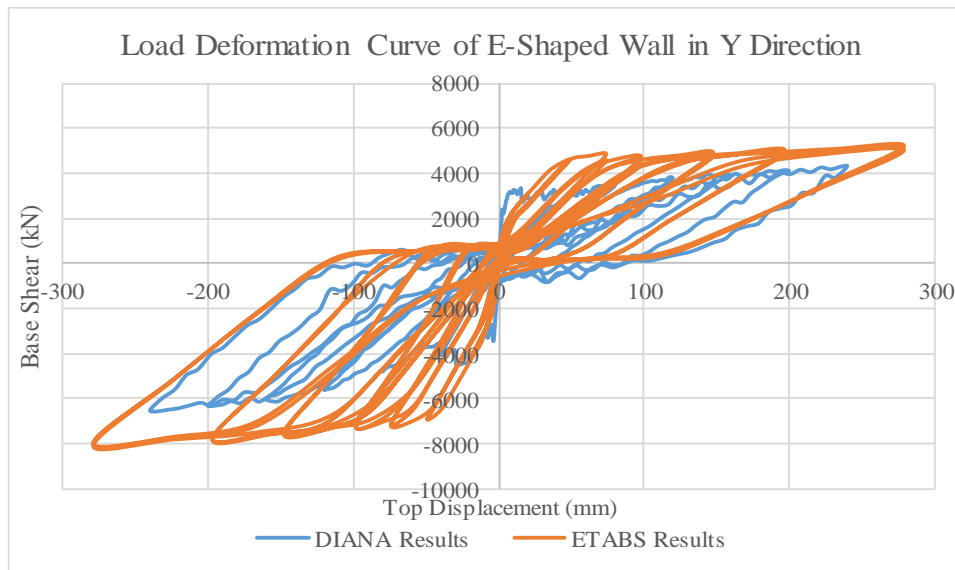


Figure 4-3 Load deformation curve of E-shaped wall in Y direction

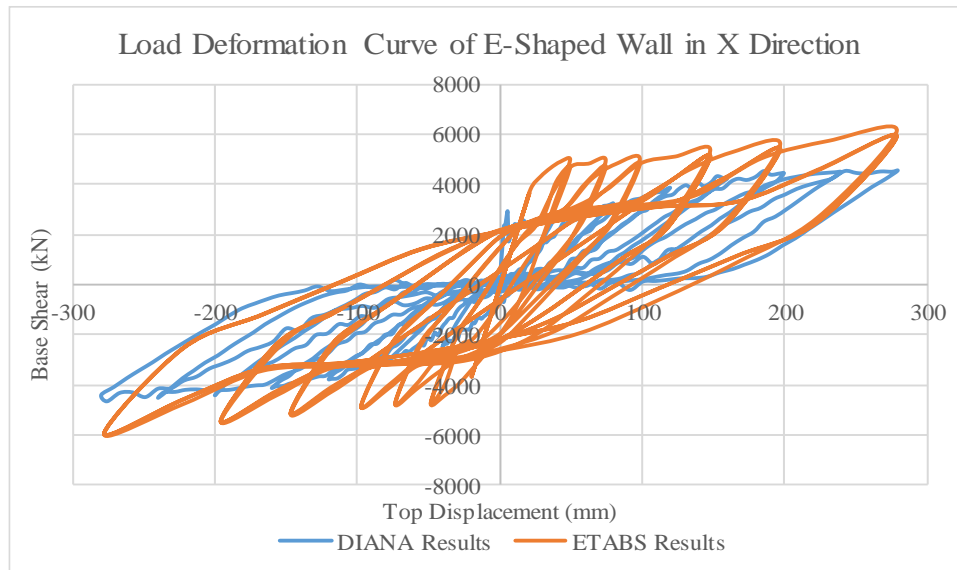


Figure 4-4 Load deformation curve of E-shaped wall in X direction

When the results of pushover analysis of a single structural wall are studied, it can be said that results of the computer programs show difference. Firstly, when the analysis results of the wall in y direction are studied (Figure 4-3), although behavior of the results look same, ETABS overestimates the capacity with 20% difference in both direction. When the results are studied in x direction, it is seen that difference is more in this direction. ETABS overestimates the capacity nearly 25% difference. Also, ETABS results show more hysteretic damping compared to DIANA results. These differences can be explained with the modeling approaches. Aspect ratios of the wall are 1.75 and 2.35 for x and y direction, respectively. This means that in x direction shear behavior governs and in y direction shear and flexural behavior govern together. Since fiber model cannot couple the nonlinear flexural and shear behavior, ETABS results show more capacity and more ductile behavior.

As a next step, pushover analysis was performed according to FEMA (FEMA 440, 2005) and results were compared with the cyclic analysis results. Below figures show the comparison of results for x and y directions. Figure 4-5 and Figure 4-6 show the DIANA results whereas Figure 4-7 shows the results obtained by ETABS. It can be said that pushover analysis results and cyclic analysis results of DIANA show good

harmony according to Figure 4-5 and Figure 4-6. On the other hand, it can be said that ETABS results look similar up to 1% drift ratio. After this nonlinear analysis did not converge to a solution. In X direction, pushover analysis did not converge at all with ETABS. After that point, all the analyses with the full structure were performed with Perform3D instead of ETABS.

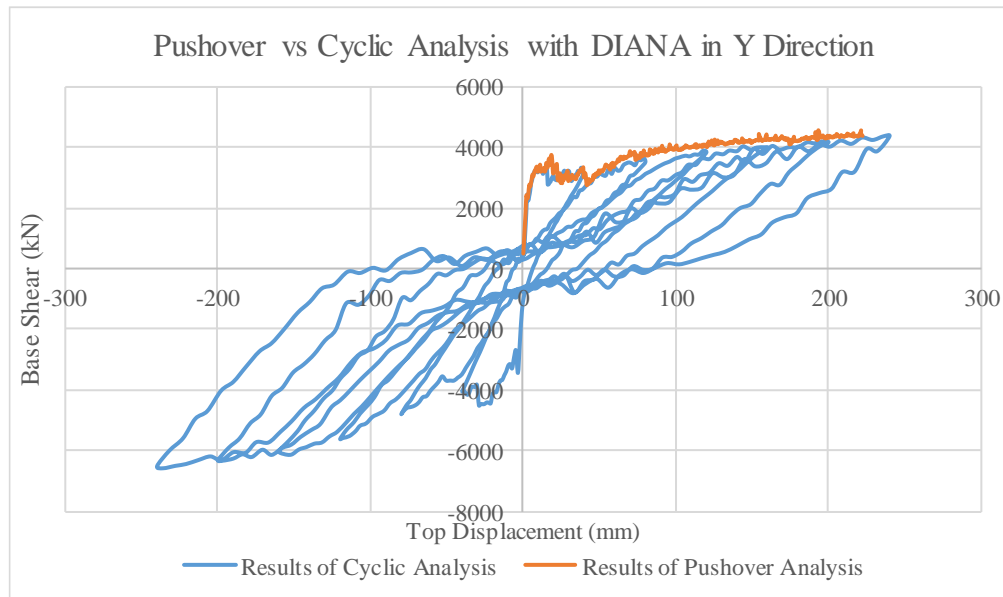


Figure 4-5 Comparison of pushover and cyclic analysis results of E-shaped wall in Y direction

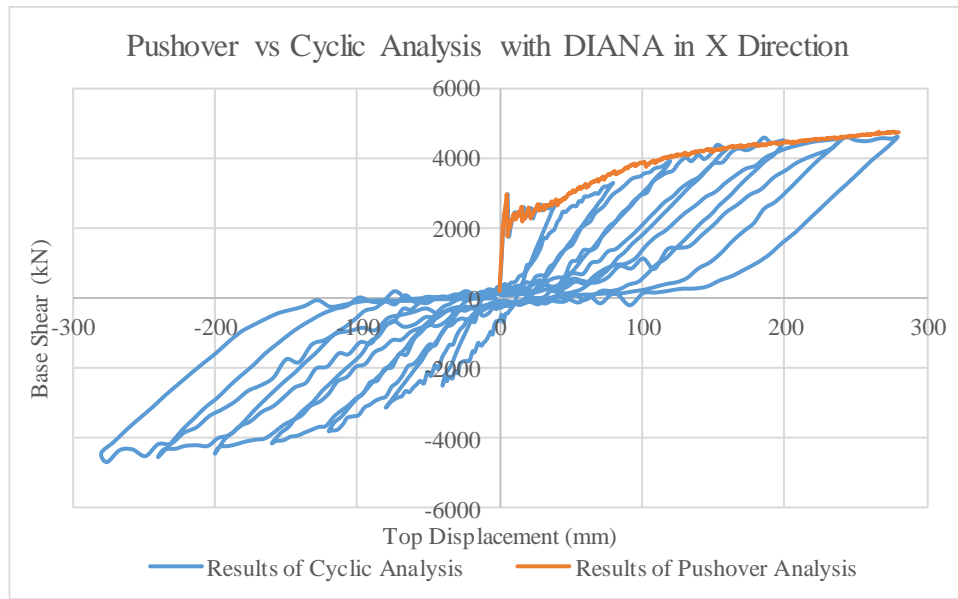


Figure 4-6 Comparison of pushover and cyclic analysis results of E-shaped wall in X direction

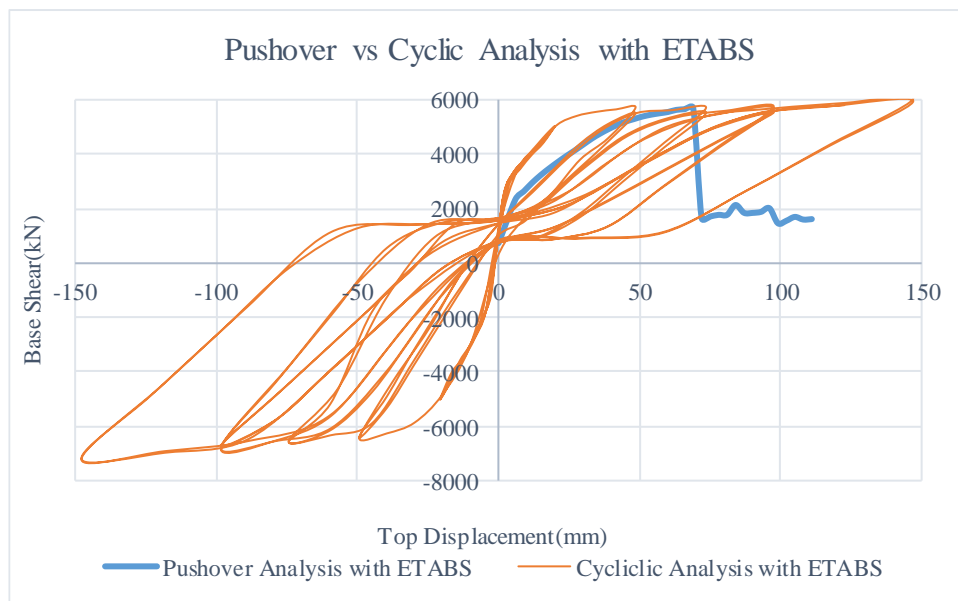


Figure 4-7 Comparison of pushover and cyclic analysis results of E-shaped wall in Y direction

4.2. Pushover Analysis

4.2.1. Pushover Analysis of 4-Storey Structure

Pushover analysis was performed for the 12 m high short building in the x and y directions with both DIANA and Perform3D. Figure 4-8 shows the analysis models in DIANA and Perform3D, respectively.

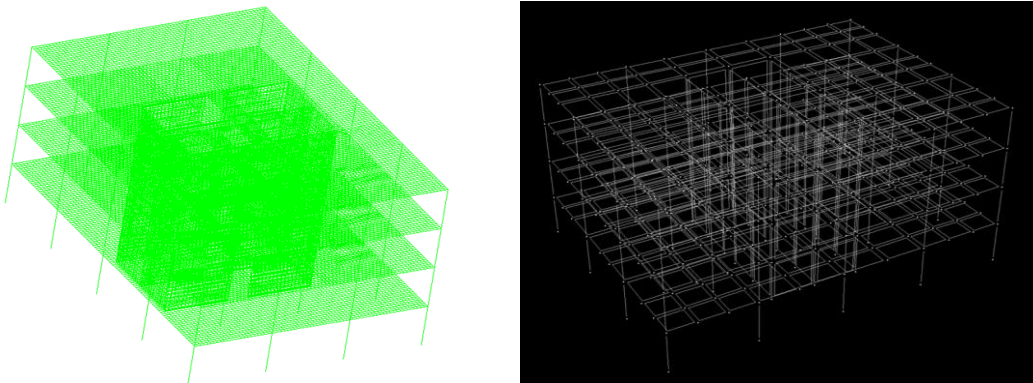


Figure 4-8 Analysis models of the building in DIANA and PERFORM3D

In DIANA, columns were modelled as frame elements and slabs and structural walls were modeled with shell elements. In DIANA, BE2 L7BEN element type was used for columns and CQ40S element type was used for slabs and structural walls. Sectional and material properties of these elements are presented in APPENDIX A. As it is stated above $2\phi 18/30^{\text{cm}}$ was used as a longitudinal reinforcement and $2\phi 16/30^{\text{cm}}$ was used as a lateral reinforcement for structural walls. In this analysis, no nonlinearity was assigned for columns and slabs but modulus of elasticity for slabs was decreased to 25% to account for cracking under gravity loads according to ACI 10.10.4.1. Figure 4-9 shows the reinforcements of the building in DIANA.

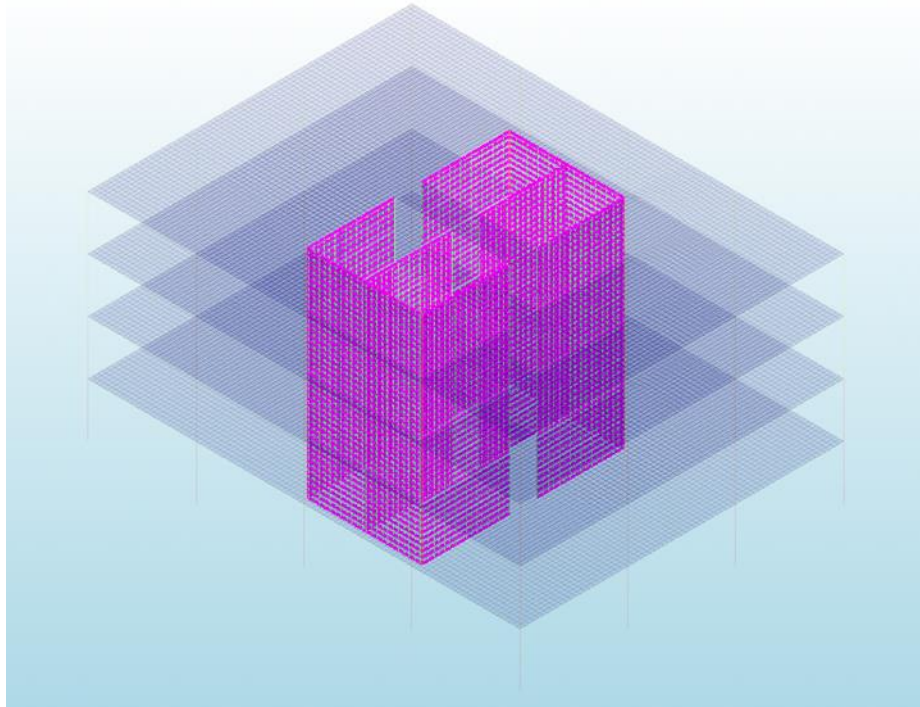


Figure 4-9 Lateral and longitudinal reinforcements of the building

In Perform3D model, columns and slabs are modeled with column elements and shell/slab element of Perform3D. In this model, columns and slabs are taken as elastic members. In order to model the walls, shear wall properties of Perform3D was used. These properties are presented in APPENDIX A. In Perform3D, in order to define the nonlinearity, structural wall sections were modeled with fibers. There is a limitation on the number of fiber sections in Perform3D, thus in order to obey this limitation some of the reinforcements were defined as a single reinforcement. While doing this, stiffness and inertia of the system were not changed.

In order to perform pushover analysis, forces were applied to the structure in the shape of inverted triangular. Figure 4-10 shows the application of forces to the structure.

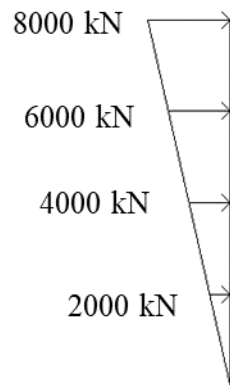


Figure 4-10 Application of forces

In analyses, forces were applied step by step to all stories. Figure 4-11 and Figure 4-12 show the pushover analysis results of the short building with both Perform3D and DIANA.

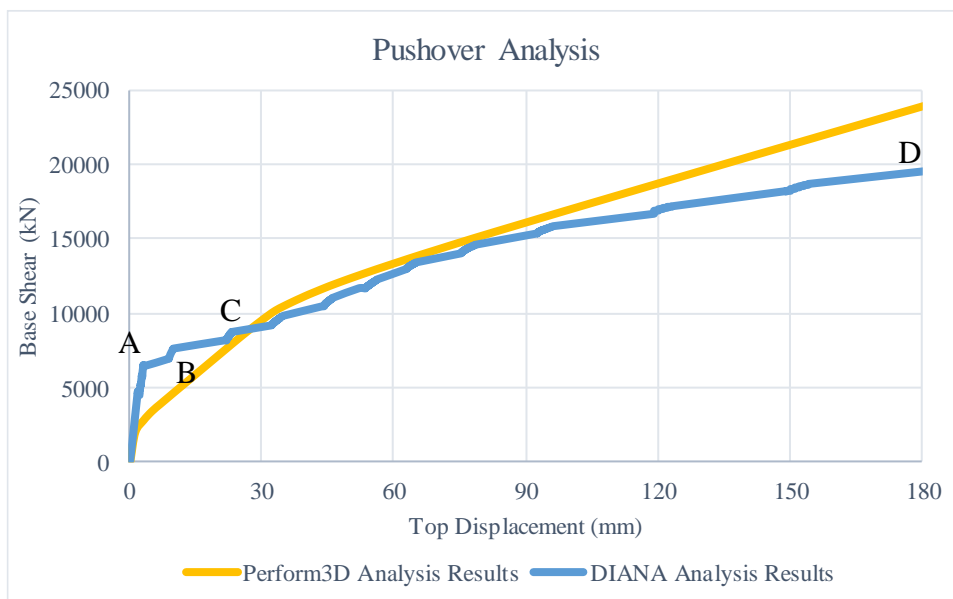


Figure 4-11 Comparison of base shear results for Y direction

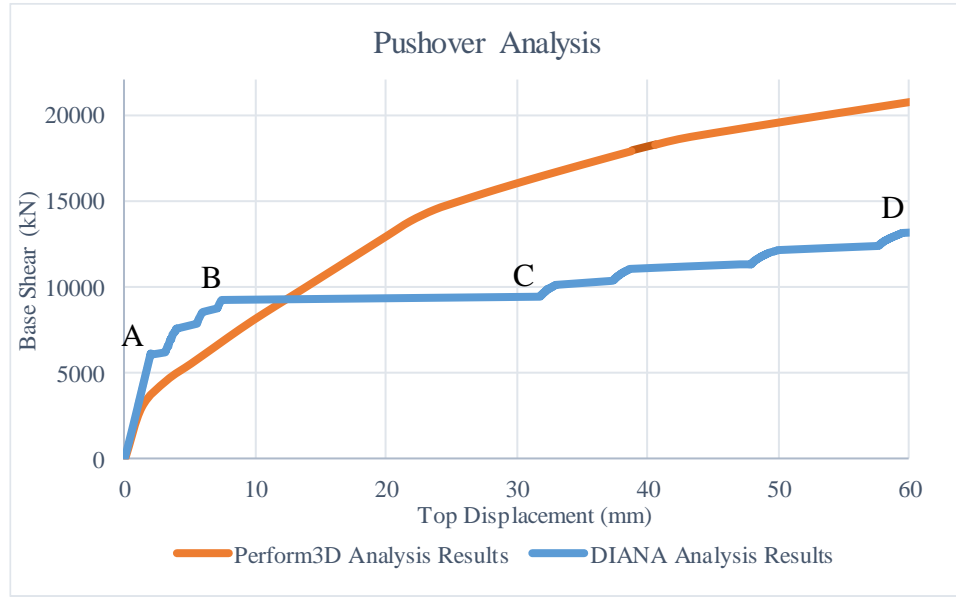


Figure 4-12 Comparison of base shear results for X direction

Figure 4-11 and Figure 4-12 show the base shear values according to pushover analysis. Analysis results can be checked by calculating the shear capacity of the wall. According to ACI section 11.9.6 shear capacity of the core wall can be calculated in two different ways and smaller one is taken as the capacity of the wall.

$$V_c = 0.27 \times h \times d + \frac{N_u \times d}{4 \times l_w} \quad 4.1$$

$$V_c = \left[0.05 \times \lambda \times \sqrt{f_c} + \frac{l_w \times \left(0.1 \times \lambda \times \sqrt{f_c} + 0.2 \times \frac{N_u}{l_w \times h} \right)}{\frac{M_u}{V_u} - \frac{l_w}{2}} \right] \quad 4.2$$

In these equations;

l_w = length of the wall (5.1^m in y direction and 6.4^m in x direction)

h = thickness of the wall (0.45^m)

d = effective shear depth (0.8 l_w)

$\lambda = 1$ for normal weight concrete

M_u = factored bending moment (6540 kN/m for y direction and 6860 kN/m for x direction)

V_u = factored shear force (834 kN for y direction and 810 kN for x direction)

N_u = factored axial force (5735 kN)

By using these formulations with the specified values shear capacity of the structural wall is calculated 14450 kN and 10160 kN in y and x direction of the building, respectively. It is seen that in DIANA, when capacity reaches these values, stiffness of the model decreases. On the other hand, Perform3D overestimates the stiffness of the structure.

When the analyses result that are presented in Figure 4-11 and Figure 4-12 are studied, it is seen that there are points of change in behavior of the structure. In order to understand the reason of these changes, the analysis results should be studied in more details. DIANA can present the results in terms of strain. But to be more understandable, results are going to be presented in terms of crack width. Crack width can be calculated by using Equation 4.3. In this equation h represents the crack bandwidth and it is equal to root of the element area (Root of the element area is equal to 0.285 m for our model).

$$w_c = \varepsilon_c \times h \quad 4.3$$

For serviceability 0.5 mm is a limit value for crack width. After that value people feel uncomfortable because of these cracks. The strain value corresponding to this crack width is 1.75×10^{-3} . So, in this study while presenting the results, instead of showing all crack values just the cracks that larger than specified value were shown in terms of strain values.

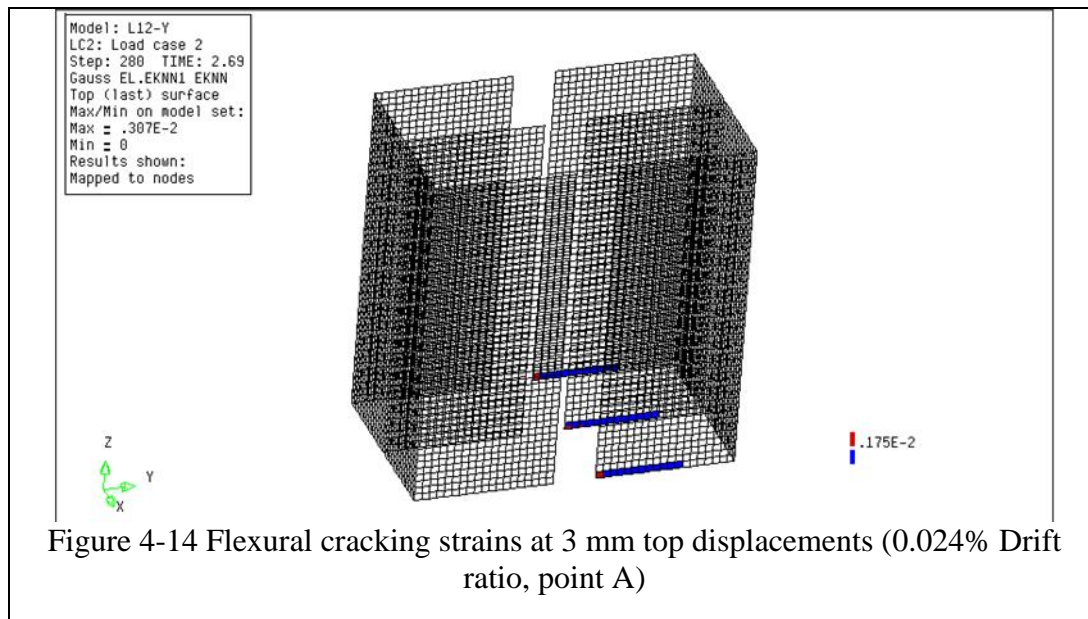
Perform3D does not show the cracking of concrete, instead it shows the concrete strain values with coloring the wall section according to limit strain value. Same strain values with DIANA was selected as limit strain value and results were presented according to this value. Figure 4-13 shows the colors according to scale factor.



Figure 4-13 Coloring of wall section according to limit strain value

When the results of DIANA in the y direction are studied, it can be said that at the beginning there is no crack and system shows linear response as it is shown from the Figure 4-11. After 3 mm top floor displacement (Figure 4-14, 0.024% drift ratio, point A in Figure 4-11) flexure cracking starts and those cracks are continued until 10 mm top displacement (Figure 4-15, point B in Figure 4-11). After this point shear cracks begin to form up to 20 mm top displacement (Figure 4-17, point C in Figure 4-11) and then strain hardening takes place. Figure 4-19 shows the crack strains of the structural wall at the end of the analysis (180 mm top displacement).

When the results of Perform3D in the y direction are studied, structure shows elastic behavior at beginning and after 2 mm top displacement nonlinearity take place. According to selected scale factor, first cracks occurred at 0.07% drift ratio as shown in Figure 4-16. At 0.24% drift ratio, strain value at the wall sections on the first floor passes the limit value as shown in Figure 4-18. Finally, Figure 4-20 shows the wall sections that have strain values more than limit value at the end of the analysis.



Model: L12-Y
 LC2: Load case 2
 Step: 410 TIME: 3.97
 Gauss EL.EKNN1 EKNN
 Top (last) surface
 Max/Min on model set:
 Max = .594E-2
 Min = 0
 Results shown:
 Mapped to nodes

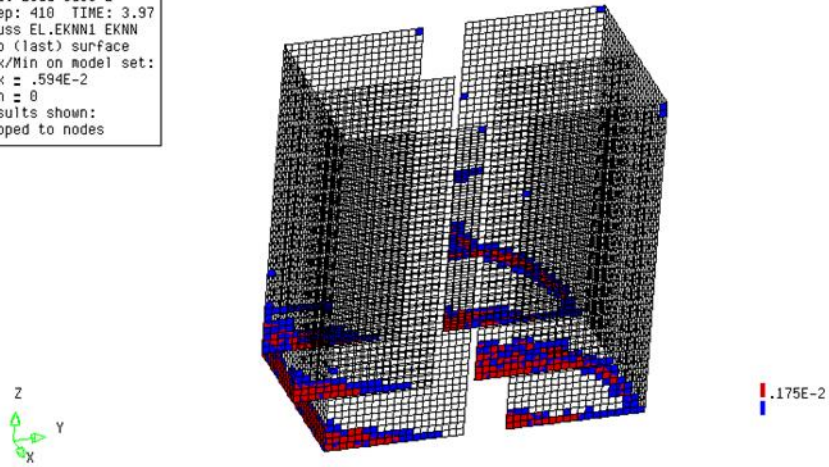


Figure 4-15 Flexural cracking strains at 10 mm top displacement (0.08% Drift ratio, point B)

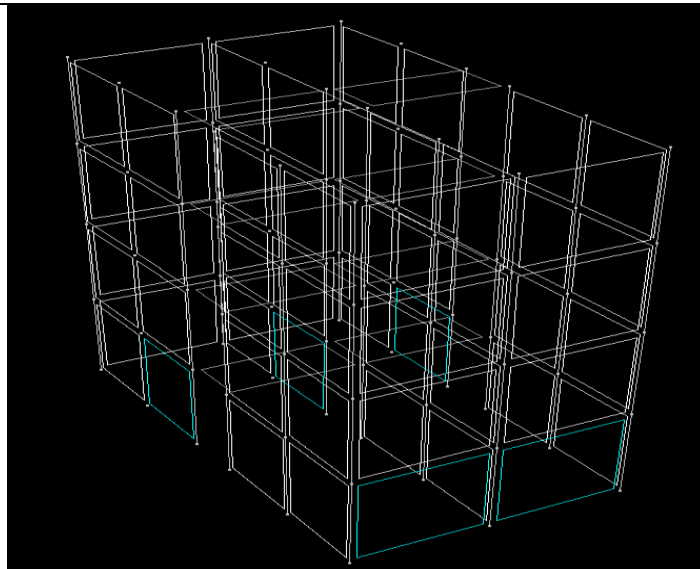


Figure 4-16 Cracked wall sections at 0.07% drift ratio

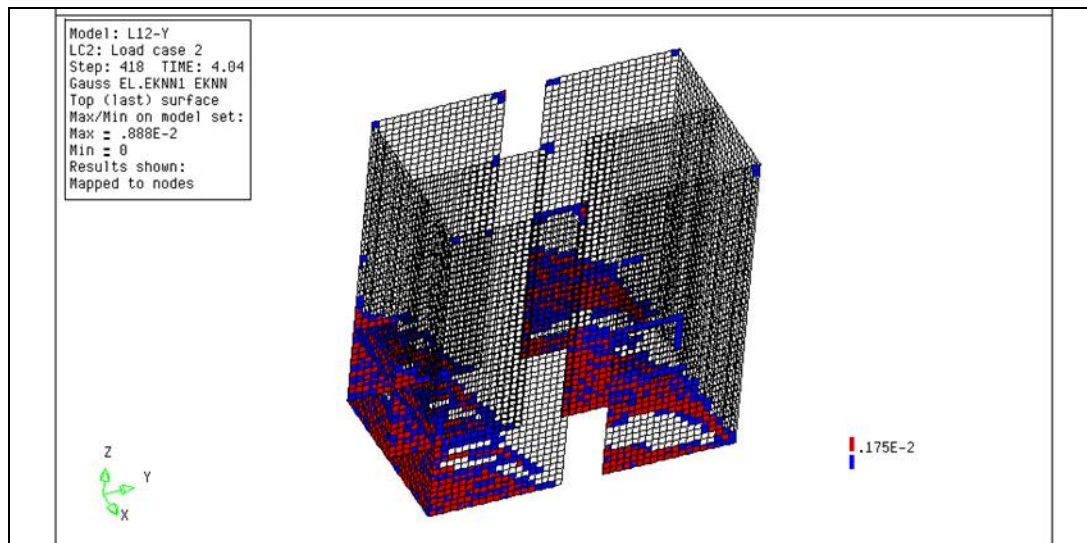


Figure 4-17 Shear cracks at 20 mm top displacement (0.17% Drift ratio, point C)

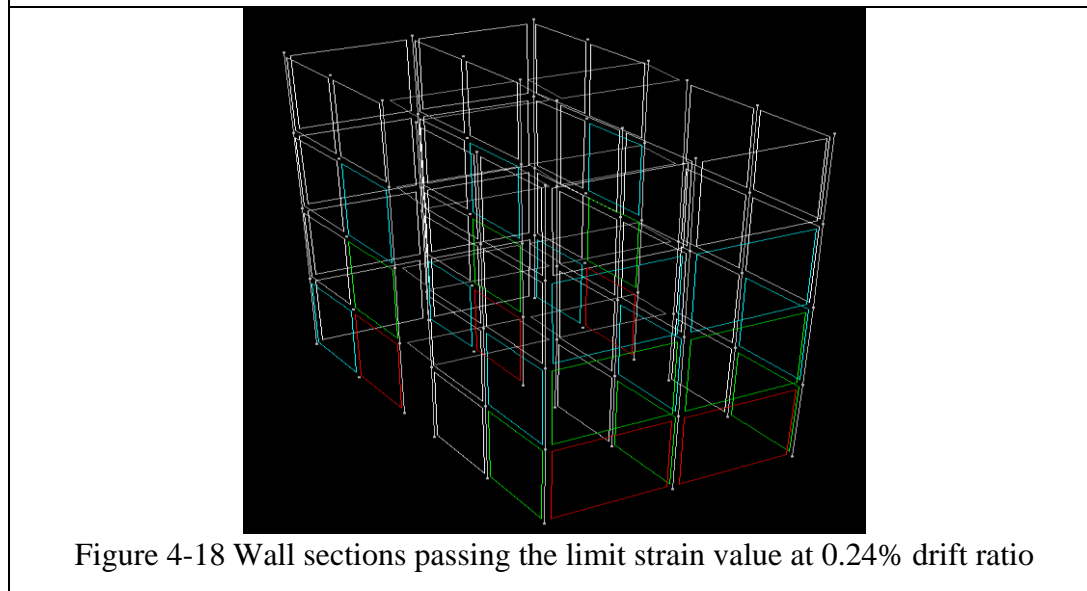
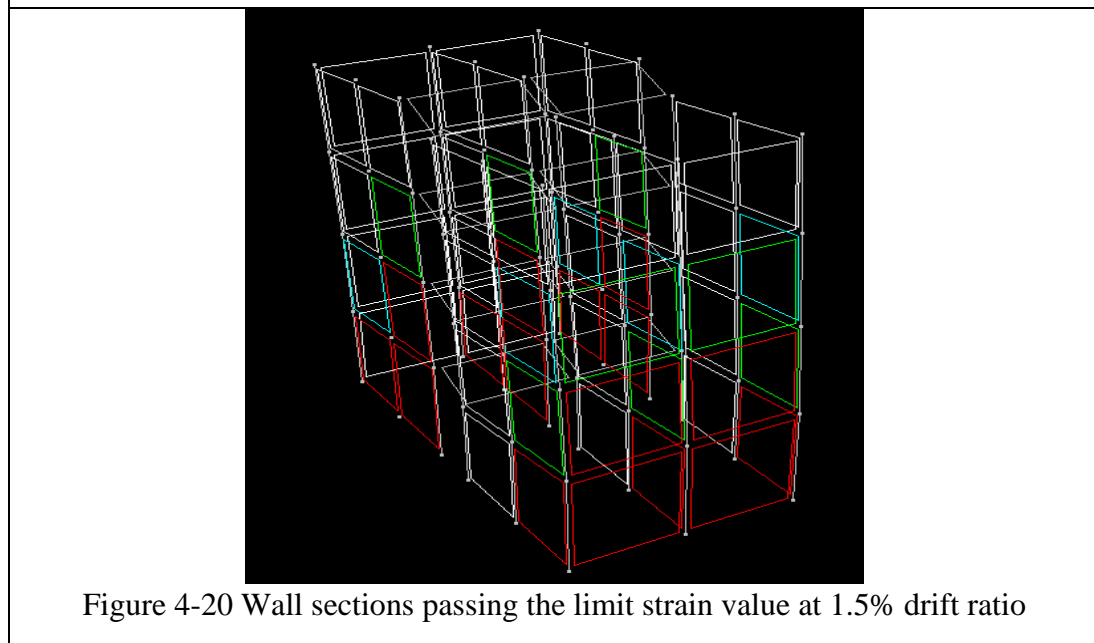
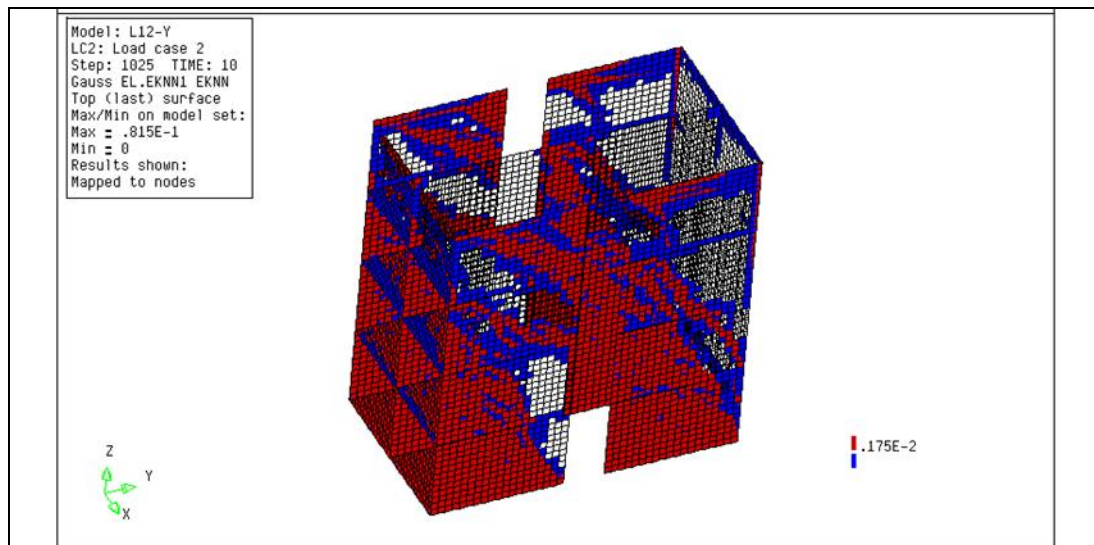


Figure 4-18 Wall sections passing the limit strain value at 0.24% drift ratio



Behavior of the reinforcement has the same importance with behavior of concrete on the response of the structure under the applied load. Therefore, when the behavior of reinforcement is studied in DIANA, it is seen that longitudinal reinforcements start yielding at 3 mm top displacement. As the results are studied, it is seen longitudinal reinforcements start yielding at the beginning of flexural cracking and this yielding continues till the end of the analysis. Figure 4-21 shows the yielded reinforcement. In

this figure, red color implies that stress value of reinforcement is greater than yield value at these points.

In Perform3D, since fiber modeling approach was used, results of reinforcement cannot be presented by itself. Instead, it can be presented by strain gages or monitored fibers. In this study, results of reinforcement is presented with the help of monitored fibers. When the results are studied in y direction, it is observed that longitudinal reinforcements start yielding after the strain value of the section that pass the limit value (2.1×10^{-3}) and continue till the end of the analysis. Figure 4-22 shows the yielded reinforcements at the end of the analysis.

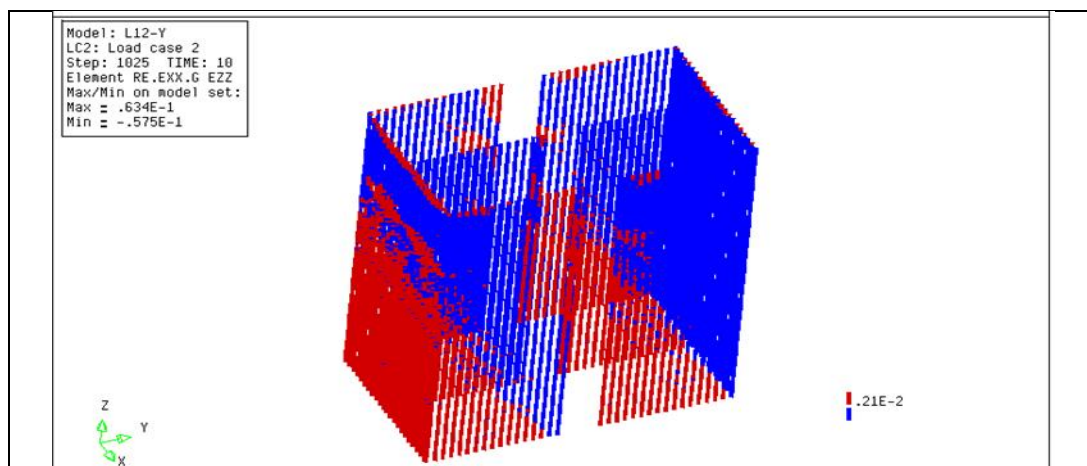


Figure 4-21 Yielding of longitudinal reinforcement at 1.5% drift ratio in DIANA

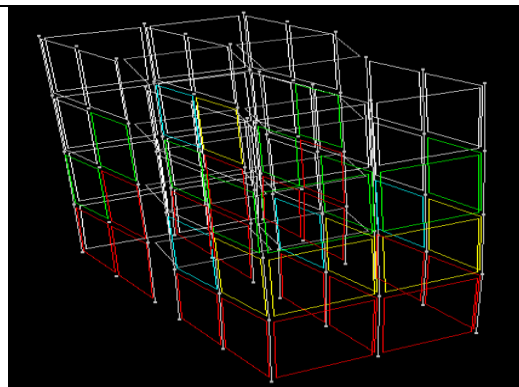


Figure 4-22 Yielding of longitudinal reinforcement at 1.5% drift ratio in Perform3D

After then results of the building in the x direction was studied. When the results of DIANA are examined, behavior of the building is almost linear up to 3 mm top displacement (0.025% drift ratio, point A) as it understood from the Figure 4-12. This figure implies that up to this point nearly no part of the wall crack. After than structure shows flexural behavior up to 7.5 mm top displacement (0.0625% drift ratio, point B in Figure 4-12). Then, shear cracks start. These cracks continue up to 30 mm top displacement (0.25% drift ratio, point C in Figure 4-12). After this point strain hardening takes place. Figure 4-28 shows the crack strains of the structural wall at the end of analysis (0.5% drift ratio, point D in Figure 4-12).

Thereafter, analysis results of Perform3D in x direction were studied. As it is seen from the Figure 4-12 structure shows elastic behavior up to 3 mm top displacement and after 3 mm top displacement, nonlinearity take place. Figure 4-25 shows the initiation of cracks at the 0.06% drift ratio. At 0.17% drift ratio strain value at the wall sections on the first floor passes the limit value as shown in Figure 4-27. Finally, Figure 4-29 shows the wall sections that have strain values more than limit value at the end of the analysis.

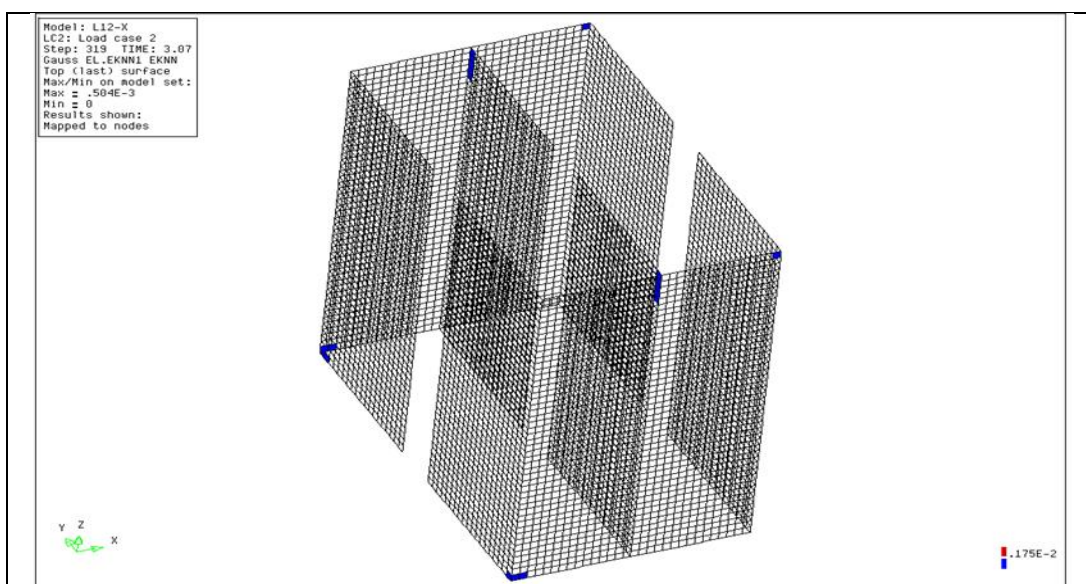


Figure 4-23 Flexural cracking strains at 3 mm top displacement (0.025% drift ratio)

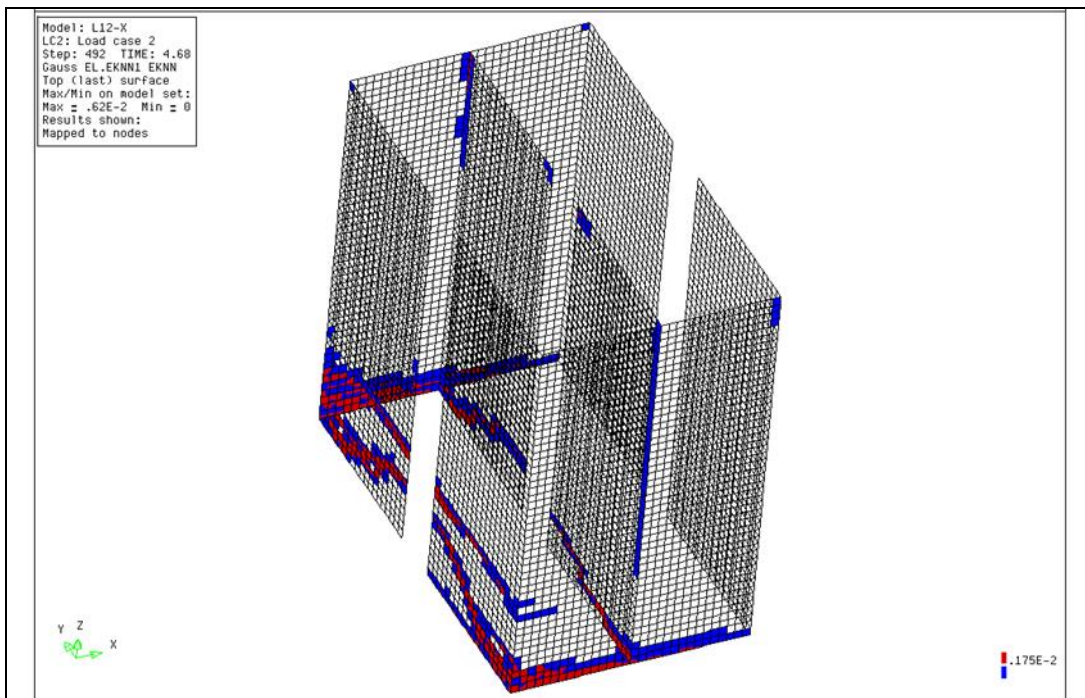


Figure 4-24 Flexural cracking strains at 7.5 mm top displacement (0.0625% Drift ratio)

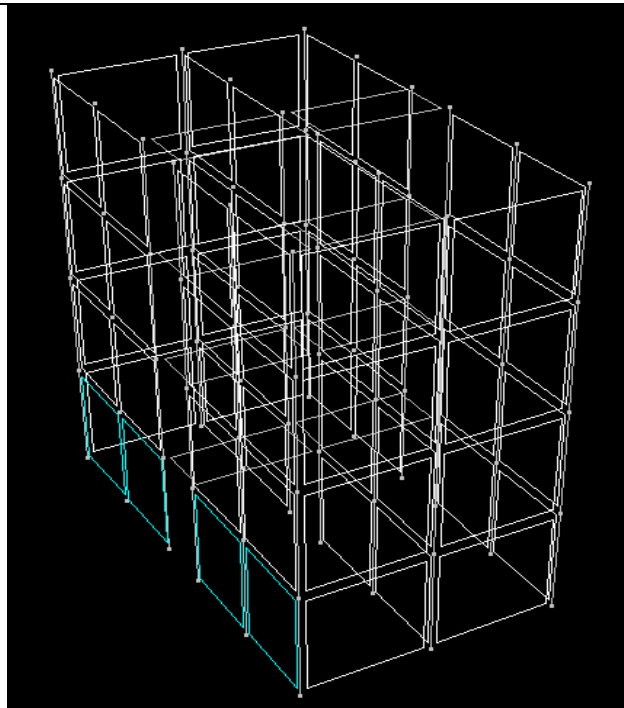


Figure 4-25 Wall strain at 0.06% drift ratio

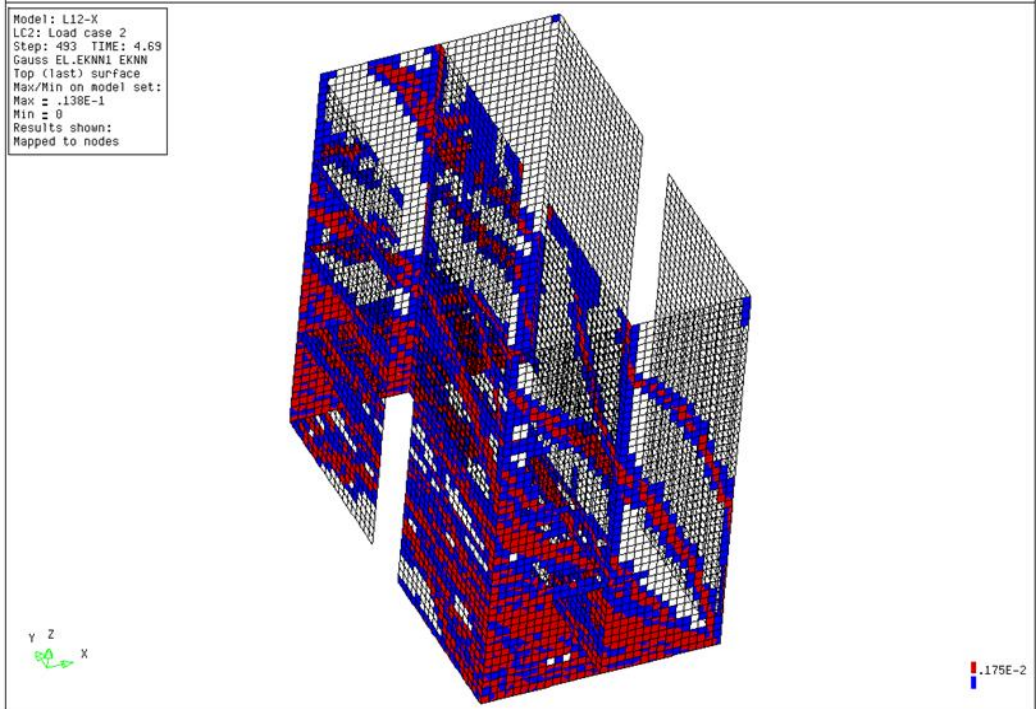


Figure 4-26 Flexural cracking strains at 30 mm top displacement (0.25% Drift ratio, Point C)

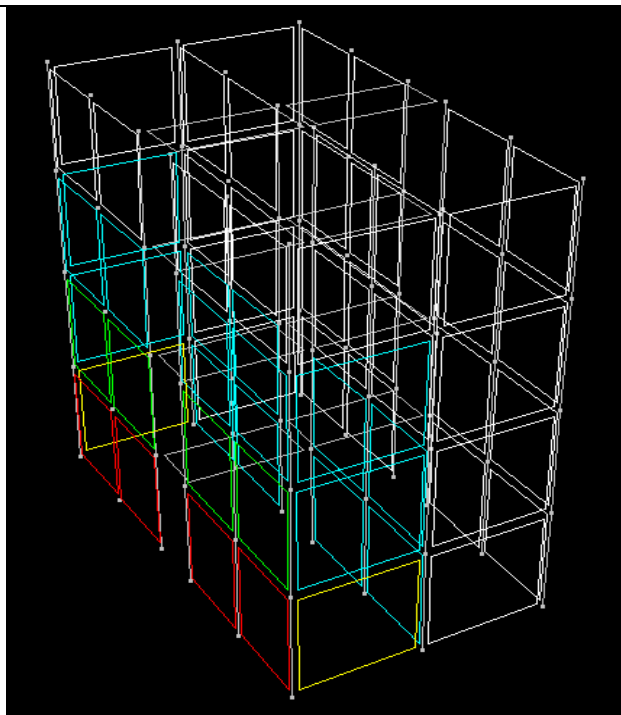


Figure 4-27 Wall sections passing the limit strain value at 0.17% drift ratio

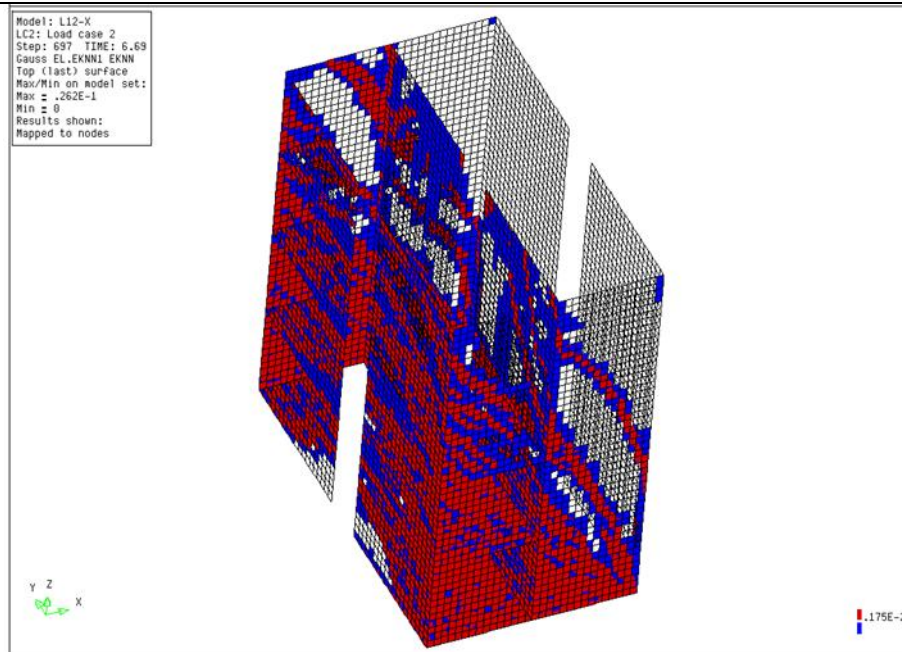


Figure 4-28 Flexural cracking strains at 0.5% drift ratio (Point D)

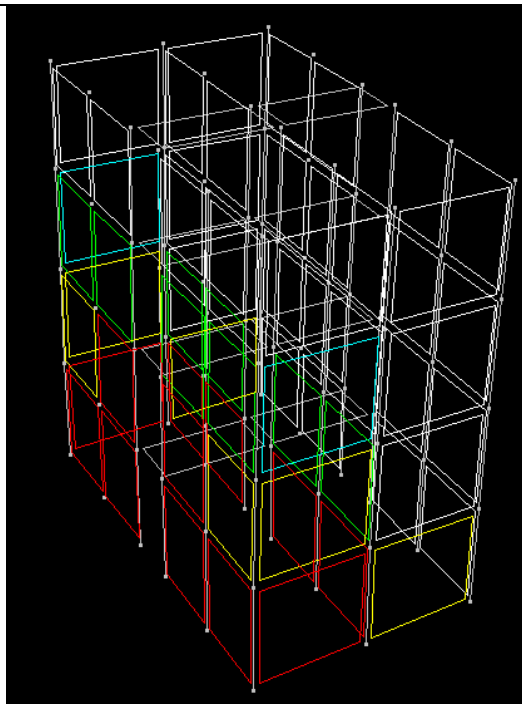


Figure 4-29 Wall sections passing the limit strain value at 0.5% drift ratio

When the behavior of the reinforcements is studied according to DIANA results it is seen that longitudinal reinforcements start yielding at 3 mm top displacement. According to analysis results up to starting point of strain hardening none of the longitudinal reinforcement yield but at the end of the analysis nearly all of the longitudinal reinforcements that stay in tension yields. Figure 4-30 shows the yielded reinforcement. In this figure, red color implies that stress value of reinforcement is greater than yield value at these points.

According to the results of Perform3D in x direction it is observed that longitudinal reinforcements start yielding after the strain value of the section pass the limit value and continue till the end of the analysis. Figure 4-31 shows the yielded reinforcements at the end of the analysis.

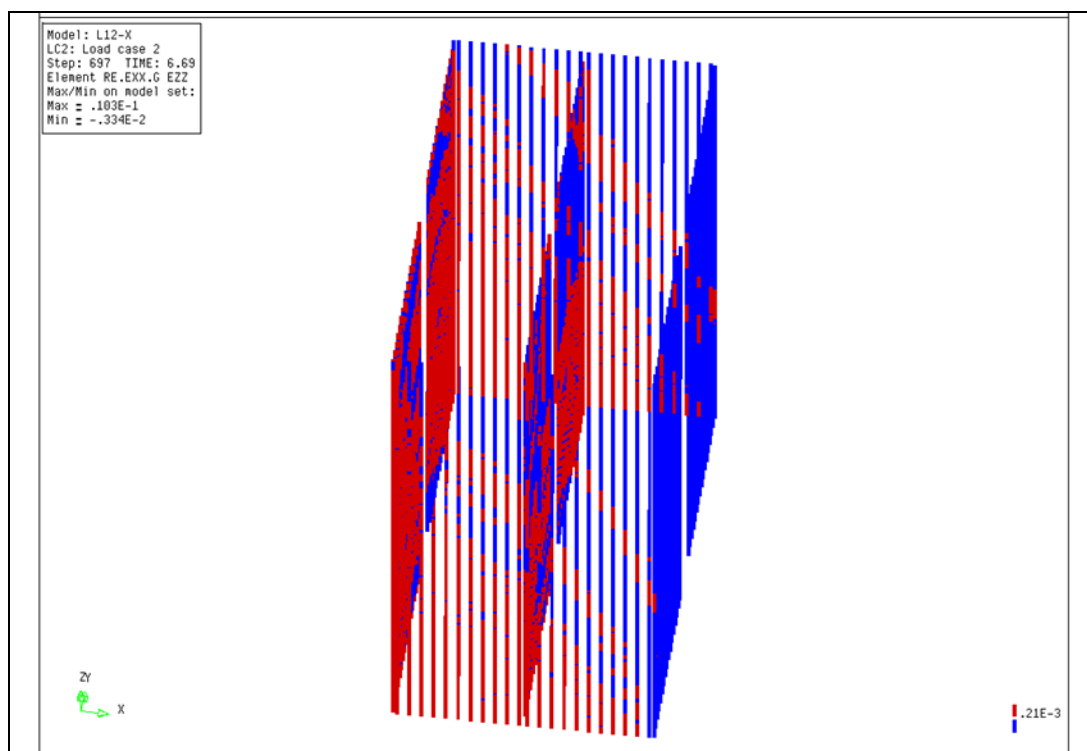


Figure 4-30 Yielding of longitudinal reinforcements in DIANA at 0.5% drift ratio

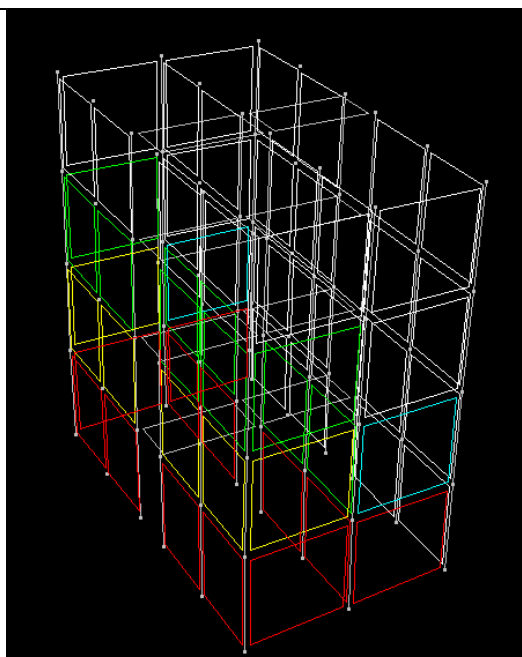


Figure 4-31 Yielding of longitudinal reinforcements in Perform3D at 0.5% drift ratio

As we study the results, it can be said that there are some differences between the results of the programs. Firstly, as it is understood from the Figure 4-11 and Figure 4-12 initial stiffness value of the structure is different in DIANA and Perform3D. Stiffness of the DIANA model is nearly equal to 10 times of the stiffness of the Perform3D model. One of the main reason of this is the difference between material properties. In DIANA, all stress and strain values can be defined but in Perform3D this cannot be done. In Perform3D, although elastic perfectly plastic material type is suggested, three linear material properties with strength loss was used and because of this reason properties of concrete cannot be defined as it was done in DIANA. Moreover, there is also a difference on the shear capacity of the structure between programs. This difference can be basically explained with some reasons. The first reason is that, in Perform3D shear behavior is modeled elastically. Thus, shear deformations cannot be captured and shear capacity is overestimated. The other reason is that, when slabs are modeled elastically, it couples the walls and increases the stiffness of the building. But this coupling behavior is not observed in DIANA, since local deformations are observed at the connections between wall and slabs. Furthermore, when the flange of the wall is under the tension, the program calculates it as flange totally resist the tension and so overestimate the capacity of the structure. This can be accepted as a reason for the capacity difference of the x direction.

4.2.2. Pushover Analysis of 15-Storey Structure

When the aspect ratio of the wall is less than 2 the wall can be considered as a squat wall. The aspect ratio of the wall that used in short building is 1.75 in x direction and 2.35 in y direction. Thus, it can be considered as a squat wall. On the other hand, aspect ratio of the wall that used in tall building is larger than 4 in each direction. Thus, it can be considered as a slender wall and flexural failures are expected.

Figure 4-32 shows the analysis models of the tall building in DIANA and Perform3D, respectively. In DIANA, as it was done for the short structure, BE2 L7BEN element type was used for columns and CQ40S element type was used for slabs and structural

walls and Figure 4-33 shows the reinforcements of the structure in DIANA. In Perform3D model, columns and slabs were modeled with column elements and shell/slab element of Perform3D. In order to model the walls, shear wall properties of Perform3D was used. In Perform3D, structural wall sections were modeled with fiber hinges to define the nonlinearity. As it is mentioned before there is a limitation on the number of fibers in Perform3D. Therefore, some of the reinforcements were described as a single reinforcement in order to agree with the limitation. Stiffness and inertia of the system were not changed while doing this arrangement.

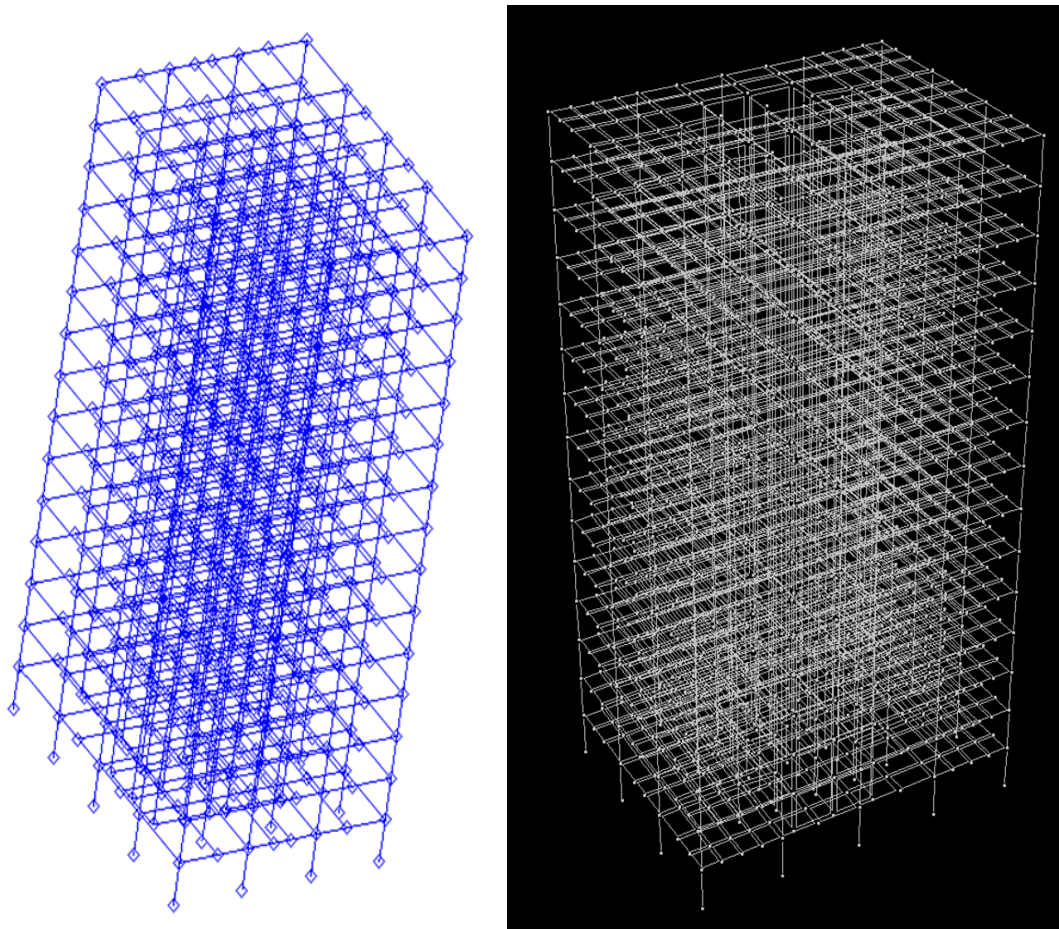


Figure 4-32 Analysis models of the tall building in DIANA and Perform3D

As it was done for 4-storey structure, in this model, columns and slabs were taken as elastic members.

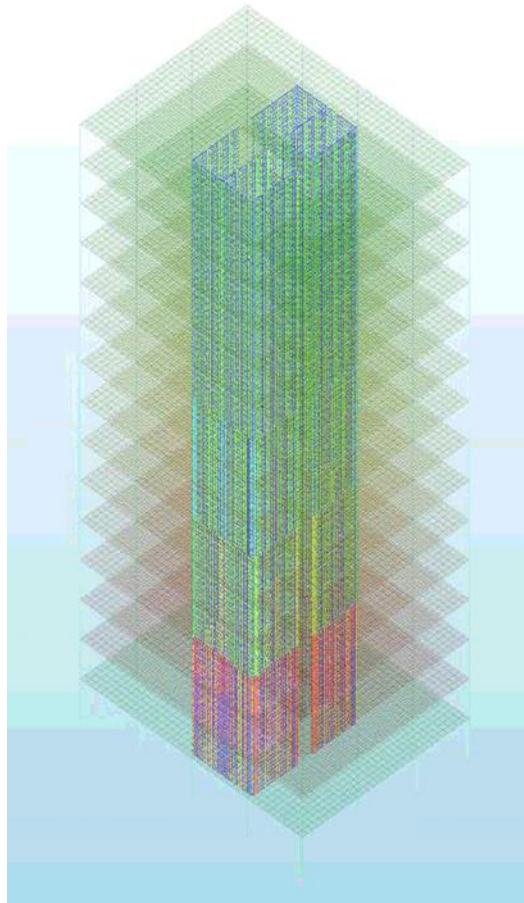


Figure 4-33 Lateral and longitudinal reinforcements of the building

Pushover analysis was performed by applying force in inverted triangular pattern and Figure 4-34 shows the application of forces to the structure.

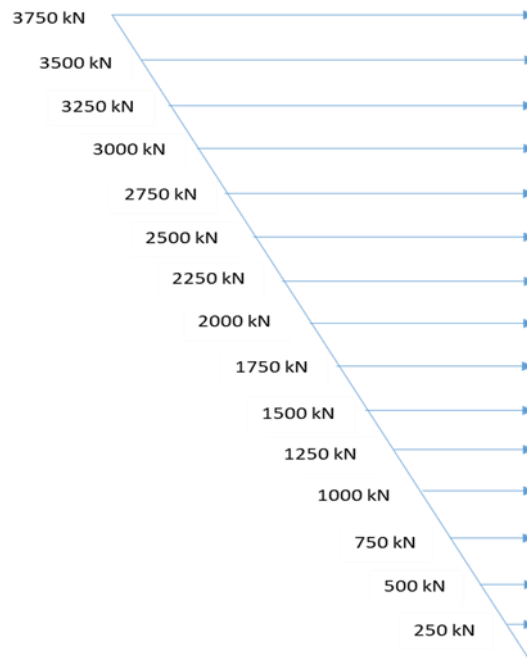


Figure 4-34 Application of forces

Forces were applied step by step to all stories. Figure 4-35 and Figure 4-36 show the pushover analysis results of the tall building with both Perform3D and DIANA.

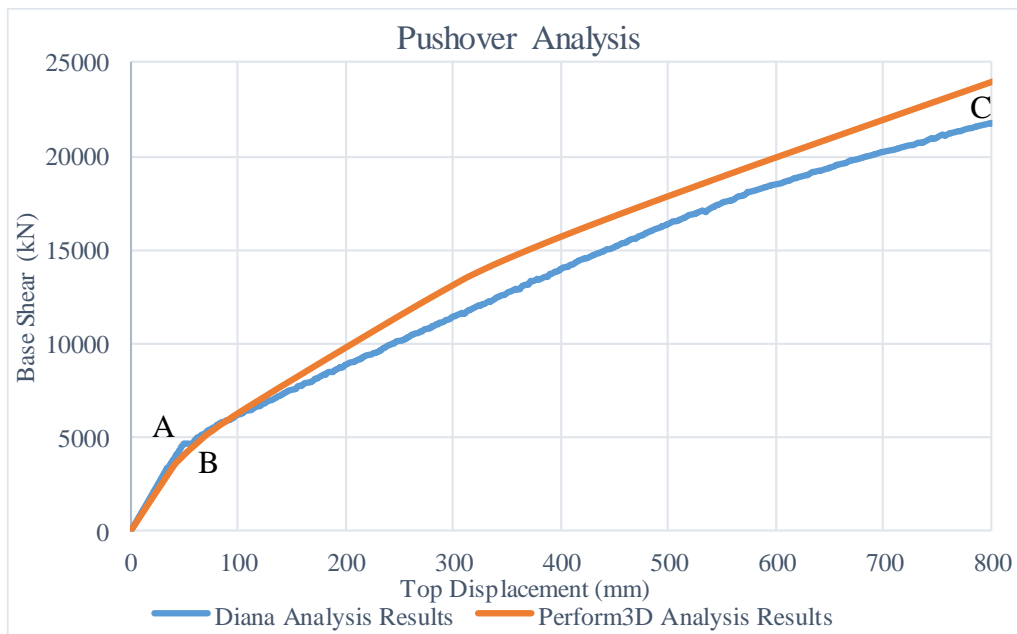


Figure 4-35 Comparison of pushover analysis results in Y direction

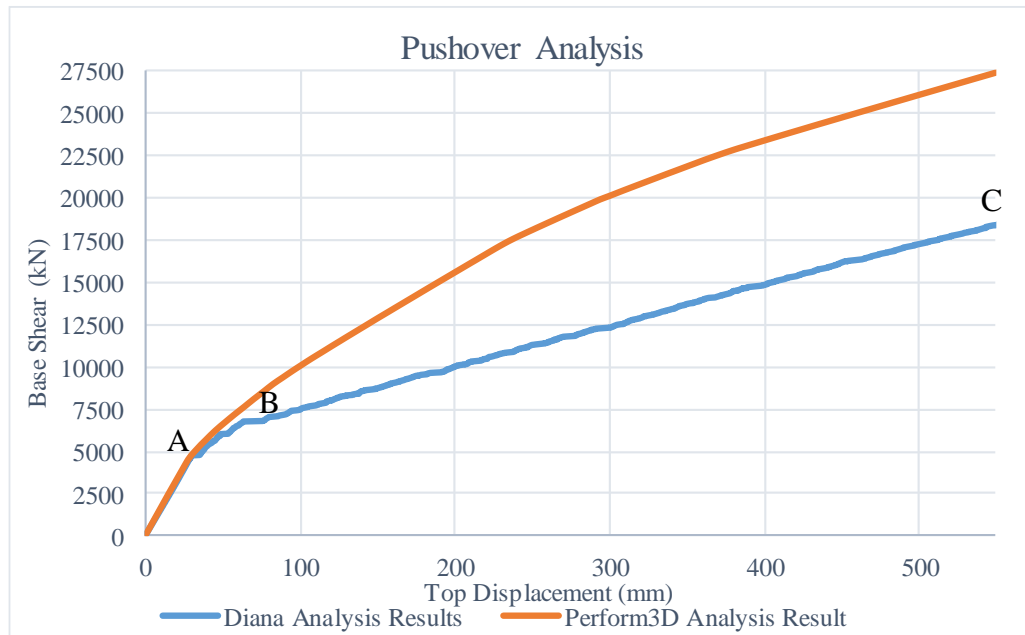
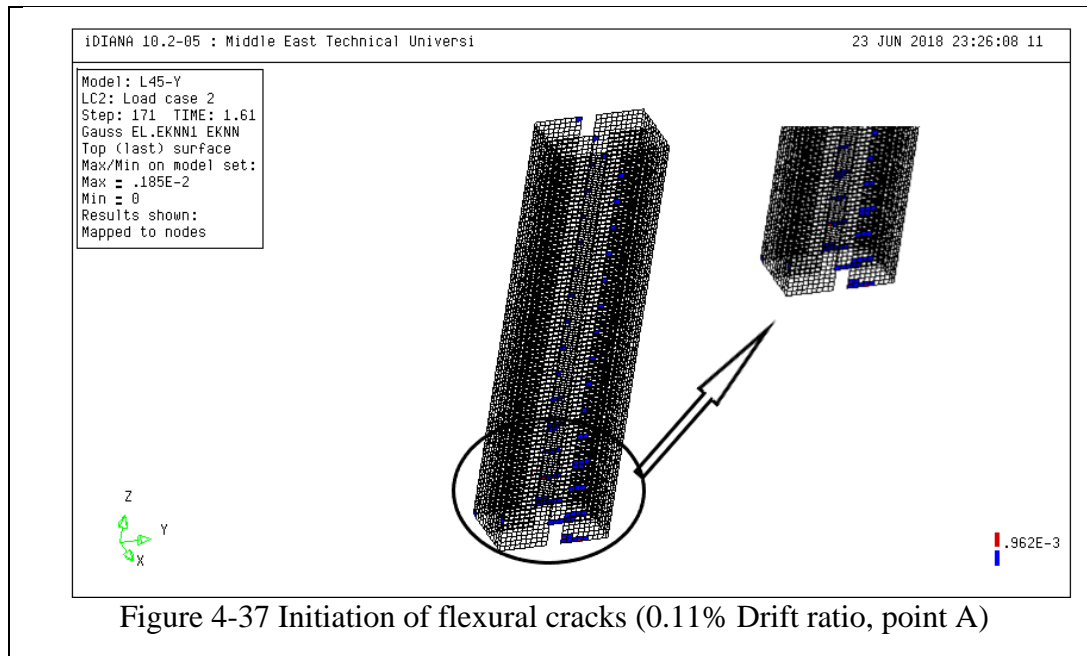


Figure 4-36 Comparison of pushover analysis results in X direction

First, results of pushover analysis on the y direction of the building were studied. When the results of DIANA are studied, the behavior of the building is linear up to 49.5 mm top displacement (0.11% drift ratio). Up to this point as it is shown from the Figure 4-37 (Point A in Figure 4-35) the flexural crack values are less than the limit value. The limit strain value for this structure was determined like the previous structure and found as 9.62×10^{-4} (Different element sizes were used by considering the run time.) After that point base shear value stays nearly constant up to 57.5 mm top displacement (0.13% drift ratio, point B in Figure 4-35) and this part of the behavior is governed by shear. Figure 4-38 shows the shear cracks. After this point longitudinal reinforcement start yields and strain hardening takes places. Figure 4-40 shows the flexural cracking strains at the end of analysis (1.8% drift ratio, Point C in Figure 4-35).

When analysis results of Perform3D in y direction is studied, it is seen that the structure shows elastic behavior up to 45 mm top displacement (0.1% drift ratio) and after that point nonlinearity takes place. Figure 4-39 shows the wall sections that have

strain values more than 25% of limit strain value at 0.18% drift ratio. Figure 4-41 shows the cracked wall section at the end of the analysis (1.8% Drift Ratio).



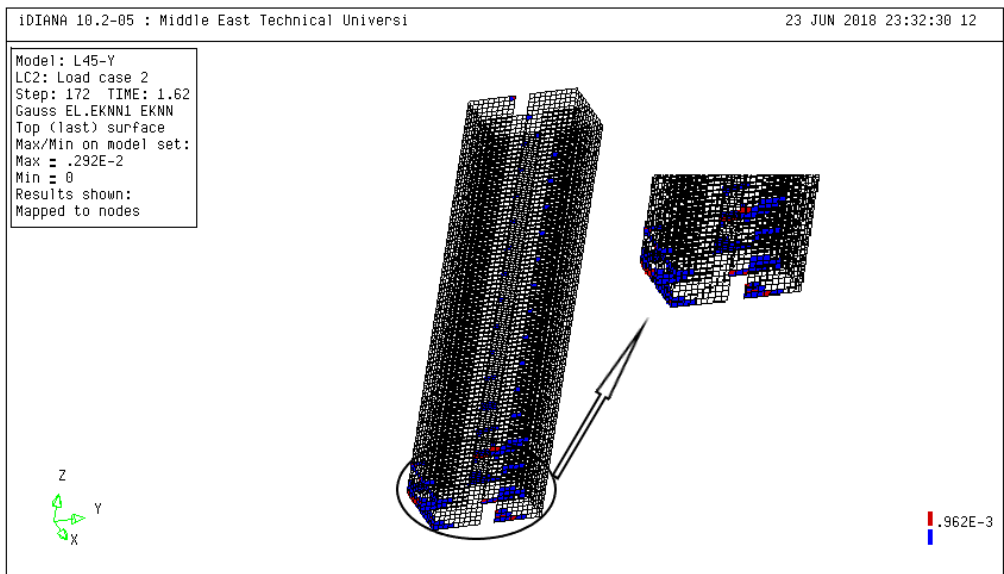


Figure 4-38 Shear cracking strains at 57.5 mm top displacement (0.13% Drift ratio, point B)

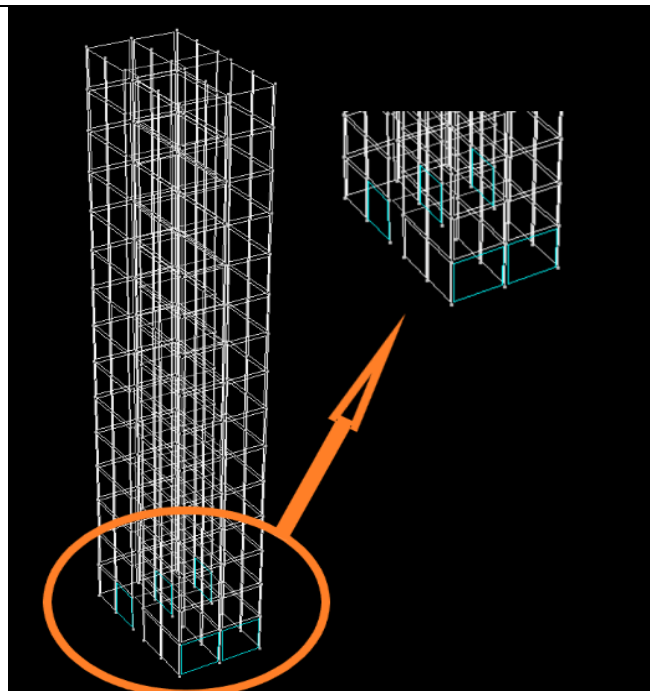
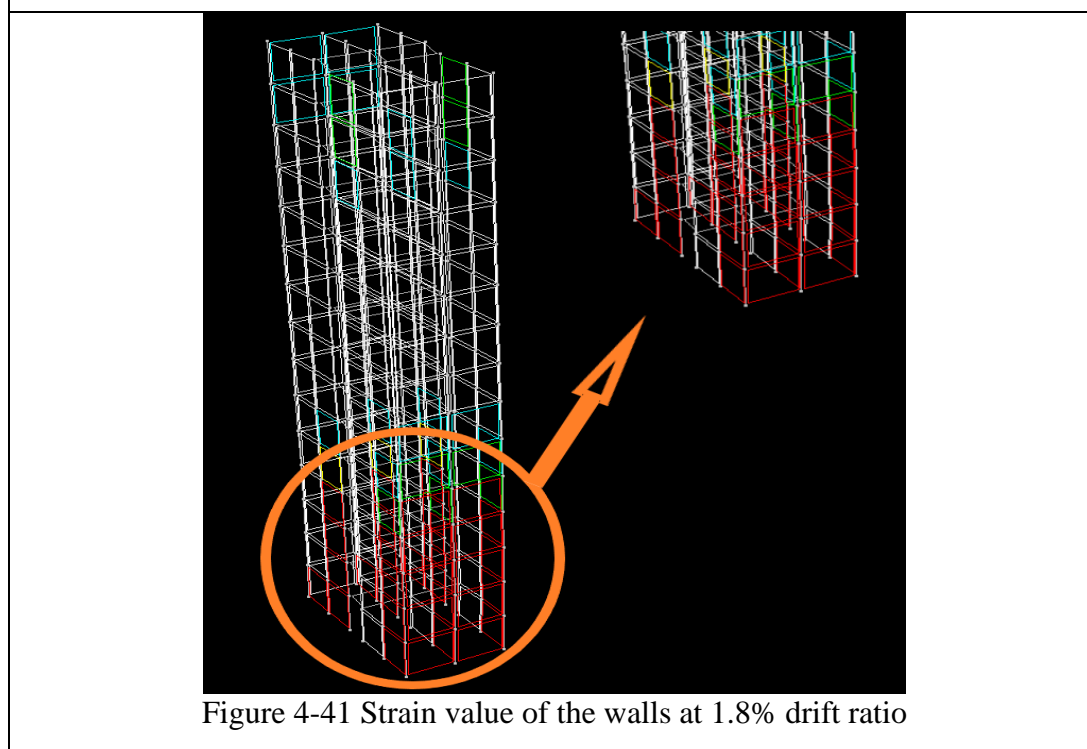
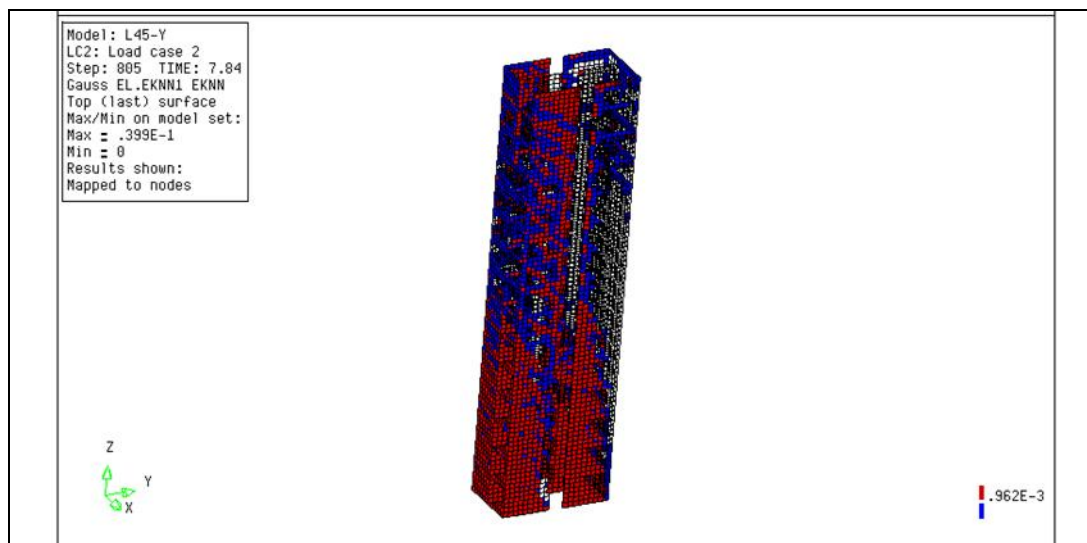


Figure 4-39 Strain value of the walls at 0.18% drift ratio



When the results of both computer programs are studied, it is observed that longitudinal reinforcements start yielding at the beginning of strain hardening. At the

end of the analysis, nearly all of the longitudinal reinforcements that stay in tension zone yield as it is shown in Figure 4-42 and Figure 4-43.

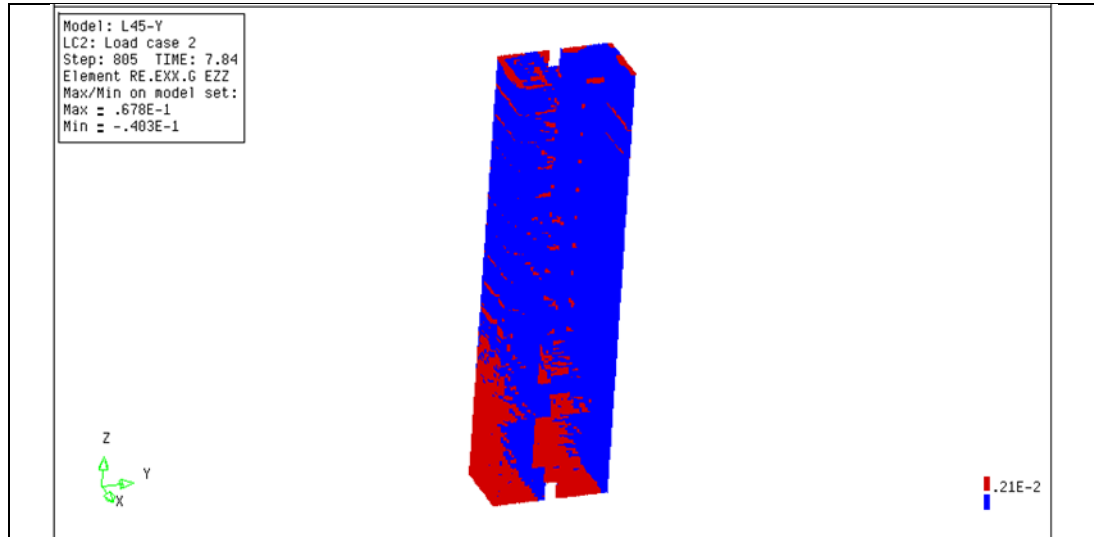


Figure 4-42 Yielding of longitudinal reinforcements in DIANA at 1.8% drift ratio

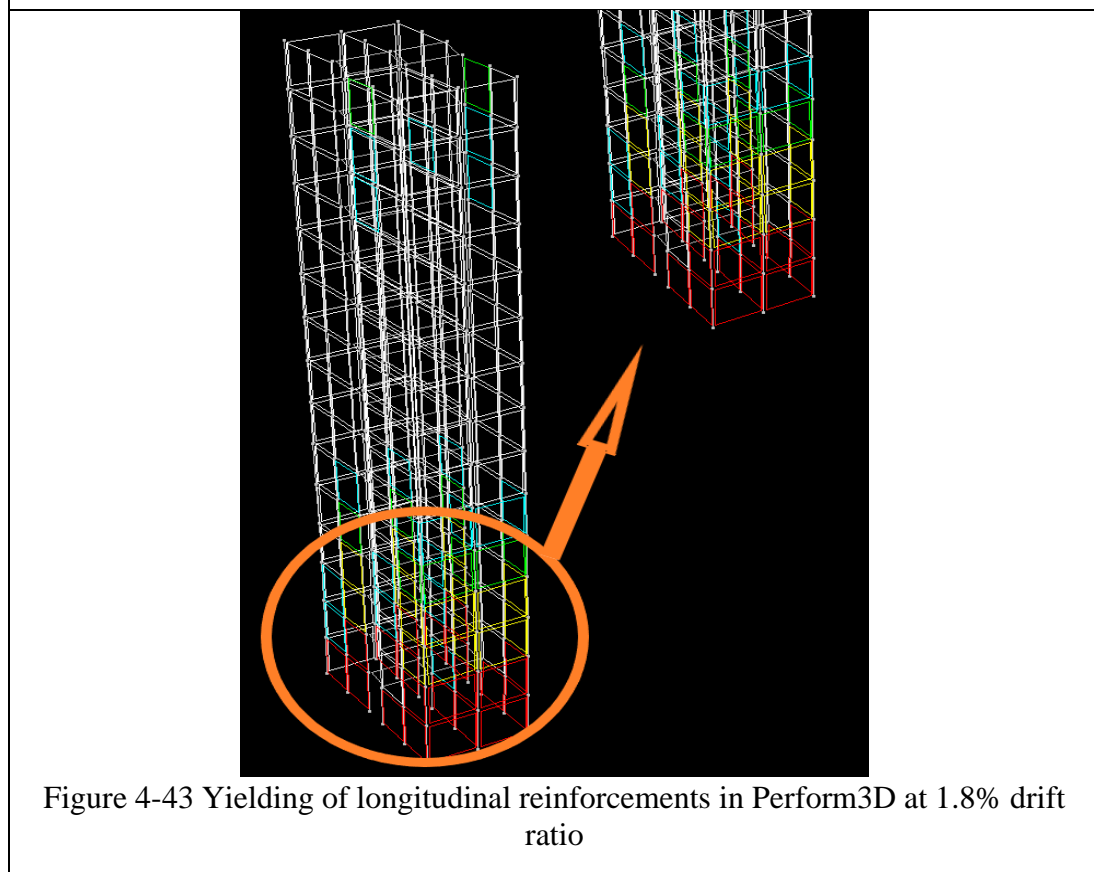
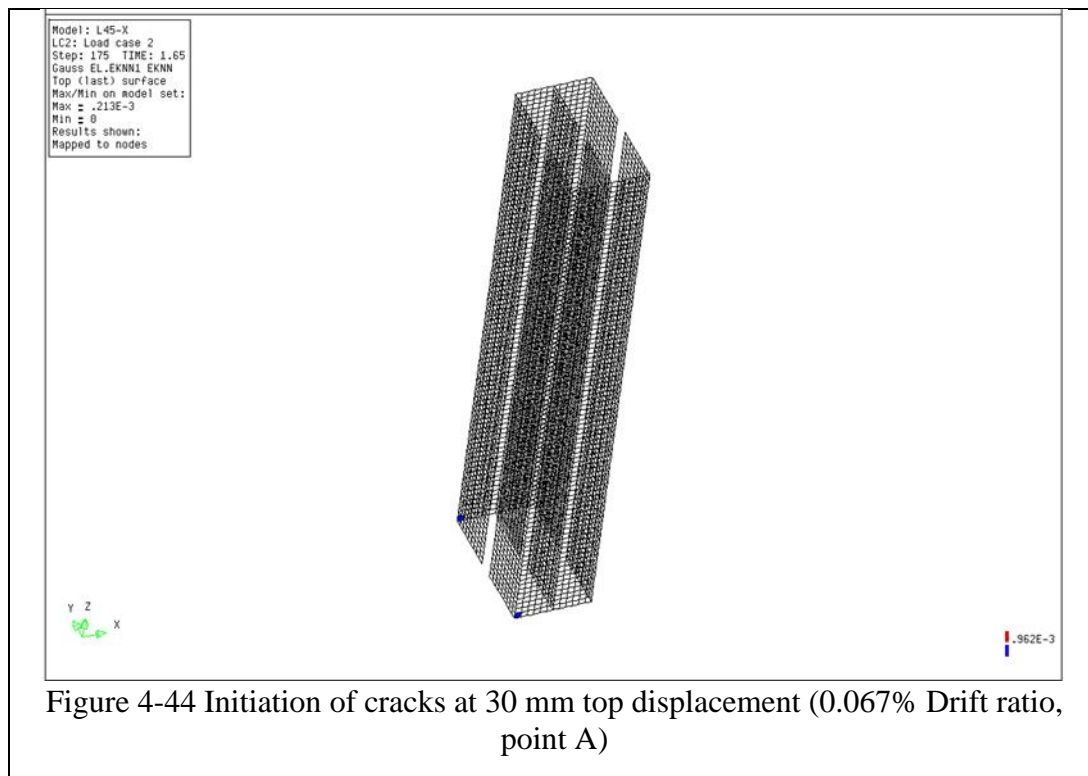


Figure 4-43 Yielding of longitudinal reinforcements in Perform3D at 1.8% drift ratio

When the results of the DIANA in the x direction are studied it is shown that building behaves elastically until 30 mm top displacement (0.067% drift ratio, point A in Figure 4-36) and all the cracks width are less than the limit value as it is shown in Figure 4-44. After that point, flexural cracks start and continue until 92.8 mm top displacement (0.21% drift ratio, point B in Figure 4-36) as it is shown in Figure 4-45. After that point strain hardening takes place and longitudinal reinforcements start yield. Figure 4-47 shows the cracks at the end of analysis (2.2% drift ratio, point C in Figure 4-36).

According to the results of Perform3D in x direction (Figure 4-36) structures shows elastic behavior up to 33 mm top displacement (0.07% Drift Ratio) and after 33 mm top displacement nonlinearity takes place. At 0.25% drift ratio strain value at the wall sections on the first floor passes the limit value as shown in Figure 4-46. Finally, Figure 4-48 shows the wall sections that have strain values more than limit value at the end of the analysis.



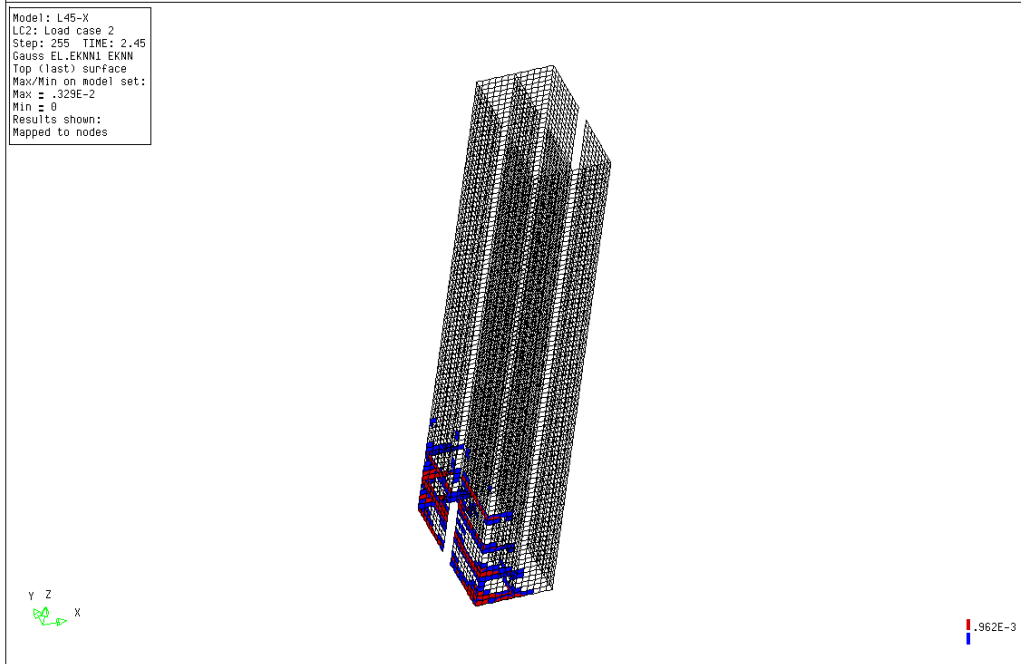


Figure 4-45 Flexural cracking strains at 92.8 mm top displacement (0.21% Drift ratio, point B)

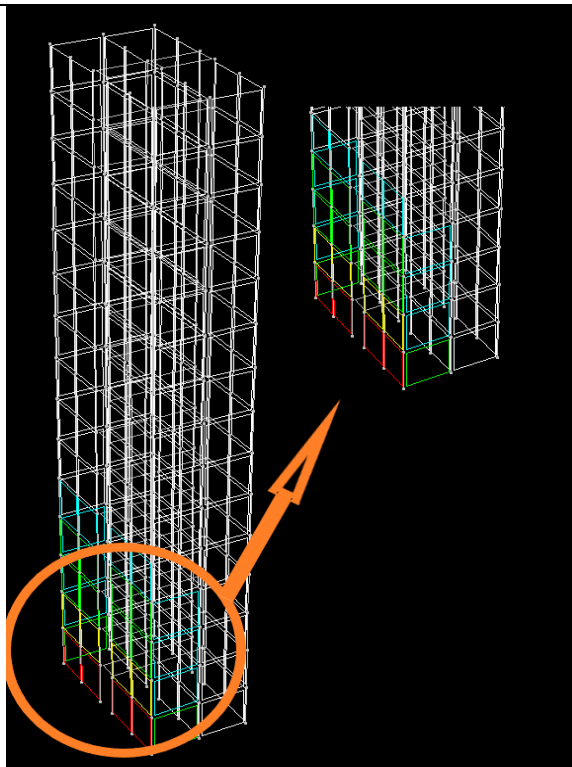


Figure 4-46 Wall sections that pass the limit strain value at 0.25% drift ratio

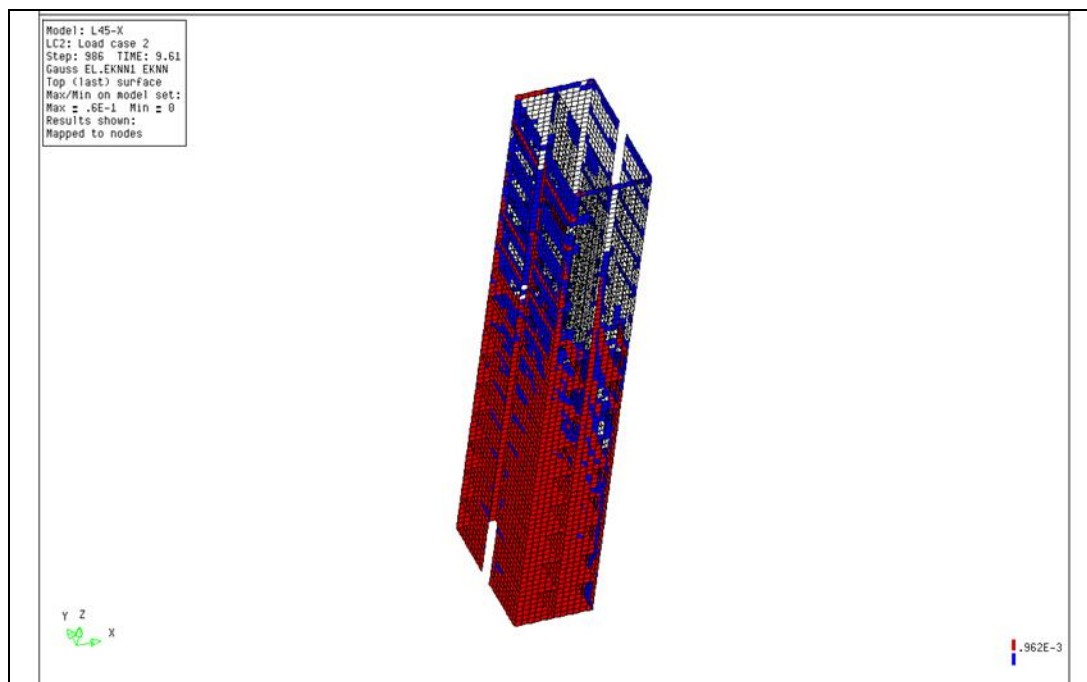


Figure 4-47 Flexural cracking strains at the end of the analysis (2.2% Drift ratio, point C)

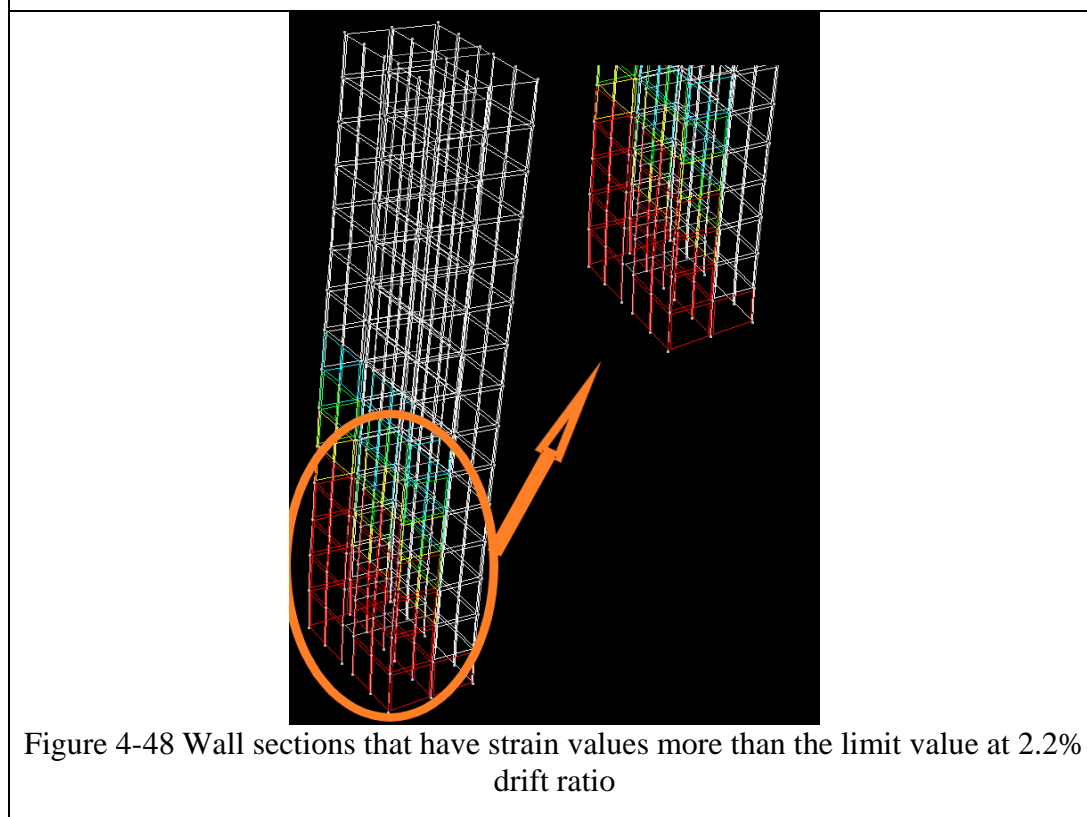


Figure 4-48 Wall sections that have strain values more than the limit value at 2.2% drift ratio

When behavior of the reinforcement is studied, results show that none of the longitudinal reinforcements yield up to strain hardening. However, at the end of the analysis, all of the longitudinal reinforcements which stay in tension zone yield as shown in Figure 4-49 and Figure 4-50.

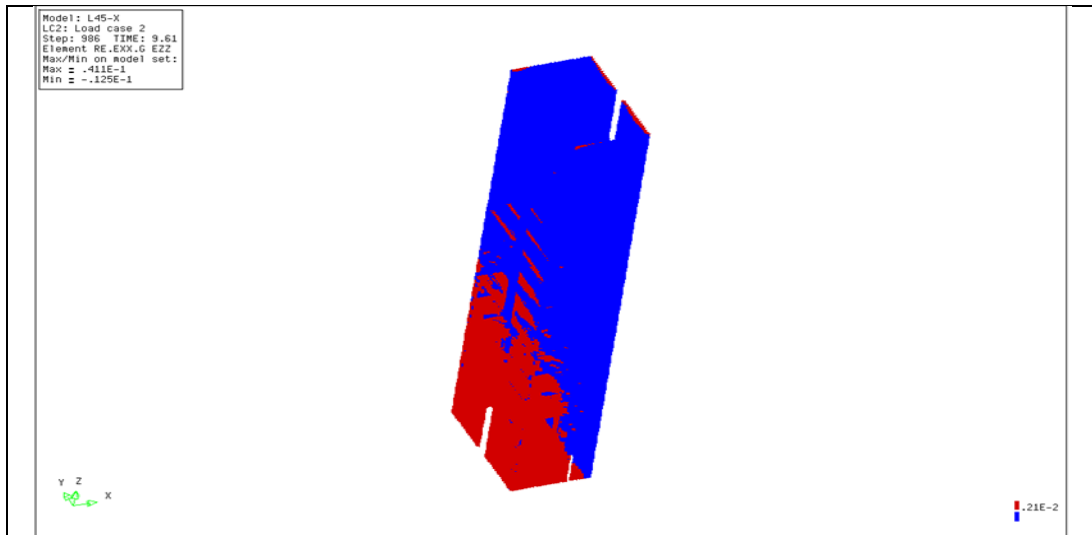


Figure 4-49 Yielding of longitudinal reinforcement in DIANA at 2.2% drift ratio

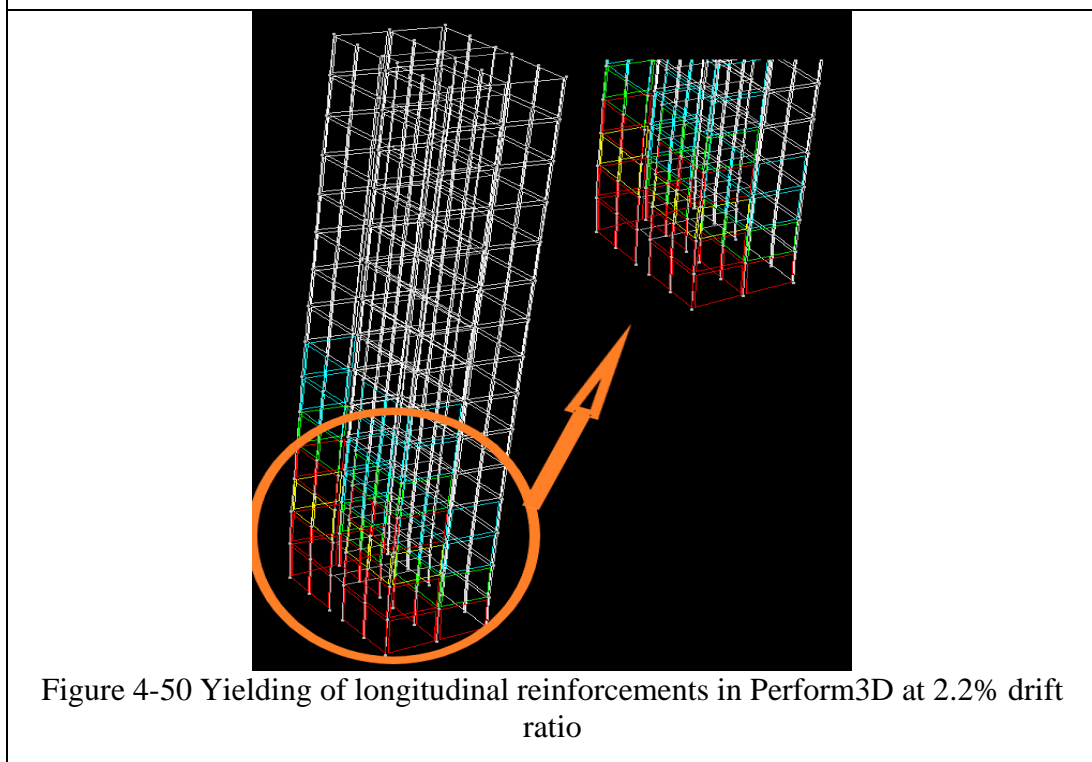


Figure 4-50 Yielding of longitudinal reinforcements in Perform3D at 2.2% drift ratio

As the pushover analysis results of tall building are studied, it can be said that results are comparably well compared to the short building. It is a known fact that as the slenderness ratio of the building increases, the effect of shear decreases. The most important deficiency of the analysis programs such as Perform3D is that they cannot couple the nonlinear flexure and shear behavior. First of all, as it is understood from the Figure 4-35 and Figure 4-36 initial stiffness value of the structure up to the end of the elastic behavior is same in DIANA and Perform3D. After than the building shows nonlinear behavior and the results of the program show difference. One of the reason of this difference is the effect of the shear. When the results in y direction is studied, the difference can also be explained with the coupling of walls in addition to shear. Since we know that slabs have coupling effect on the walls in Perform3D and this increases the capacity of the structure. In x direction, the difference is too much compared to y direction and this can be explained with the overestimation of the capacity when the flange section is under tension.

4.3. Time-History Analysis

After completing pushover analysis, before finishing this study, it was decided to perform nonlinear time history analysis with asymmetric structures in order to see the effect of torsion. Cross section properties of the asymmetric structure are presented in Figure 4-51. Reinforcements of the asymmetric structures were selected as same with the symmetric structures. Reinforcements and properties of ground motions that were used in the analyses are presented in APPENDIX B.

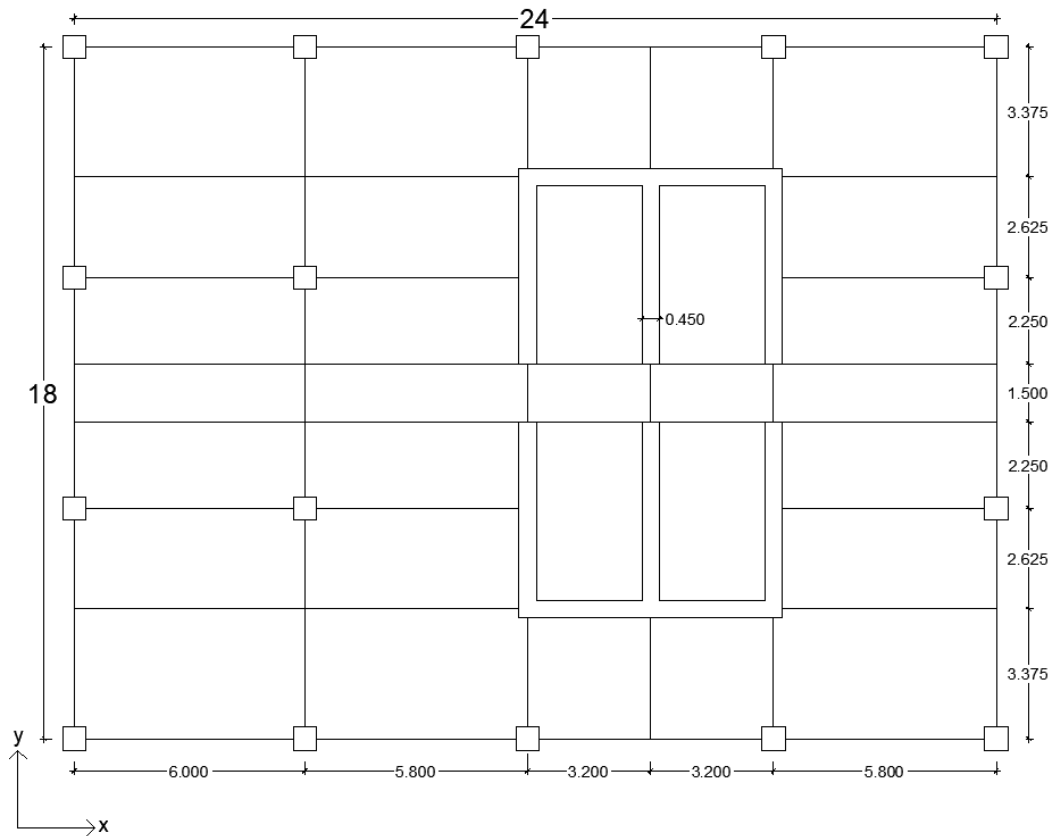


Figure 4-51 Floor plan of the asymmetric buildings (in meters)

4.3.1. Time-History Analysis of 4-Storey Structures

Time history analyses were firstly performed for the short buildings with utilizing Perform3D and DIANA. In analyses, 2.5% damping ratio was used for all structures (PEER and ATC72-1,2010).

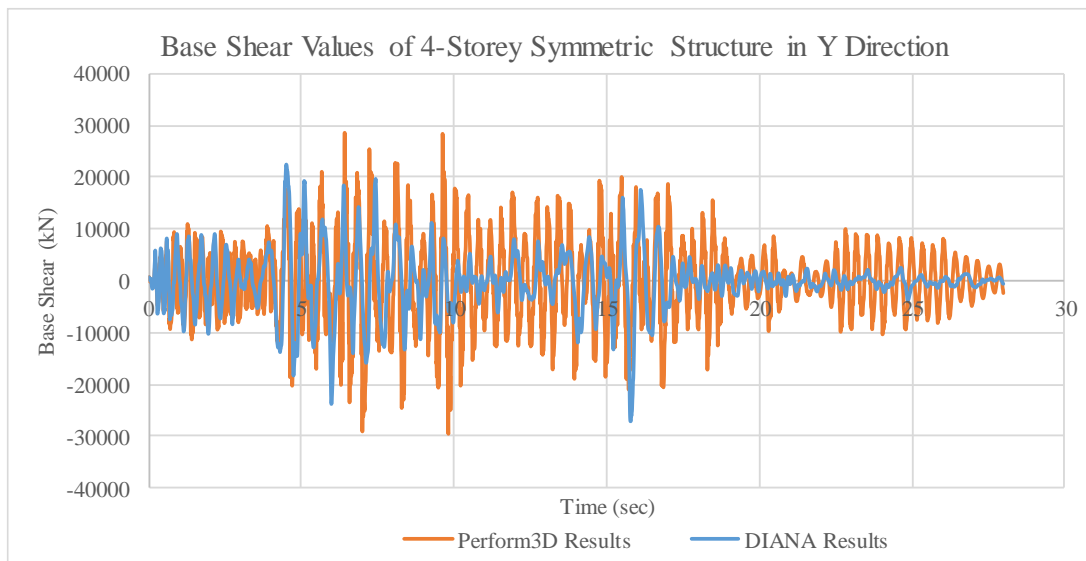


Figure 4-52 Time history analysis results of 4-storey symmetric structure in Y direction

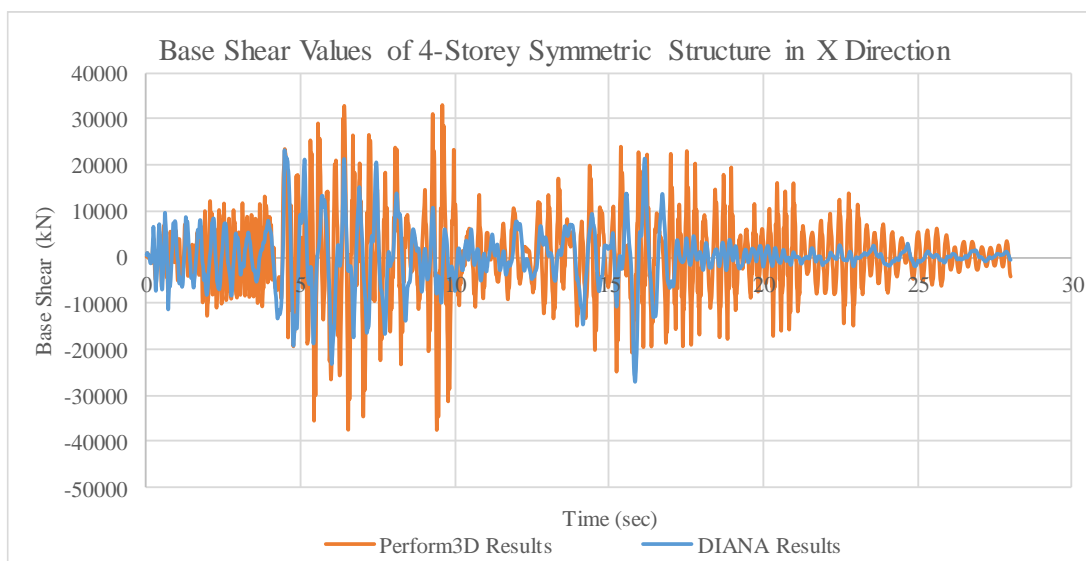


Figure 4-53 Time history analysis results of 4-storey symmetric structure in X direction

Figure 4-52 and Figure 4-53 show the time history analysis results of 4-storey symmetric structure. When the output of the computer programs compared, it seems that results are as expected. It is known that for short structures shear behavior governs but as it is stated before, Perform3D cannot calculate the nonlinear shear and flexural

behavior together. Therefore, Perform3D gives higher shear capacity value than DIANA.

Time history analysis results were studied in terms of drift ratio and displacement. Table 4-2 and Table 4-3 show the analysis results in tabular form. Since the structure is symmetric too much rotation is not expected. Therefore, rotation of the building is not studied.

Table 4-2 Time history analysis results of 4-storey symmetric structure in Y direction

	DIANA Results		Perform3D Results	
	Max. Displacement (mm)	Drift Ratio (%)	Max. Displacement (mm)	Drift Ratio (%)
Storey 1	22	0.73	15	0.50
Storey 2	70	1.16	46	0.77
Storey 3	112	1.24	80	0.89
Storey 4	147	1.23	113	0.94

Table 4-3 Time history analysis results of 4-storey symmetric structure in X direction

	DIANA Results		Perform3D Results	
	Max. Displacement (mm)	Drift Ratio (%)	Max. Displacement (mm)	Drift Ratio (%)
Storey 1	29	0.96	11	0.37
Storey 2	75	1.26	32	0.54
Storey 3	119	1.32	55	0.61
Storey 4	155	1.29	77	0.64

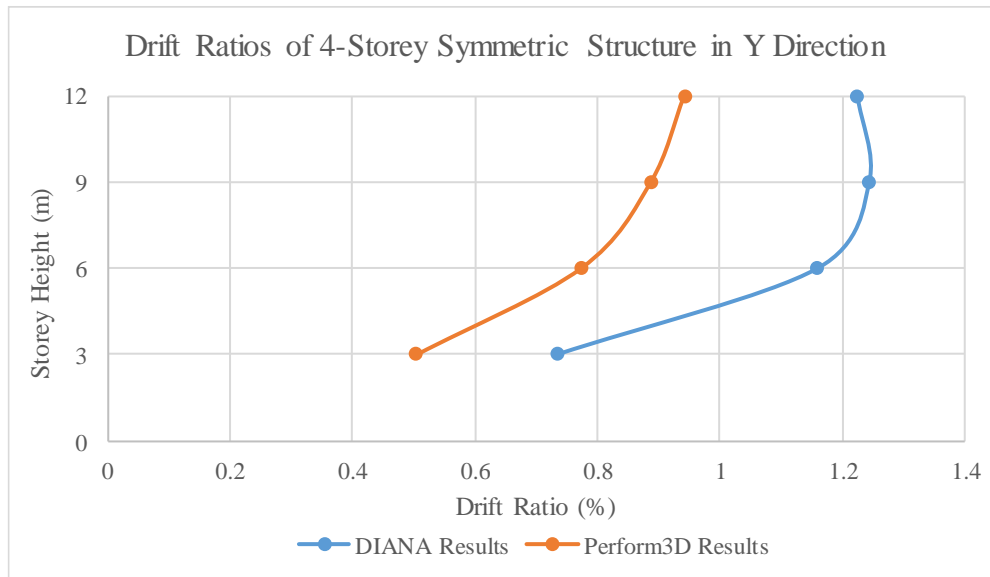


Figure 4-54 Comparison of drift ratios in Y direction for 4-storey symmetric structure

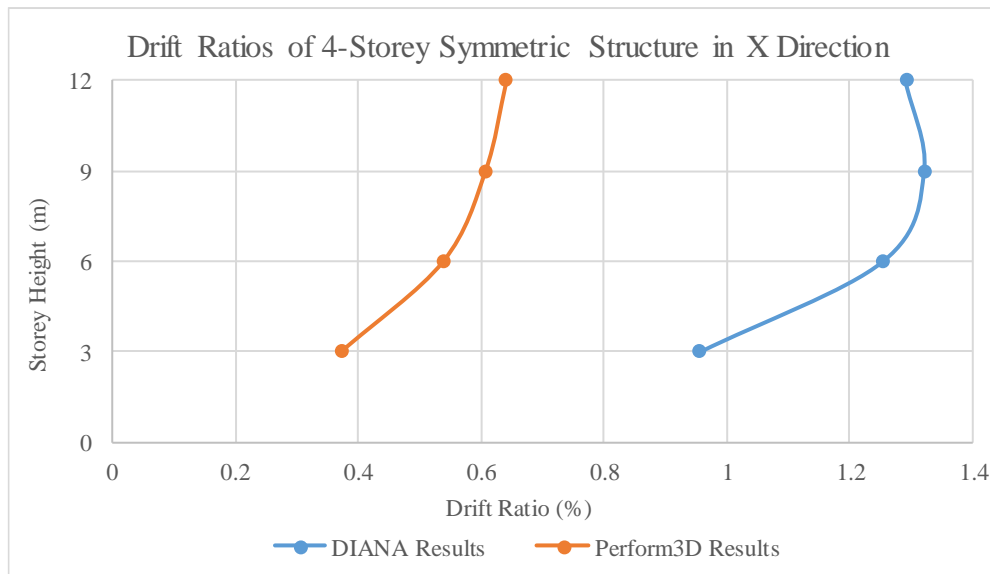


Figure 4-55 Comparison of drift ratios in X direction for 4-storey symmetric structure

When the analysis results are studied in terms of displacements and drift ratios, the difference between the stiffness of the model in different programs became more clear. Percent difference between the programs reaches 60% and 30% in x and y direction, respectively. As the pushover and time history analysis results are studied, it is seen

that stiffness of the model in Perform3D is more than the stiffness of the model in DIANA. This means that the model in DIANA is more fragile and make more displacement compared to Perform3D model especially in x direction.

Time history analyses of 4-storey asymmetric structure were performed with DIANA and Perform3D. Base shear results of 4-storey asymmetric structure are presented in Figure 4-56 and Figure 4-57. Table 4-4 and Table 4-5 show the analysis results in terms of displacement, drift ratio and rotation. As it is understood from these tables, percent difference between the programs reaches 54% and 20% in x and y direction, respectively. Although structure is asymmetric, in Perform3D, no rotation is observed.

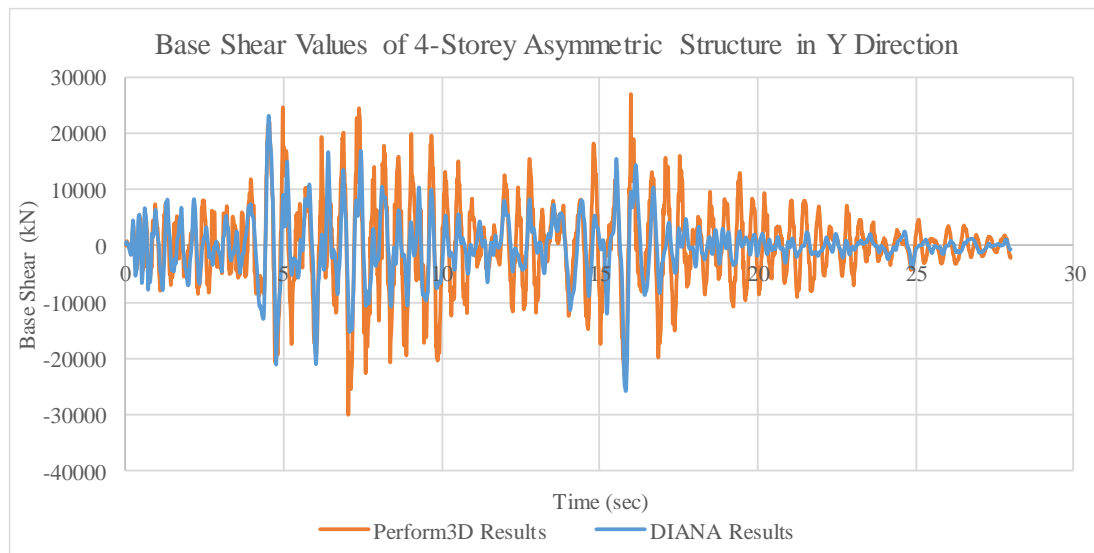


Figure 4-56 Time history analysis results of 4-storey asymmetric structure in Y direction

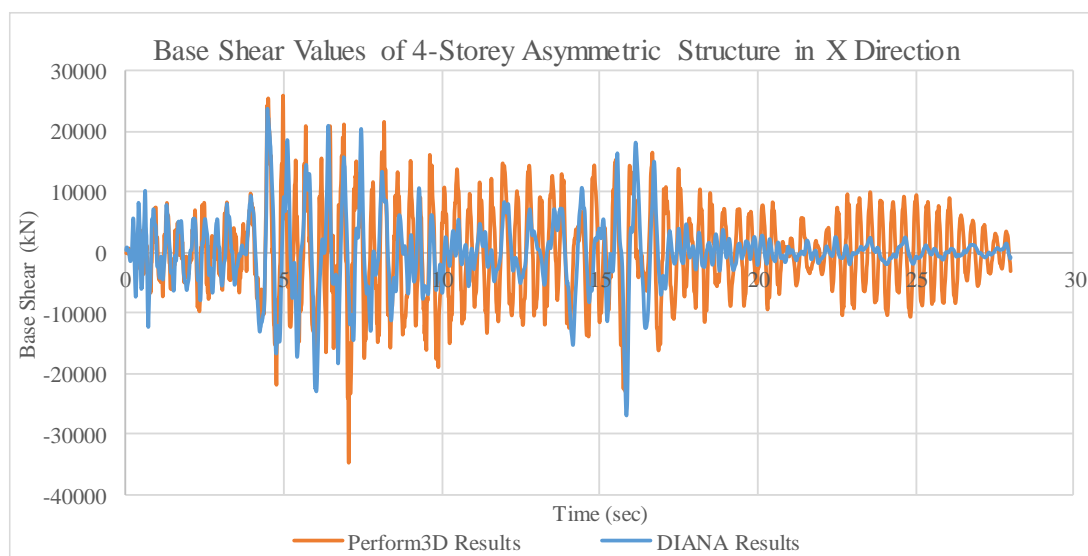


Figure 4-57 Time history analysis results of 4-storey asymmetric structure in X direction

Table 4-4 Time history analysis results of 4-storey asymmetric structure in Y direction

	DIANA Results			Perform3D Results		
	Max. Disp. (mm)	Drift Ratio (%)	Rotation (degree)	Max. Disp. (mm)	Drift Ratio (%)	Rotation (degree)
Storey 1	24	0.81	0.005	19	0.64	0.009
Storey 2	60	1.00	0.009	58	0.97	0.031
Storey 3	98	1.09	0.036	100	1.11	0.057
Storey 4	132	1.10	0.069	140	1.17	0.079

Table 4-5 Time history analysis results of 4-storey asymmetric structure in X direction

	DIANA Results			Perform3D Results		
	Max. Disp. (mm)	Drift Ratio (%)	Rotation (degree)	Max. Disp. (mm)	Drift Ratio (%)	Rotation (degree)
Storey 1	29	0.98	0.028	13	0.45	0
Storey 2	75	1.24	0.065	40	0.66	0
Storey 3	116	1.29	0.086	68	0.75	0
Storey 4	151	1.26	0.092	96	0.80	0

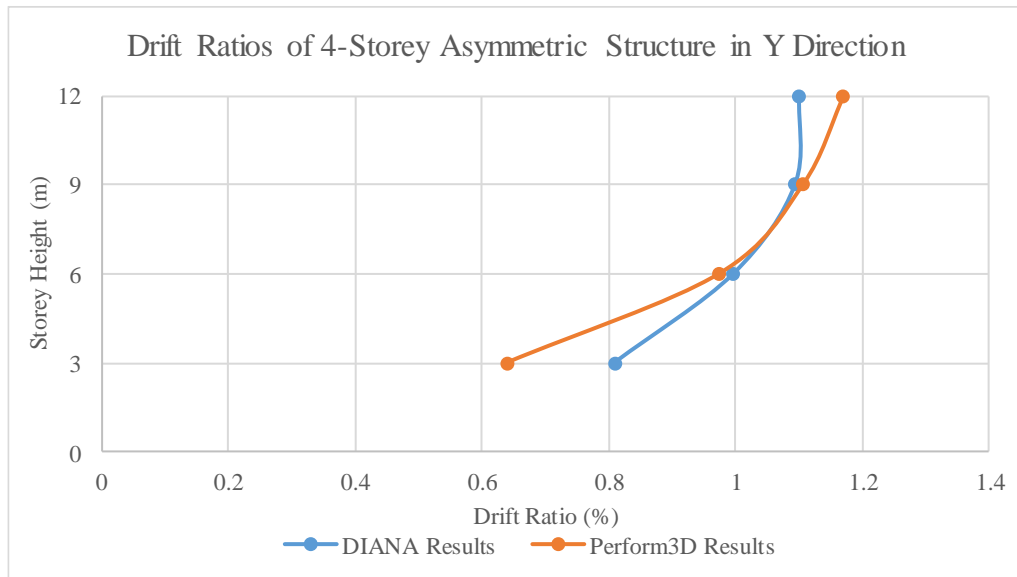


Figure 4-58 Comparison of drift ratios in Y direction for 4-storey asymmetric structure

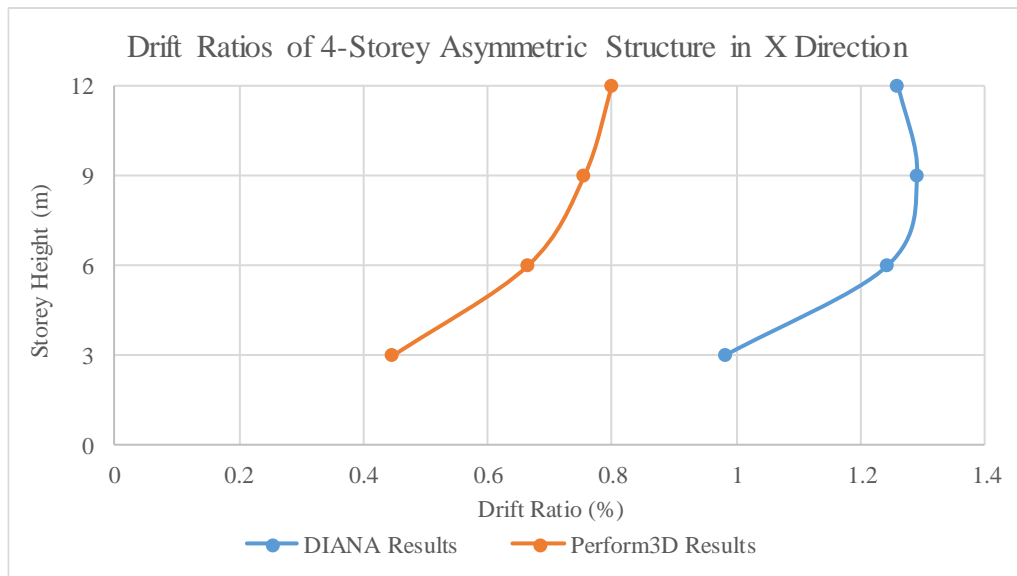


Figure 4-59 Comparison of drift ratios in X direction for 4-storey asymmetric structure

Asymmetric structure has asymmetry in y direction. So it is expected to get smaller base shear capacity in y direction compared to the symmetric structure. Results of both programs are as expected. Since Perform3D cannot take into account the torsion effectively, the capacity of the asymmetric structure is nearly same with symmetric

structure in x direction. This is more understandable from drift ratio graphs. In DIANA, stiffness of the structure decreases in both directions especially in y direction because of the asymmetry. Hence, the difference between drift ratios in x direction is more compared to symmetric structure. On the other hand, in y direction, since capacity of the structures in different programs is more convenient compared to symmetric structure, drift ratios became more similar.

As a general conclusion, for short buildings since shear governs the behavior of the structure, complete finite element programs that can couple the nonlinear shear and flexural behavior should be used in analysis.

4.3.2. Time-History Analysis of 15-Storey Structures

After completing time history analysis of short buildings, time history analyses were performed for 15-storey structures. Figure 4-60 and Figure 4-61 show the time history analysis results of 15-storey symmetric structure in terms of base shear.

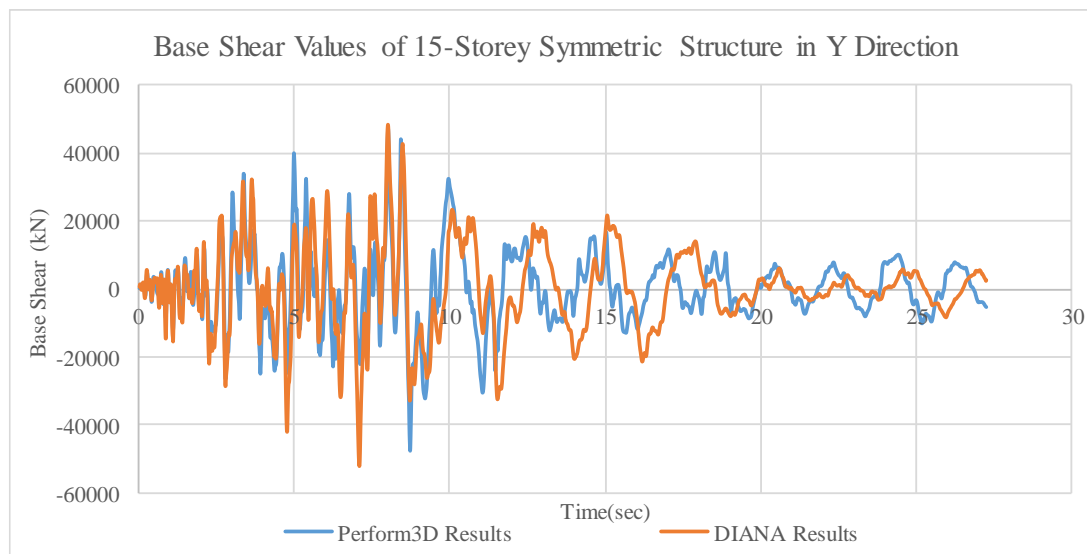


Figure 4-60 Time history analysis results of 15-storey symmetric structure in Y direction

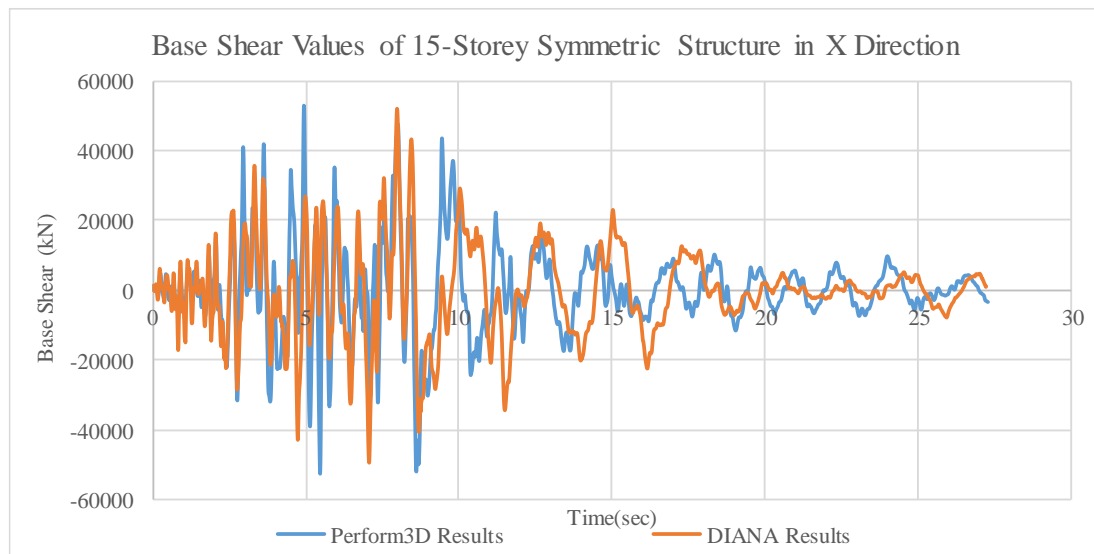


Figure 4-61 Time history analysis results of 15-storey symmetric structure in X direction

As these results are studied, it is seen that analyses results are compatible with the pushover analysis results. According to pushover analysis results, stiffness of the Perform3D model is more than the stiffness of the DIANA model and this means that under the same earthquake load, displacements became more in DIANA model.

Time history analysis results were studied in terms of drift ratio and displacement. Table 4-6 and Table 4-7 show the analysis results in tabular form. Rotation of the building is not studied, since the structure is symmetric.

Table 4-6 Time history analysis results of 15-storey symmetric structure in Y direction

	DIANA Results		Perform3D Results	
	Max. Displacement (mm)	Drift Ratio (%)	Max. Displacement (mm)	Drift Ratio (%)
Storey 1	30	1.01	22	0.73
Storey 2	82	1.37	71	1.19
Storey 3	147	1.63	129	1.43
Storey 4	222	1.85	195	1.62
Storey 5	304	2.03	267	1.78
Storey 6	390	2.17	341	1.90
Storey 7	478	2.28	415	1.98
Storey 8	568	2.37	490	2.04
Storey 9	656	2.43	563	2.09
Storey 10	742	2.47	637	2.12
Storey 11	825	2.50	710	2.15
Storey 12	904	2.51	784	2.18
Storey 13	980	2.51	858	2.20
Storey 14	1050	2.50	932	2.22
Storey 15	1120	2.49	1008	2.24

Table 4-7 Time history analysis results of 15-storey symmetric structure in X direction

	DIANA Results		Perform3D Results	
	Max. Displacement (mm)	Drift Ratio (%)	Max. Displacement (mm)	Drift Ratio (%)
Storey 1	31	1.04	22	0.55
Storey 2	87	1.45	71	0.75
Storey 3	150	1.67	129	0.92
Storey 4	221	1.84	195	1.05
Storey 5	295	1.97	267	1.17
Storey 6	372	2.07	341	1.26
Storey 7	450	2.14	415	1.33
Storey 8	530	2.21	490	1.39
Storey 9	610	2.26	563	1.45
Storey 10	689	2.30	637	1.49
Storey 11	768	2.33	710	1.54
Storey 12	845	2.35	784	1.58
Storey 13	919	2.36	858	1.61
Storey 14	990	2.36	932	1.64
Storey 15	1060	2.36	1008	1.67

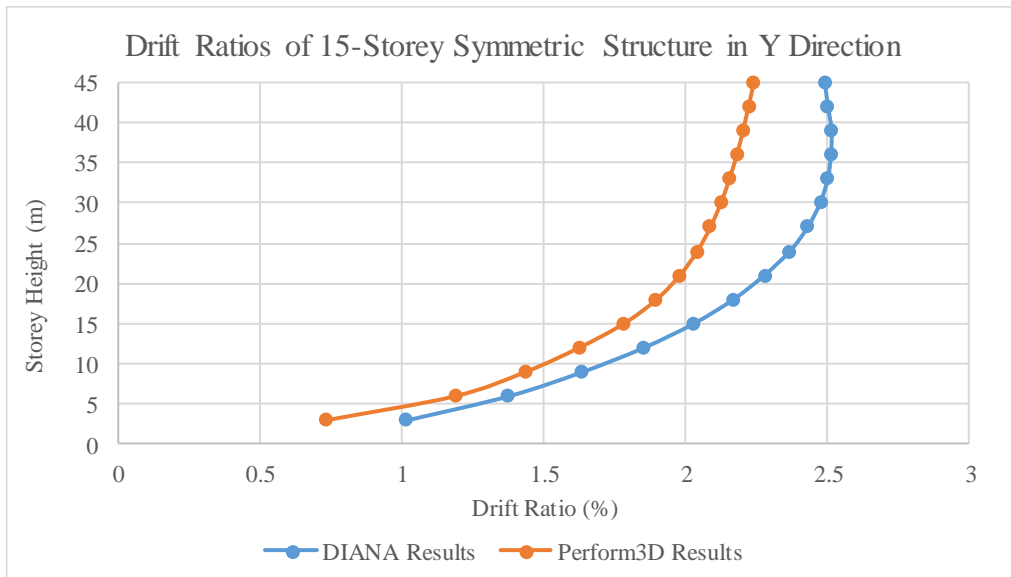


Figure 4-62 Comparison of drift ratios in Y direction for 15-storey symmetric structure

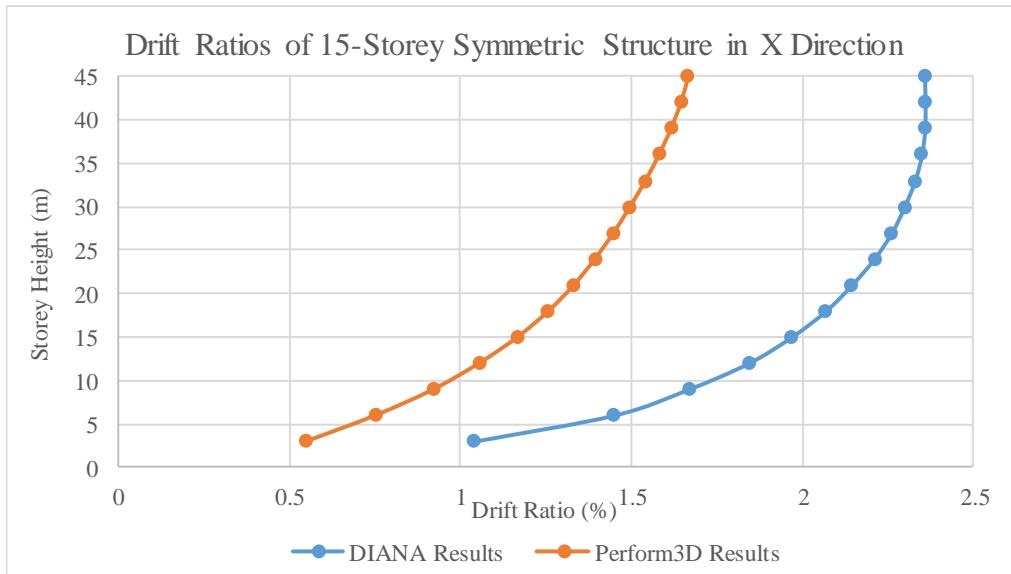


Figure 4-63 Comparison of drift ratios in X direction for 15-storey symmetric structure

As it is understood from the results of pushover analysis, stiffness of the models in different programs are nearly same in y direction and difference in x direction is less compared to short building. The difference is also seen from the Table 4-6 and Table 4-7, percent difference between the programs is about 35% and 15% in x and y

directions, respectively. This can also be interpreted from the drift ratios. In y direction, drift ratios look similar but in x direction drift ratios are different because of the difference in stiffness.

15-storey asymmetric structure was modeled with Perform3D and DIANA with the same assumptions such as columns and slabs are taken as elastic and slab stiffness decreases to 25%. Analysis results of asymmetric structure in terms of base shear versus time are presented in Figure 4-64 and Figure 4-65. Table 4-8 and Table 4-9 show the results in terms of displacement, drift ratio and rotation.

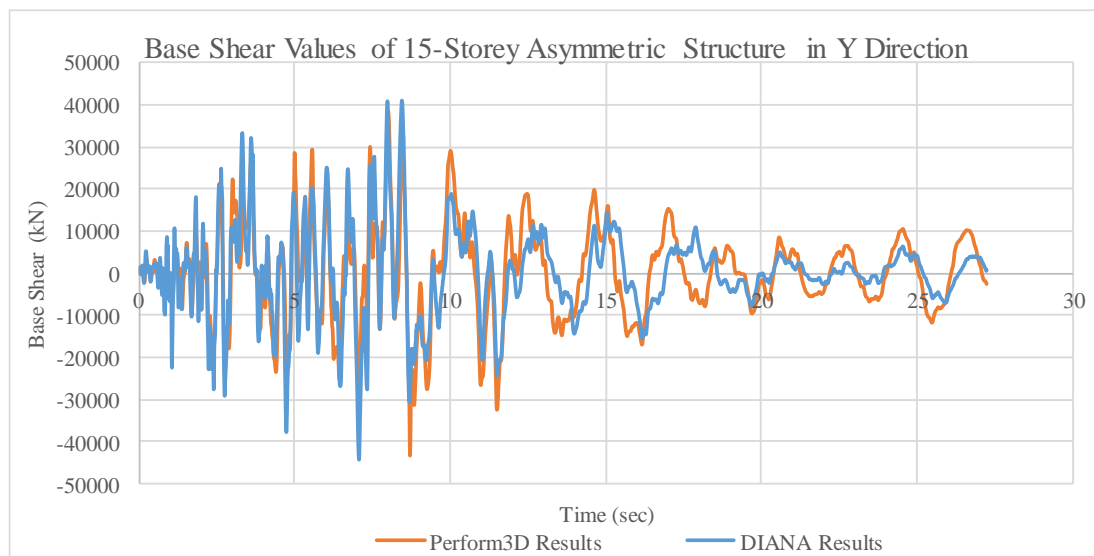


Figure 4-64 Time history analysis results of 15-storey asymmetric structure in Y direction

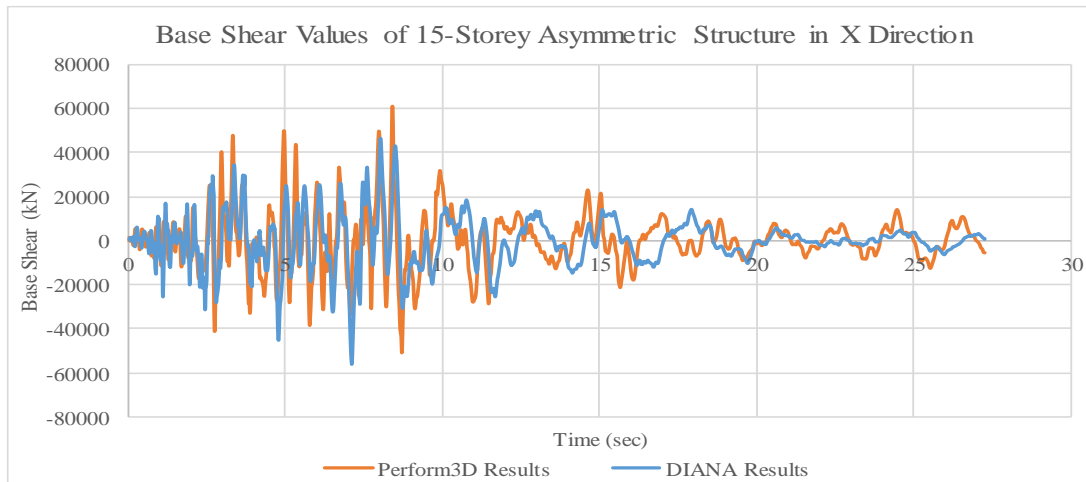


Figure 4-65 Time history analysis results of 15-storey asymmetric structure in X direction

Table 4-8 Time history analysis results of 15-storey asymmetric structure in Y direction

	DIANA Results			Perform3D Results		
	Max. Disp. (mm)	Drift Ratio (%)	Rotation (degree)	Max. Disp. (mm)	Drift Ratio (%)	Rotation (degree)
Storey 1	25	0.85	0.016	25	0.82	0.022
Storey 2	68	1.14	0.076	78	1.30	0.073
Storey 3	121	1.34	0.165	138	1.54	0.142
Storey 4	180	1.50	0.265	204	1.70	0.219
Storey 5	246	1.64	0.365	276	1.84	0.301
Storey 6	314	1.74	0.463	350	1.95	0.388
Storey 7	386	1.84	0.544	425	2.02	0.479
Storey 8	459	1.91	0.609	499	2.08	0.568
Storey 9	532	1.97	0.647	573	2.12	0.652
Storey 10	605	2.02	0.666	646	2.15	0.727
Storey 11	676	2.05	0.661	720	2.18	0.792
Storey 12	745	2.07	0.637	798	2.22	0.846
Storey 13	809	2.07	0.664	880	2.26	0.910
Storey 14	869	2.07	0.740	964	2.29	0.983
Storey 15	924	2.05	0.807	1045	2.32	1.055

Table 4-9 Time history analysis results of 15-storey asymmetric structure in X direction

	DIANA Results			Perform3D Results		
	Max. Disp. (mm)	Drift Ratio (%)	Rotation (degree)	Max. Disp. (mm)	Drift Ratio (%)	Rotation (degree)
Storey 1	20	0.68	0.032	18	0.60	0
Storey 2	57	0.96	0.074	51	0.86	0
Storey 3	104	1.16	0.105	95	1.05	0
Storey 4	160	1.33	0.140	146	1.21	0
Storey 5	224	1.49	0.169	204	1.36	0
Storey 6	293	1.63	0.201	267	1.48	0
Storey 7	368	1.75	0.280	334	1.59	0
Storey 8	447	1.86	0.366	404	1.68	0
Storey 9	529	1.96	0.458	476	1.76	0
Storey 10	612	2.04	0.547	547	1.82	0
Storey 11	696	2.11	0.633	618	1.87	0
Storey 12	779	2.16	0.702	689	1.91	0
Storey 13	860	2.21	0.786	759	1.95	0
Storey 14	938	2.23	0.850	830	1.98	0
Storey 15	1010	2.24	0.926	901	2.00	0

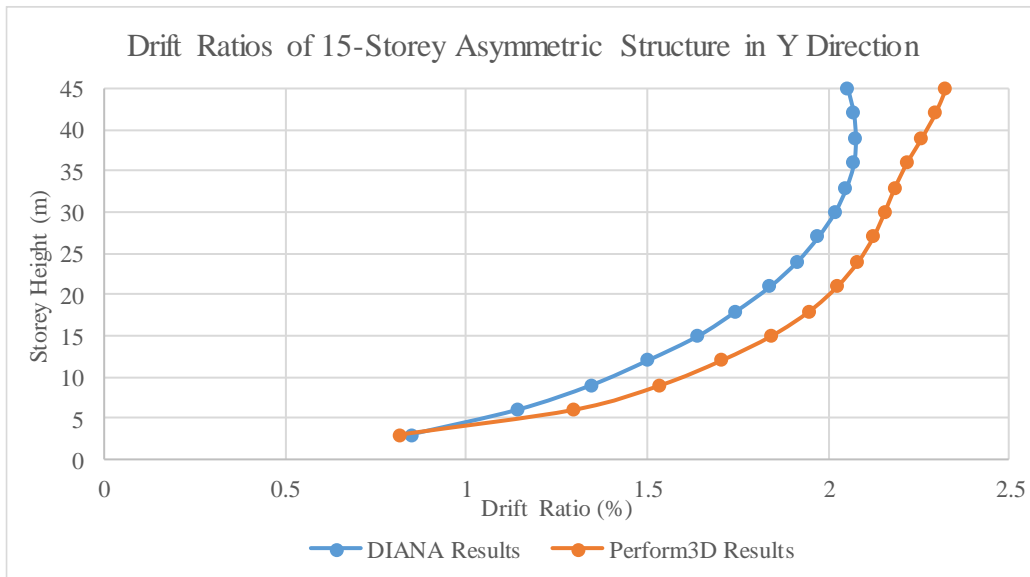


Figure 4-66 Comparison of drift ratios in Y direction for 15-storey asymmetric structure

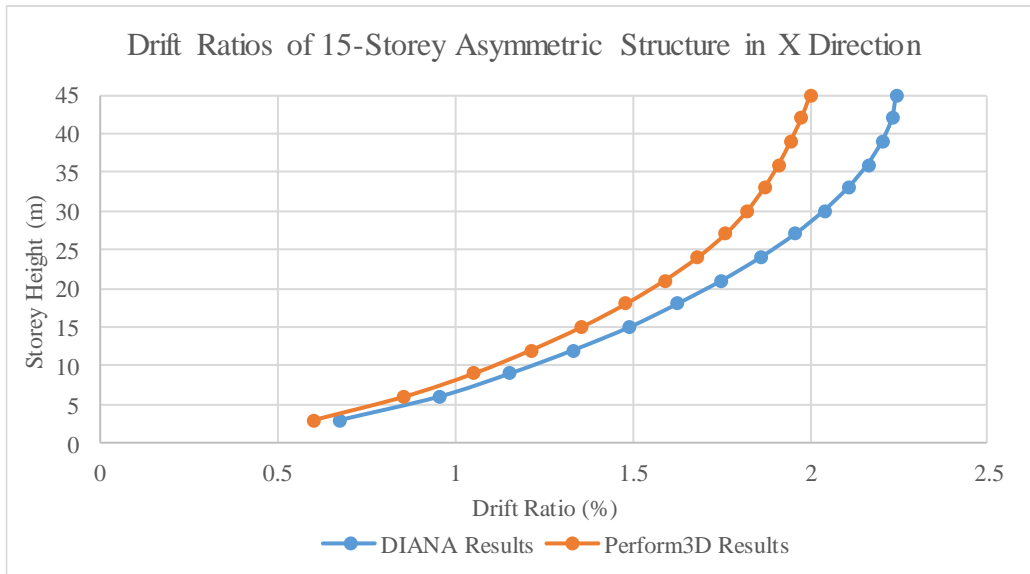


Figure 4-67 Comparison of drift ratios in X direction for 15-storey asymmetric structure

As it is understood from the results of time history analysis, stiffness of the models decreased because of the asymmetry. The difference between computer programs become less as it is also seen from the Table 4-8 and Table 4-9. Percent difference

between the programs is about 10% both for x and y directions. Although structure is asymmetric, Perform3D cannot capture any rotation in x direction.

4.4. Discussion of the Results

In this chapter, nonlinear analyses were performed for both squat and slender walls with different computer programs. Pushover analyses and time history analyses were performed for both walls. Moreover, in order to see the effect of torsion, asymmetric structures were modeled and time history analyses were performed. When the results of computer programs are compared it is seen that there are similarities and differences.

First, when the results of short building are compared, it is seen that the general behavior for both programs are same but in Perform3D capacity is always overestimated. Most important reason of this overestimation is that in Perform3D shear behavior is modeled elastically. In order to consider the effect of shear for the analysis of short buildings, complete finite element programs should be used.

Moreover, when the results of tall building are studied, it can be understood that results are more appropriate compared to short building. In y direction there is a small difference and this difference can be explained again with the definition of shear behavior in Perform3D. Also, in Perform3D slab has a coupling effect for walls and this also increases the capacity of the structure. But in the x direction, the difference is more compared to y direction. In Perform3D, when tension force applied to the flange section, it is calculated as flange section resist this force as a whole. This can be the reason of the difference.

Finally, the last part of this chapter is related with the torsion. In this part, in order to see the effect of torsion, asymmetric structures were modeled. As expected, because of the additional torsion, stiffness of the structural decreased. Related with this, base shear capacity also decreased and displacements were increased.

CHAPTER 5

SUMMARY AND CONCLUSION

Need for tall building is increasing consistently and approximately nearly thousands of structures over 100 meters are being constructed and more than this number are currently planned all over the world. Analysis of tall buildings under reversal loadings is confusing problem in civil engineering. Because of this reason, performance based and design approach is generally preferred. Although this method of analysis is more reliable, there are some complexities in modeling of structural walls. For example, modeling of flanged wall section and calculation of the interaction of the connecting members such as slabs and columns. Thus, this thesis mainly focused on comparison of different nonlinear modeling approaches for structural walls.

At first, elastic analyses were performed for calibration. For this purpose, by using different modeling approaches, typical wall layouts were analyzed. Box section and C-shaped section were selected for wall layouts and pure torsion and pure bending analyses were performed. Finite element method, mid-column method and modified mid-column method were used in analyses. When the elastic analysis results of box section are studied for pure torsion, it can be concluded that mid column method calculate stiffness of the system too much. Therefore, provide smaller displacement values compared to approximate solution (for selected section, result of this method is nearly 5 times smaller than the approximate result). Stiffness calculation problem of mid-column method can be solved by the modified mid-column method up to acceptable level. Modified mid-column method decreases the stiffness of the system by arranging the torsional stiffness of the members. Although modified mid-column method provides acceptable results, closest results to theoretical solution can be obtained from finite element method. When torsion analysis results of C-shaped section are considered, same words can be said. Mid-column method again

overestimates the capacity of the system and cannot calculate the effect of warping. On the other hand, finite element method gives most acceptable results by considering warping effect. Same sections were also analyzed for pure bending with mid-column method and finite element method. In bending analysis, modified mid-column method was not used, since it was proposed for torsion analysis. As in the torsion analyses, mid-column method overestimates the stiffness of the system but finite element method can provide acceptable results. Thus, as a conclusion of these analyses, it can be said that finite element method is the best modeling approach for the elastic analysis of structural walls.

As a second step, behavior of planar and flanged structural walls were modeled nonlinearly. The distributed inelasticity (fiber) modeling approach and the continuum based nonlinear modeling approach were used for these analyses. In order to use the fiber model, ETABS and Perform3D were used and to use the continuum model, DIANA was used. Analysis results were compared with each other by taking experimental results as a reference. When the results of RW2 are compared, it is seen that the fiber model overestimates the initial stiffness of the wall. But as a general conclusion, it can be said that for regular sections such as rectangular, the fiber method predicts the nonlinear behavior of the structure at acceptable level. When the results of TW2 are compared, again fiber model overestimates the initial stiffness of the section in both directions. But in addition, when the flange of the specimen is under tension, the fiber model assumes it as all flange resist the tension and so over-estimates the capacity. The reason of the difference between the analysis results and experimental results can also be explained with the nonlinear tensile strain distribution of the flange. As the experimental results studied, it is seen that tensile strain along the width of the flange follow a nonlinear distribution and this distribution cannot be captured by the fiber model. But, if the results of the continuum model are compared with the experimental results, it can be said that the continuum model perfectly estimate the nonlinear behavior of reinforced concrete structures even for irregular geometries.

As a final step, in order to see the effect of nonlinear shear and flexure together, behavior of squat and slender walls were compared. In order to represent the squat wall and slender wall 4-storey and 15-storey structures were used. These buildings were modeled elastically with ETABS and designed according to ASCE 7-10 and ACI-318R-08. Then by using the fiber and the continuum modeling approaches, these buildings were modeled nonlinearly. First, nonlinear pushover analyses were performed according to FEMA to compare the behavior of these structures. First, pushover analyses were performed with 4-storey structure. In these analyses, slabs and columns were taken elastic and the only nonlinearity was defined for structural walls. As the analyses results studied, it can be seen that although the general behavior of the building is same there are some differences between the results of the programs. Perform3D overestimates the capacity of the structure. As it is known, shear governs the behavior of the short building and since Perform3D cannot couple the nonlinear shear and flexural behavior together, capacity is over-estimated in Perform3D. Moreover, the capacity difference in weak direction can also be explained with the coupling of the walls. In Perform3D, slabs work as a coupling beam and this increases the capacity. In addition, as it is known from the nonlinear calibration studies, in the fiber modeling approach when flange section is under tension force, it is assumed as all section resist this force and thus capacity is overestimated. This can be shown as a reason for the capacity difference in strong direction.

Later, pushover analyses were performed for 15-storey structure. In contrast to analyses of short structure, results of computer programs are more convenient for tall building. One of the main reason of this convenience is that the effect of shear is low for tall buildings. In weak direction, results of computer programs are nearly same. The difference can be explained with the coupling effect of slabs and small effect of shear. The difference in strong direction attracts the attention. In Perform3D, when tension force applied to the flange section, it is calculated as flange section resist this force as a whole. This can be the reason of the difference.

Time history analyses were performed in order to see the effect of the torsion and the capability of the program for calculating torsion effect. In order to do this, 4 and 15-storey asymmetric structures were modeled and analyzed. First, pushover analysis results and time history analysis results were studied for symmetric structures in terms of base shear values. Later, time history analysis results of symmetric and asymmetric structures were studied in terms of base shear, displacements and drift ratio. When the analyses results are studied for symmetric structure, it is seen that time history analyses results and pushover analyses results are coinciding. For example, for short buildings, Perform3D overestimates the stiffness of the structure because of the effect of shear does not taken into account. On the other hand, for tall buildings pushover analysis results and time history analysis results of the programs look similar, since effect of shear decreases for tall buildings. When the results are studied according to asymmetry, it can be seen that because of the additional torsion effect, stiffness of the structures decrease and structures become more fragile.

Final conclusions of this study can be summarized as follows;

- Finite element method is the best modeling approach for the linear elastic analysis of structural walls.
- Fiber modeling approach has the capability to predict the nonlinear behavior of planar structural walls. However, this approach overestimates the capacity of the flanged structural walls when the flange section is under tension.
- Continuum modeling approach can capture the nonlinear behavior of both planar and flanged structural walls.
- Fiber modeling approach cannot couple the nonlinear shear and flexural behavior. For structures in which shear governs such as squat wall, fiber modeling approach should not be preferred.
- When strong structural walls are used, rotation of the structure is expected but this rotation cannot be captured by the fiber modeling approach.

- Elastically modeled slabs cause coupling of the wall in the fiber modeling approach but this coupling effect is not observed in the continuum modeling approach.
- As the height increases, the slenderness ratio decreases which causes decreasing in the effect of shear. Therefore, fiber modeling approach can be used for the analysis of tall buildings.

REFERENCES

- ACI. (2008). *Building Code Requirements for Structural Concrete and Commentary* . Farmington Hills, Mishigan : American Concrete Institue .
- Akış, T. (2004). *Lateral Load Analysis of Shear Wall-Frame Structures*.
- Alendar, V., & Milicevic, M. (2015). *Study of Capabilities of Etabs 2015 Software for Performance Based Design*.
- ASCE 7-10. (2010). *Minimum Design Loads for Buildings and Other Structures*. Reston, Virginia: American Society of Civil Engineers.
- Belarbi, A., & Hsu, T. T. (1994). Constitutive Laws of Concrete in Tension and Reinforcing Bars Stiffened By Concrete. *Structural Journal*, 465-474.
- Chang, & Mander. (1994). *Seismic Energy Based Fatigue Damage Analysis of Bridge Columns: Part I-Evaluation of Seismic Capacity*. Buffalo: NCEER Technical Report.
- Coleman, J., & Spacone, E. (2001). Localization Issues in Force-Based Frame Elements. *ASCE*, 403-419.
- DIANA FEA User's Manual - Release 9.5*. (n.d.). Retrieved from DIANA FEA: <https://dianafea.com/manuals/d95/Diana.html>
- ETABS. (2017). *CSi Analysis Reference Manual*. Computer&Structures, INC.
- FEMA 440. (2005). *Improvement of Nonlinear Static Seismic Analysis Procedures*. Wahington, D.C.: Applied Technology Council for the Federal Emergency Management Agency.
- Fischinger, M. T. (1990). Validation of Macroscopic Model for Cyclic Response Prediction of RC Walls. In N. B. MAng, *Computer Aided Analysis and Design of Concrete Structures* (pp. 1131-1142). Swansea: Pineridge Press.

- Gerometta, M. (2009, December). *Height: Council on Tall Buildings and Urban Habitat*. Retrieved from Council on Tall Buildings and Urban Habitat: <http://www.ctbuh.org/>
- Kazaz, İ., Gülkan, P., & Yakut, A. (2012). Performance Limits for Structural Walls: An Analytical Perspective. *Engineering Structures*, 105-119.
- Kazaz, İ., Gülkan, P., & Yakut, A. (2012a). Deformation Limits for Structural Walls with Confined Boundaries. *Earthquake Spectra*, 1019-1046.
- Kutay Orakcal, L. M. (2006). *Analytical Modeling of Reinforced Concrete Walls for Predicting Flexural and Coupled-Shear-Flexural Responses*. Los Angeles.
- Mander, J. B., Priestley, M. J., & Park, R. (1988). Theoretical Stress-Strain Model for Confined Concrete. *Journal of Structural Engineering*, 1804-1826.
- Mc Guire, W. (1968). *Steel Structures*. Prentice Hall.
- Menegotto, & Pinto. (1973). Method of Analysis for Cyclically Loaded R.C. Plane Frames Including Changes in Geometry and Non-Elastic Behaviour of Elements Under Combined Normal Force and Bending. *IABSE Symposium on Resistance and Ultimate Deformability of Structures Acted on by Well-Defined Repeated Loads*, 15-22.
- Mullapudi, R., & Ayoub, A. (2009). Fiber Beam Element Formulation Using the Softened Membrane Model. *Aci Structural Journal*.
- Oosterle, R. (1979). *Earthquake Resistant Rtructural Walls-Tests of Isolated Walls*. Skokie.
- Orakcal, K. J. (2004). Flexural Modeling of Reinforced Concrete Walls - Model Attributes. *ACI Structural Journal* , 688-699.
- Özcebe, G., & Saatcioglu, M. (1989). Hysteretic Shear Model for Reinforced Concrete Members. *Journal of Structural Engineering*, 132-148.

- PEER, & ATC72-1. (2010). *Modeling and Acceptance Criteria for Seismic Design and Analysis of Tall Buildings*.
- Perform3D. (2016). *CSI, Components and Elements*. Computer&Structures, Inc.
- Petrangeli M, P. P. (1999). Fiber Element for Cyclic Bending and Shear of RC Structures. *Engineering Mechanics*, 994-1001.
- Saatcioglu, M. a. (1988). Response of reinforced concrete columns to simulated seismic loading. *ACI Structure*.
- Smith, B. S., & Girgis, A. (1986). Deficiencies in the Wide Column Analogy for Shearwall Core Analysis. *Concrete International*.
- Thomsen, J. H. (1995). *Displacement Based Design of Reinforced Concrete Structural Walls: An Experimental Investigation of Walls with Rectangular and T-Shaped Cross-Sections*.
- Timoshenko, S., & Goodier, J. (n.d.). *Theory of Elasticity*. McGraw-Hill.
- Vasquez, J. A., Llera, J. C., & Hube, M. A. (2016). A Regularized Fiber Element Model for Reinforced Concrete Shear Walls. *Earthquake Engineering and Structural Dynamics*, 2063-2083.
- Vecchio, F. C. (1986). The Modified Compression-Field Theory for Reinforced Concrete Elements Subjected to Shear. *ACI Structural Journal*, 219-231.
- Vulcano, A. B. (1988). Analytical Modeling of RC Structural Walls. *9th World Conference on Earthquake Engineering*, (pp. 41-46). Tokyo-Kyoto, Japan.
- Wallace, J. E. (1994). A New Methodology for Seismic Design of Reinforced Concrete Shear Walls. *Journal of Structural Engineering*, 465-474.
- Wallace, J. W. (1995). Seismic Design of RC Structural Walls. Part 1: New Code Format. *Journal of Structural Engineering*, 75-87.

- Wallace, J. W. (2007). Modelling Issues for Tall Reinforced Concrete Core Wall Buildings. *The Structural Design of Tall Reinforced Concrete Core Wall Buildings*, 615-632.
- Young, W. C., & Budynas, R. G. (2002). *Roark's Formulas for Stress and Strain*. McGraw-Hill.
- YR., R. (1968). Analysis of Reinforced Concrete Pressure Vessels. *Nuclear Engineering and Design* , 334-344.

APPENDIX A

UTILIZED COMPUTER PROGRAMS

As it is explained in the first Chapter, the aim of this study is to make a comprehensive comparison between the nonlinear modeling approaches for structural walls. In parallel with this purpose, three nonlinear modeling approaches; distributed inelasticity method, lumped plasticity method and continuum method were used with three computer programs; ETABS, Perform3D and Diana. In ETABS, simple shear walls and coupling beams were modeled with distributed inelasticity method and lumped plasticity method respectively. Simple structural walls and complete structures were analyzed with distributed inelasticity method in Perform3D. All the mentioned structures were analyzed with continuum model in DIANA. In the next section, element and material properties of these programs are briefly reviewed.

A.1 TNO DIANA Element Library

In this study as is stated DIANA was used to perform continuum based nonlinear analysis. This software has the capacity of nonlinear analyses with 2D and 3D (plane stress and plane strain both with symmetric and axisymmetric elements). A variety of element types were used according to performed analyses. CQ16M element is an eight-node quadrilateral isoperimetric plane stress element. CQ40S element is an eight-node quadrilateral isoperimetric curved shell element. L12BE element is a two-node, three-dimensional Class-I beam element. Details about these element types are given below.

A.1.1 CQ16M Element

The CQ16M element is an isoperimetric plane stress element with eight nodes. This element is on the basis of Gauss integration and quadratic interpolation. For this element, unknowns are the translation in x and y directions and these unknowns can

be calculated by the help of Equation (A.1 (DIANA FEA User's Manual - Release 9.5, n.d.).

$$u_i(\xi, \eta) = a_0 + a_1\xi + a_2\eta + a_3\xi\eta + a_4\xi^2 + a_5\eta^2 + a_6\xi^2\eta + a_7\xi\eta^2 \quad (\text{A.1})$$

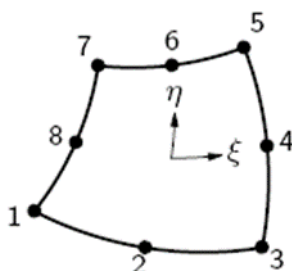


Figure A- 1 CQ16M element (DIANA FEA User's Manual - Release 9.5, n.d.)

As usual, this element yields a strain value ϵ_{xx} that changes linearly and quadratically in x and y directions respectively (vice versa for strain value ϵ_{yy}). Moreover, the shear strain γ_{xy} changes quadratically in both directions. As default, program performs 2x2 integration that yield at optimum stress point. 3x3 integration is also suitable but more than this is not usable because of the run time.

A.1.2 CQ40S Element

The CQ16M element cannot be used in three-dimension analyses. For this reason, CQ40S element was used. The CQ40S element is a quadrilateral isoperimetric curved shell element with eight nodes and it is on the basis of Gauss integration and quadratic interpolation over the $\xi\eta$ element area. The integration in thickness (ζ direction) may be Simpson or Gauss. For this element, unknowns are the translations and rotations and these unknowns can be determined by the help of Equations A.2 and A.3 (DIANA FEA User's Manual - Release 9.5, n.d.).

$$u_i(\xi, \eta) = a_0 + a_1\xi + a_2\eta + a_3\xi\eta + a_4\xi^2 + a_5\eta^2 + a_6\xi^2\eta + a_7\xi\eta^2 \quad (\text{A.2})$$

$$u_i(\xi, \eta) = b_0 + b_1\xi + b_2\eta + b_3\xi\eta + b_4\xi^2 + b_5\eta^2 + b_6\xi^2\eta + b_7\xi\eta^2 \quad (\text{A.3})$$

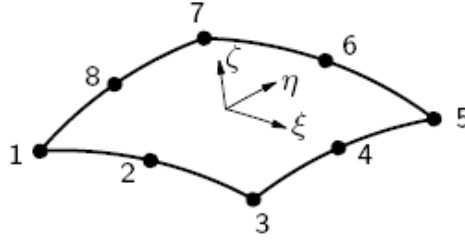


Figure A- 2 CQ40S element (DIANA FEA User's Manual - Release 9.5, n.d.)

For a rectangular element, these elements yield nearly the stress strain distribution along the element area in thickness. The shear force q_{xz} , the membrane force n_{xx} , the moment m_{xx} , the curvature κ_{xx} and strain ϵ_{xx} changes linearly in x direction and quadratically in y direction. The shear force q_{yz} , the membrane force n_{yy} , the moment m_{yy} , the curvature κ_{yy} and the strain ϵ_{yy} changes linearly in y direction and quadratically in x direction.

A.1.3 L12BE Element

The L12BE element is a three dimensional Class-I beam element with two nodes. For this element, unknowns are translations and rotations. For displacements the interpolation polynomials can be expressed as in Equations A.4, A.5, and A.6 (DIANA FEA User's Manual - Release 9.5, n.d.).

$$u_x(\xi) = a_0 + a_1\xi \quad (\text{A.4})$$

$$u_y(\xi) = b_0 + b_1\xi + b_2\xi^2 + b_3\xi^3 \quad (\text{A.5})$$

$$u_z(\xi) = c_0 + c_1\xi + c_2\xi^2 + c_3\xi^3 \quad (\text{A.6})$$

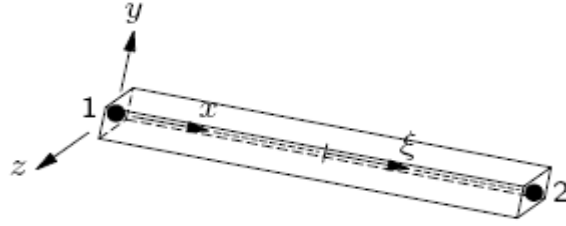


Figure A- 3 L12BE element (DIANA FEA User's Manual - Release 9.5, n.d.)

The strain values are constant through the center line of the beam because of these polynomials. The primary strains for this element are the elongation, the torsion and the curvature.

$$\varepsilon = \begin{Bmatrix} \Delta u_x \\ \Delta \phi \\ \kappa_y \\ \kappa_z \end{Bmatrix} \quad (\text{A.7})$$

$$\Delta u_x = u_x^{(2)} - u_x^{(1)} \quad (\text{A.8})$$

$$\Delta \phi = \phi_x^{(2)} - \phi_x^{(1)} \quad (\text{A.9})$$

$$\kappa_y = -\frac{d^2 u_z}{dx^2} \quad (\text{A.10})$$

$$\kappa_z = -\frac{d^2 u_y}{dx^2} \quad (\text{A.11})$$

The primary stresses for this element are normal force N and the moments M.

$$\varepsilon = \begin{Bmatrix} N_x \\ M_x \\ M_y \\ M_z \end{Bmatrix} \quad (\text{A.12})$$

DIANA performs a 2-point Gauss integration through the bar axis as default.

A.1.4 Bar Reinforcement

Reinforcements can be embedded in lots of element types such as beams, shell elements, solid elements and so on. In finite element models bar reinforcements are represented as lines. The total length of the bar must stay in the element and this length is divided into several parts. Usually, DIANA determine the location points automatically.

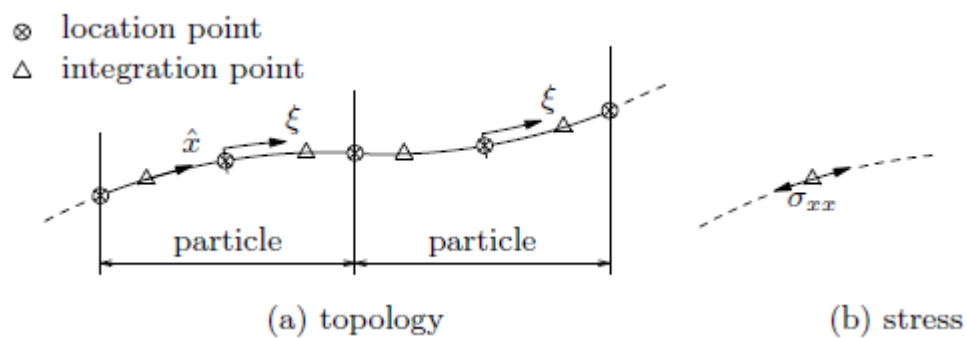


Figure A- 4 Bar reinforcement in DIANA (DIANA FEA User's Manual - Release 9.5, n.d.)

The unknowns for the bar reinforcements are the material properties, integration scheme and the cross section area.

For this study reinforcements are modelled as embedded reinforcements that do not have their own degrees of freedom of but add stiffness to the global system. For standard reinforcements by using the displacement field of the structural elements that include the reinforcements, strains of the reinforcement are calculated. This states the perfect bond between concrete and reinforcement are assumed.

A.2 TNO DIANA Material Library

Concrete crack models can be categorized into two groups. One of them is discrete crack models and the other one is smeared crack models. Figure A- 5 shows the schema of concrete crack models.

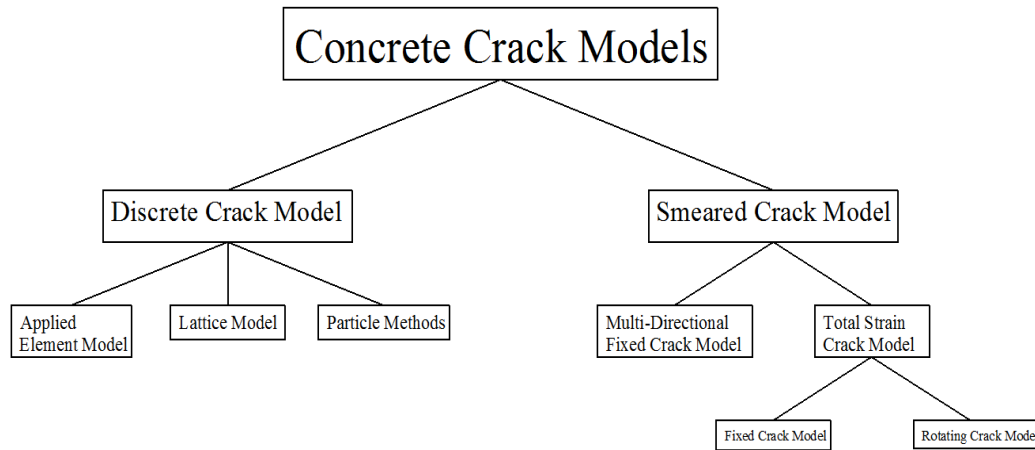


Figure A- 5 Schema of concrete crack models

In the first approach, the purpose is simulating the occurrence and propagation of only dominant cracks. In the discrete crack model, dominant cracks are represented by the separation of the nodes. These cracks are forced to progress through the element boundaries. This introduces a mesh bias system. This model can be suitable if crack locations are known in advance.

On the other hand, smeared crack model use heterogeneity of concrete. Since concrete is a heterogeneous material and presence of reinforcement contribute this heterogeneity many small cracks that may trigger the formation of dominant cracks occur. The cracked structure keeps its continuum. As an assumption behavior of the structure is taken almost linear and follows the isotropic stress strain law up to cracking. After cracking, the structure follows the orthotropic law that axes of the orthotropy are determined according to crack orientation.

When these approaches are compared, both models have advantages and disadvantages. But in this study, smeared crack model is used because of some reasons. First, topology of the finite element mesh was not revised since the cracked structure is still a continuum. Furthermore, it is not necessary to predict the orientation of cracks. By considering all these advantages, it was decided to use smeared crack model in this study.

Smeared crack model is divided into two categories as shown in Figure A- 5. Moreover, total strain crack model is also divided into two group rotating and fixed crack models (Rotating crack model was used in the analyses because of the advantages that are explained in the below section).

A.2.1 Rotating Crack Model

Total Strain Rotating Crack Models introduced by Rashid (1968) and developed by Vecchio (1986).

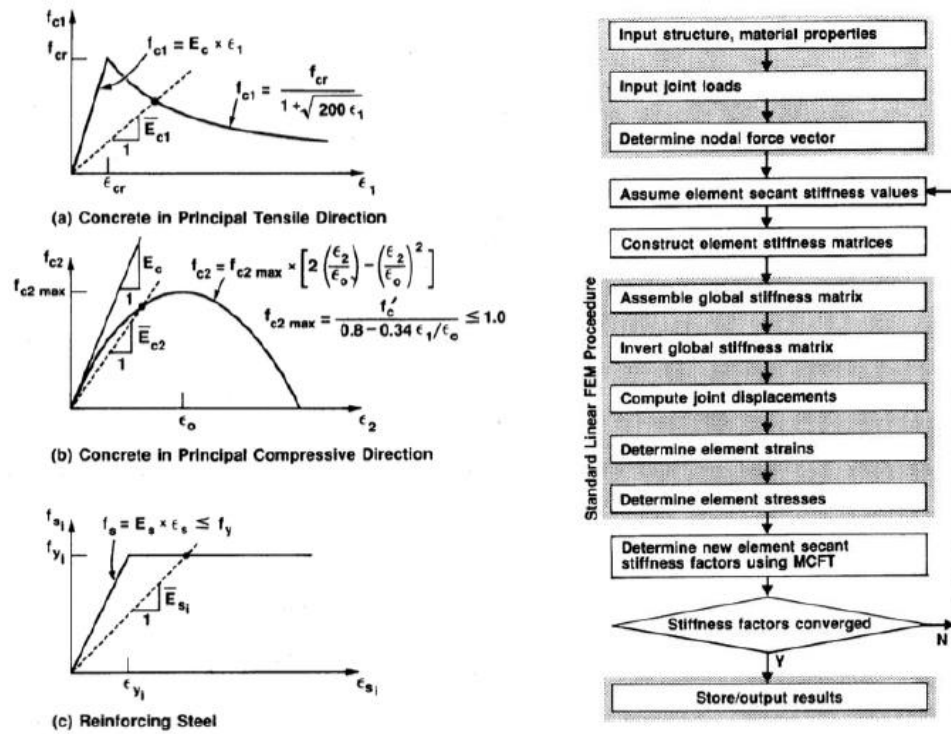


Figure A- 6 Total strain rotating crack approach (Vecchio, 1986)

One of the advantage of this model is that in this model direction of the principal stress and direction of the principal strain coincide. As a result of this, by using uniaxial stress-strain models just two normal stress components can be calculated without shear strain that occur perpendicular to the crack orientation.

Formulation of total strain rotating crack concept in 2D analysis is explained in the next part. Stiffness matrix of an individual element (k) is determined by using the

material stiffness matrix (D) that is required to associate stresses and strains. In this concept, by using suitable transformation after combining the contribution of reinforcement and concrete the k matrix that is described according to the global coordinate system is found. Concrete and reinforcement component are described in element global coordinate system as shown in Figure A- 7. In order to consider the anisotropy of materials, material stiffness matrices of concrete components and each of the reinforcement components are identified separately. Principal average tensile strain and compressive stain are found by using the principal axes system of the cracked reinforced concrete. Later on, by using transformation matrices global stiffness matrix is determined.

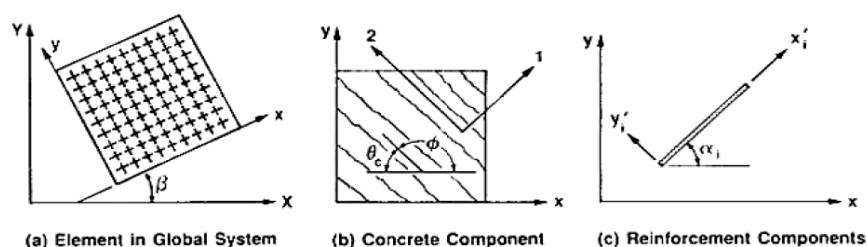


Figure A- 7 Elements' Reference Coordinate Systems

A.2.1.1 Multi-Linear Compressive Behavior

Compressive behavior of Total Strain Crack Model is usually nonlinear and can be defined in many ways such as elastic, Thorenfeldt, multi-linear, parabolic and so on as shown in Figure A- 8. In this study, in order to define the compression behavior multi-linear functions were used. Multilinear relations can be determined by the stress values and corresponding strain values. In this study, experimental results and material modeling results such as Hognestad model were used. Hognestad model was selected because of its simplicity.

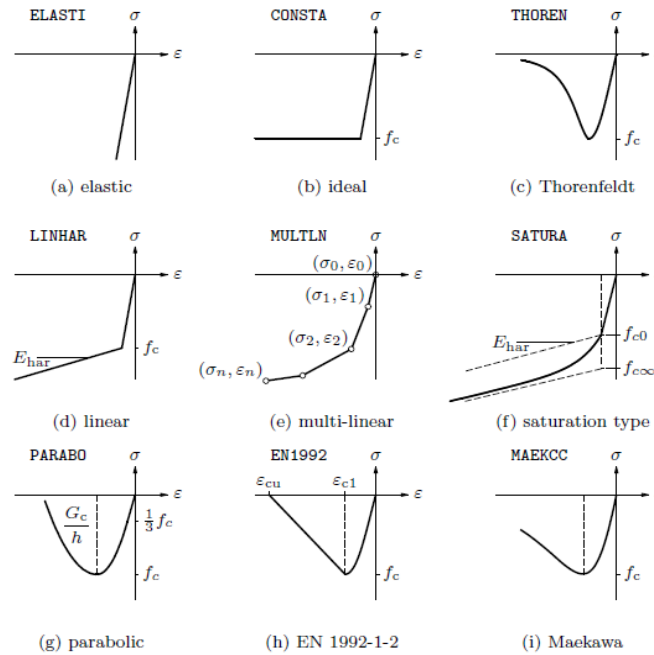


Figure A- 8 Compression behavior for total strain crack model (DIANA FEA User's Manual - Release 9.5, n.d.)

A.2.2 Von Mises Plasticity

Yielding of a ductile material such as reinforcement begins when the second deviatoric stress invariant reaches the stated value according to von Mises plasticity. Response of the material can be assumed to be linearly elastic prior to yielding.

Von Mises plasticity can also be formulated by the help of equivalent tensile stress that is a scalar value.

A.2.3 Post-Peak Behavior

In order to represent the post peak behavior of the concrete many tension softening relations such as brittle, linear, multilinear and nonlinear (Hordijk) tension softening function can be used. As it is shown in Figure A- 9, after reaching tensile strength of concrete these functions behave differently. Since high strength concrete will be used in the analysis brittle tension softening relation was used for this study.

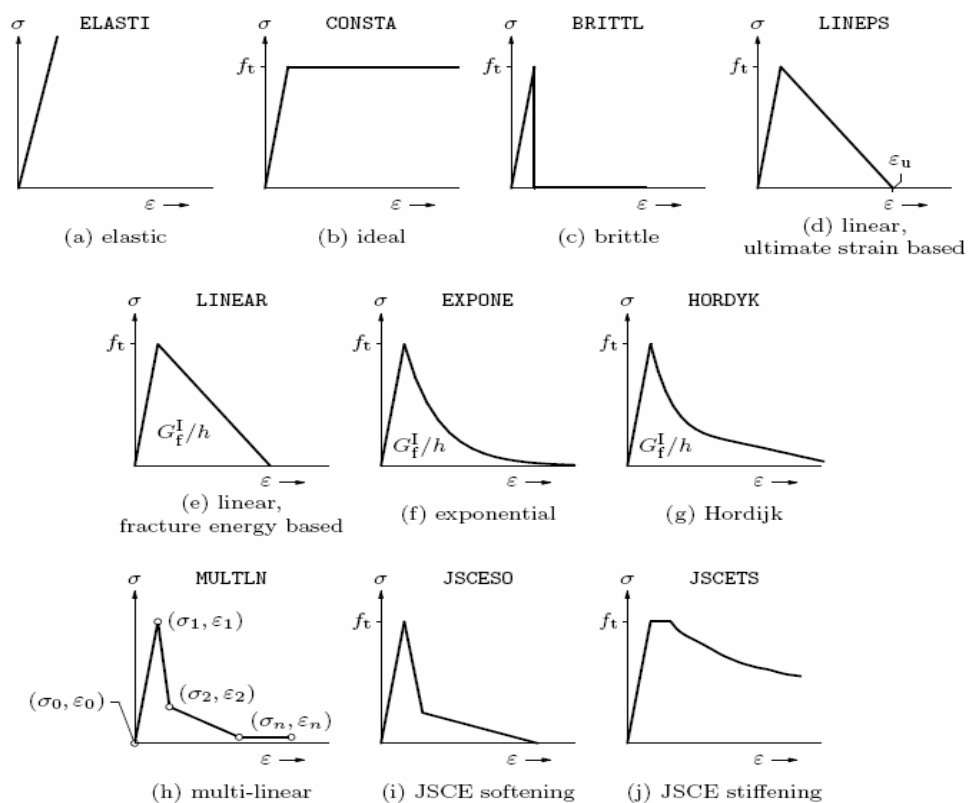


Figure A- 9 Tension softening models for concrete (DIANA FEA User's Manual - Release 9.5, n.d.)

A.2.3.1 Brittle Tension Softening

Behavior of brittle cracking can be defined as full reduction of the capacity after the stress-strain criteria has been exceeded. Before, the peak system behaves linearly but stress drops to zero just after beyond the peak. After stress drop, system involves energy dissipation that is related to the crack band width and peak strain.

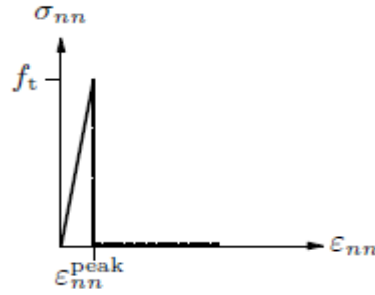


Figure A- 10 Brittle cracking behavior (DIANA FEA User's Manual - Release 9.5, n.d.)

$$G_f = \frac{1}{2} f_t \varepsilon_{nn}^{peak} h \quad (A.13)$$

In the Equation A.13 peak value of ε_{nn} is equal to f_t/E . Thereby, changing the element size affect the energy consumption in this case. This condition implies the mesh dependency but this problem is especially important for unreinforced structures.

A.3 ETABS Element Library

ETABS was also used to perform nonlinear analysis. ETABS was used to simulate the nonlinear behavior of reinforced concrete structures but has not the capability to capture the shear behavior. A series of element types are used according to analysis types. These element types are explained in the next part.

A.3.1 ETABS Frame Element

In ETABS, frame element is a very useful element type in order to model columns, beams, braces and trusses in 2D and 3D structures. By using frame hinges, nonlinear material behavior can be attributed to the frames.

A frame element is defined with a line that connect two points and this line can be divided into multiple lines. Each frame element has local coordinate system to define loads, section properties and interpreting results (ETABS, 2017). In this study, frame elements were used for coupling beams and columns.

A.3.2 Hinge Element

In ETABS, plastic hinges are used to represent concentrated nonlinear behavior in one or more degrees of freedom. Plastic hinges can be inserted to any number of locations of frame elements and also in vertical shear wall elements (ETABS, 2017). Hinges only work for nonlinear static and nonlinear time history analyses.

Uncoupled shear, moment, torsion and axial force hinges are available. In this study, shear hinge was used for coupling beam and P-M3 hinge was used for shear walls. For shear hinge, force-displacement relationship is specified for each degree of freedom.

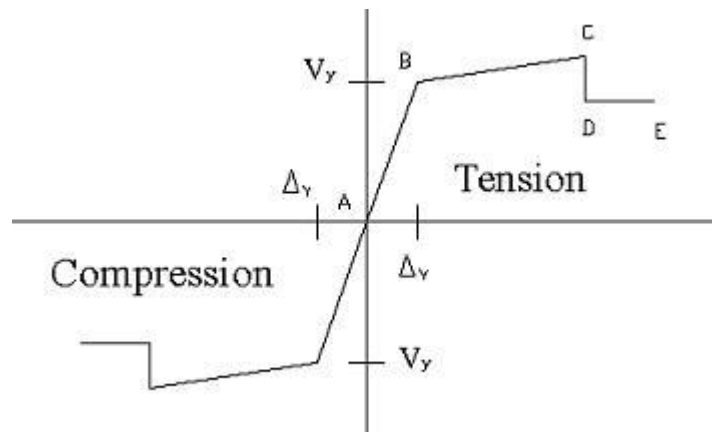


Figure A- 11 Force-Displacement relationship of shear hinge (ETABS, 2017)

Fiber (P-M3) hinges can be defined with material points through the cross section and each point represents a tributary area and its own stress strain curve (ETABS, 2017). For the section, plane sections remain plane assumption is valid.

Fiber hinges give more realistic results compared to force-moment hinges but they are computationally demanding.

A.3.3 Shell Element

Shell element is used to model shell behavior in 2D and 3D structures and includes three or four node formulation. Material of shell element can be homogeneous or layered through thickness. For layered shell, material nonlinearity can be taken into consideration (ETABS, 2017).

In the element local coordinate system, in order to calculate moments, internal forces and stresses are evaluated at 2 by 2 Gauss integration points are used and extrapolated to the joints of element. Moreover, stiffness of shell element is calculated with four-point numerical integration formulation (ETABS, 2017).

Shell elements were used to model floors of the structures and shear walls for this study.

A.4 ETABS Material Library

Material properties can be defined as isotropic, orthotropic and anisotropic and these properties depends on element type. Material properties are assumed constant regardless of any temperature changes. For each element, material temperature can be assigned to determine the material properties (ETABS, 2017). For fiber hinges in frame elements and shell elements, nonlinear stress strain curves can be defined.

A.4.1 Isotropic Materials

For isotropic material, behavior is independent of orientation of the material and direction of the loading. Moreover, for isotropic material shear behavior is not coupled from extensional behavior. Although this is not always the case, isotropic behavior is always assumed for steel and concrete. Below figure shows the calculation of mechanical properties for isotropic materials.

$$\begin{Bmatrix} \varepsilon_{11} \\ \varepsilon_{22} \\ \varepsilon_{33} \\ \gamma_{12} \\ \gamma_{13} \\ \gamma_{23} \end{Bmatrix} = \begin{bmatrix} \frac{1}{E_1} & \frac{-\nu_{12}}{E_1} & \frac{-\nu_{12}}{E_1} & 0 & 0 & 0 \\ & \frac{1}{E_1} & \frac{-\nu_{12}}{E_1} & 0 & 0 & 0 \\ & & \frac{1}{E_1} & 0 & 0 & 0 \\ & & & \frac{1}{G_{12}} & 0 & 0 \\ & & & & \frac{1}{G_{12}} & 0 \\ & & & & & \frac{1}{G_{12}} \end{bmatrix} \begin{Bmatrix} \sigma_{11} \\ \sigma_{22} \\ \sigma_{33} \\ \sigma_{12} \\ \sigma_{13} \\ \sigma_{23} \end{Bmatrix} + \begin{Bmatrix} \alpha_1 \\ \alpha_1 \\ \alpha_1 \\ 0 \\ 0 \\ 0 \end{Bmatrix} \Delta T \quad (\text{A.14})$$

In Equation A.14, E_1 , ν_{12} , G_{12} , and α_1 represent the young modulus, poison ratio, shear modulus, and coefficient of thermal expansion, respectively. It should be noted that value of the young modulus is positive and poison ratio is between -1 and 0.5.

A.4.2 Uniaxial Materials

Uniaxial materials are used for rebar, tendon and cable elements. For rebar that used in layered shell section, shearing behavior can be considered. Below figure shows the calculation of mechanical properties for uniaxial materials.

$$\begin{Bmatrix} \varepsilon_{11} \\ \varepsilon_{22} \\ \varepsilon_{33} \\ \gamma_{12} \\ \gamma_{13} \\ \gamma_{23} \end{Bmatrix} = \begin{bmatrix} \frac{1}{E_1} & \frac{-\nu_{12}}{E_1} & \frac{-\nu_{12}}{E_1} & 0 & 0 & 0 \\ & \frac{1}{E_1} & \frac{-\nu_{12}}{E_1} & 0 & 0 & 0 \\ & & \frac{1}{E_1} & 0 & 0 & 0 \\ & & & \frac{1}{G_{12}} & 0 & 0 \\ & & & & \frac{1}{G_{12}} & 0 \\ & & & & & \frac{1}{G_{12}} \end{bmatrix} \begin{Bmatrix} \sigma_{11} \\ 0 \\ 0 \\ \sigma_{12} \\ \sigma_{13} \\ 0 \end{Bmatrix} + \begin{Bmatrix} \alpha_1 \\ 0 \\ 0 \\ 0 \\ 0 \\ 0 \end{Bmatrix} \Delta T \quad (\text{A.15})$$

It should be noted that uniaxial material is a kind of isotropic material with stresses σ_{22} , σ_{33} and σ_{23} equal to zero.

A.4.3 Nonlinear Material Behavior

For certain elements, nonlinear material behavior is available by directional material model. In these models for one or more stress strain component, uncoupled stress strain behavior is modeled (ETABS, 2017). This is a simple and useful modeling approach for beams, columns, shear walls and so on but the applicability of the model should be carefully studied before using it in a general continuum model.

A.4.4 Hysteresis Material Behavior

Hysteresis is the energy dissipation process through displacement (deformation). In ETABS, in order to characterize the material, many hysteresis models are available. These hysteresis models are different from each other in terms of dissipated amount of energy in a given cycle of deformation. All of the hysteresis models can be used for the following aims (ETABS, 2017):

- Material stress-strain behavior that affects frame fiber hinges
- Single degree of freedom hinges and interacting hinges
- Link/support elements of multi linear plasticity type

A.4.4.1 Backbone Curve

Uniaxial action vs deformation curve specifies the nonlinear behavior for each material, hinge and link under monotonic loading in both positive and negative directions. Action and deformation are defined stress vs strain for materials and force vs deformation or moment vs rotation for links and hinges (ETABS, 2017).

A.4.4.2 Degrading Hysteresis Model

This model uses degrading hysteretic loop that can take into unloading stiffness and decreasing energy dissipation with increasing plastic deformation. For plastic

deformation two measures are used. The first one is the maximum plastic deformation for positive and negative directions and the second is the cumulative plastic deformation. Figure A- 12 shows the degrading hysteresis model.

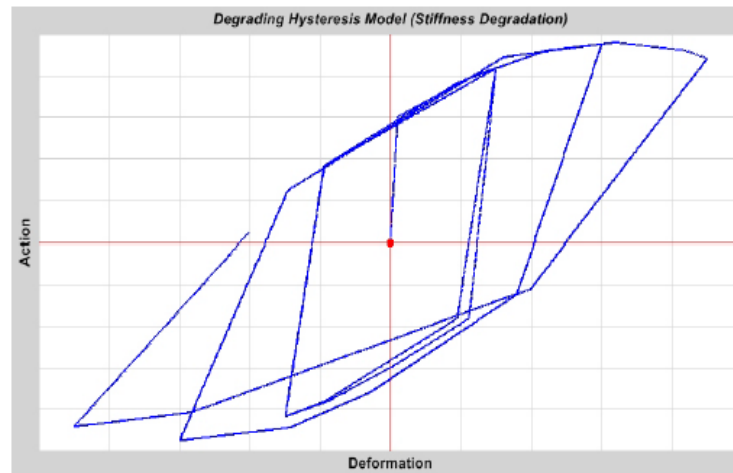


Figure A- 12 Degrading hysteresis model under increasing cycling load (ETABS, 2017)

A.4.4.3 Concrete Hysteresis Model

Compression and tension behavior are independent for this model and behave differently. Stress vs strain or force deformation curve is used to determine the compression sign. Force vs deformation curve for tension can be all zero but for compression a non-zero force vs deformation curve should always be defined. Below figure is an example of concrete hysteresis model.

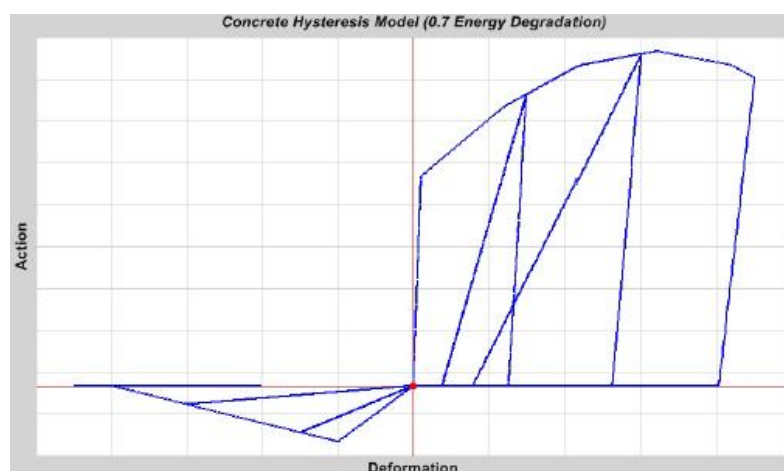


Figure A- 13 Concrete hysteresis model under increased cyclic load

A.5 Perform3D Element Library

At the beginning of this study, usage of Perform3D was not aimed but after seeing that ETABS cannot perform the nonlinear analysis of 3D model, we decided to use Perform3D. Perform3D is also used to simulate the nonlinear behavior of reinforced concrete but has not the capability to capture the nonlinear shear behavior. A variety of element types are used according to analysis types. These element types are defined in the following part.

A.5.1 Column Element

In Perform3D, column elements use frame compound components. Since column elements have the capability to carry axial force, it is different than frame elements. Moreover, since columns are also subjected biaxial bending, it is necessary to take into account the P-M-M interaction (Perform3D, 2016).

A.5.2 Shear Wall Element

Defining of inelastic behavior of shear walls in Perform3D is not a simple task and limitations of the models should be known. In Perform3D shear and axial-bending properties of shear wall can be specified as follows;

i. Shear properties

Shear properties are defined by using shear material and this shear material can be elastic or inelastic. Moreover, for shear wall element, component cross section must be specified.

ii. Axial-bending properties

These properties can be defined by using fiber cross section. This section can be elastic or inelastic. While defining the shear wall element, component cross section of the wall should be specified.

In addition to these properties, out of plane and transverse stiffness of the wall must be defined. But it should be kept in mind that shear wall elements in Perform3D behave elastic in both of these directions.

In Perform3D each shear wall element connects 4 nodes and has 6 degrees of freedom for each node. For shear walls in plane behavior is more important than the out of plane behavior. The wall element can be inelastic for the in plane direction. Transverse in plane behavior is secondary and wall element is elastic in this direction. Also, out of plane bending is secondary and assumed to be elastic (Perform3D, 2016).

As an assumption depth of cross section is taken constant through the element length according to the element width at its mid-height in order to calculate the element stiffness.

Axial strain, curvature and shear strain are taken to be constant through the element length. Therefore, a shear wall element is a lower order element than a standard beam element. Figure A- 14 explains the consequence of this. For instance, if one single element is used for a one storey wall, from beam theory the calculated elastic bending deflection is only 75% of the exact value but total deflection including both bending and shear is more accurate. So more than one element can be used in a storey according to user.

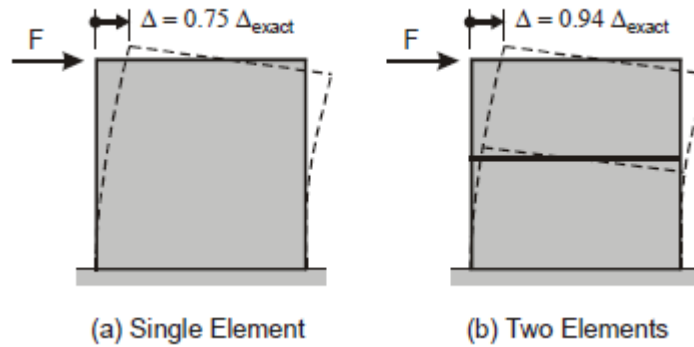


Figure A- 14 Error in bending stiffness (Perform3D, 2016)

A.5.3 Elastic Slab/Shell Element

The slab element has in plane (membrane) and out of plane (plate bending) stiffness. This element can be used to model slabs, elastic walls and curved shells. For Perform3D the most useful application of slab element is modeling the deformable floor diaphragms. In the diaphragm membrane behavior of elements are used to take into account to plane effects and plate bending behavior can be used for application and distribution of gravity loads (Perform3D, 2016).

A slab element has four nodes and three local axes as shown in Figure A- 15. As a rule, slab elements should be rectangular or near rectangular.

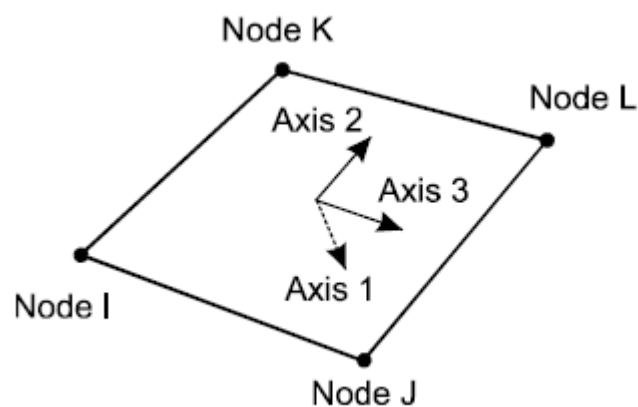


Figure A- 15 Local axis and nodes of slab element (Perform3D, 2016)

A.6 Perform3D Material Library

Perform3D allows a trilinear stress-strain relationship for concrete and steel materials. Trilinear material behavior can be specified but because of the uncertainties in the behavior of walls and modeling, it is suggested to use elastic and perfectly plastic behavior (Perform3D, 2016).

A.6.1 Concrete Material

In Perform3D, for concrete material the loading stiffness and initial elastic stiffness are always equal. Dissipated energy is controlled by changing the reloading stiffness. For concrete either finite or zero strength can be specified in tension. Below figures summarize the concrete material behaviors.

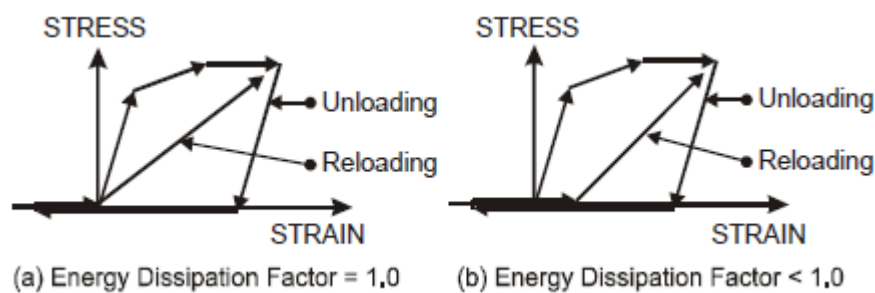


Figure A- 16 Concrete material behavior in compression (Perform3D, 2016)

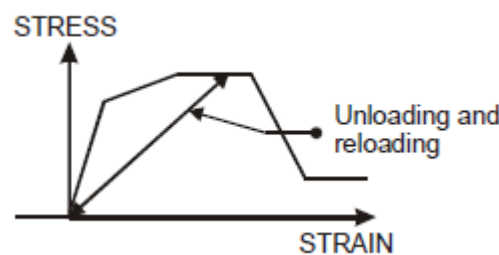


Figure A- 17 Concrete material behavior in tension (Perform3D, 2016)

In Perform3D, behavior in compression and tension are independent from each other. So, cracking in tension does not affect the subsequent compression behavior and tensile behavior is not affected by crushing in compression.

APPENDIX B

DESIGN OF 4 AND 15-STOREY STRUCTURES

Nonlinear modeling approaches were tested in this thesis. It was aimed to figure out the capabilities of modeling approaches. In order to do this, behavior of tall and short buildings was compared. It was assumed as these structures were located at Istanbul, Kağıthane and design response spectrum was determined according to this location. Response spectrum was determined according to ASCE 7-10 and Table B- 1 shows the parameters that used in the determination of design response spectrum.

Table B- 1 Parameters that used in determination of response spectrum

Parameter	Explanation
S_{DS}	The design spectral response acceleration at short periods
S_{D1}	The design spectral response acceleration at 1-s period
S_{MS}	The mapped spectral response acceleration at short periods
S_{M1}	The mapped spectral response acceleration at 1-s period
T	The fundamental period of the structure
T_L	Transition period (taken as 8 sec.)
I	Importance factor
R	Response modification coefficient
F_a and F_v	Site coefficients

These structures were designed according to 475 years return period. S_1 and S_s values were determined as 0.216 g and 0.753 g, respectively. These values were taken from Turkish earthquake seismic hazard map. It was also assumed that these structures are located in D type of site class and according to this site class site coefficient values, F_a and F_v were determined as 1.2 and 2, respectively. Figure B- 1 shows the determination of design response spectrum according to ASCE 7-10.

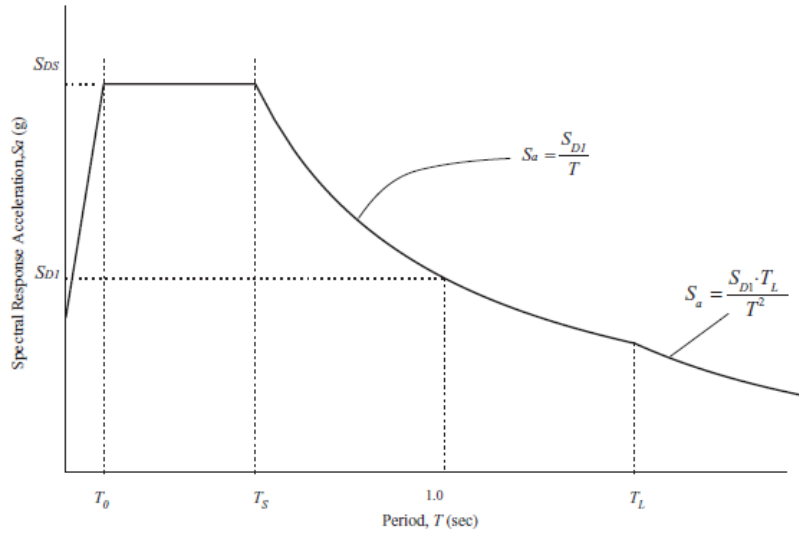


Figure B- 1 Determination of design response spectrum

$$S_{MS} = F_a \times S_S \quad (B.1)$$

$$S_{M1} = F_v \times S_1 \quad (B.2)$$

$$S_{DS} = 2S_{MS}/3 \quad (B.3)$$

$$S_{D1} = 2S_{M1}/3 \quad (B.4)$$

$$T_0 = 0.2S_{D1}/S_{DS} \quad (B.5)$$

$$T_S = S_{D1}/S_{DS} \quad (B.6)$$

Design response spectrum was determined by using Equation B.1 ~ Equation B.6 and presented in Figure B- 2.

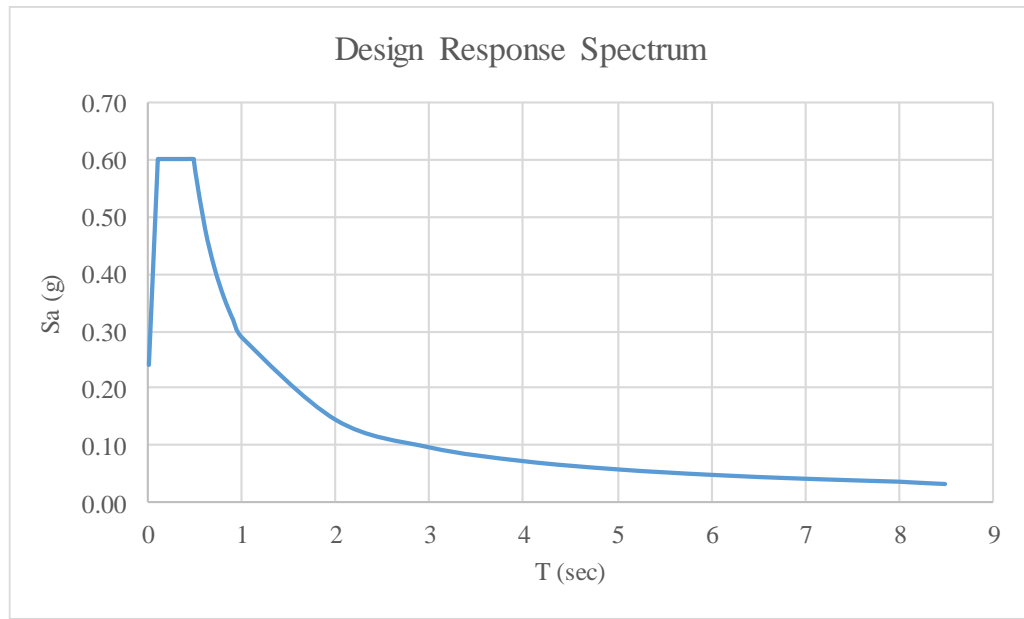


Figure B- 2 Design response spectrum

B.1 Design of E-Shaped Structural Wall

Design of E-shaped structural wall was performed with ETABS. For 12-meter height structural wall, minimum amount of reinforcements was used both for longitudinal and horizontal directions without any confinement. For 45-meter height structural wall, different reinforcement placements were selected for first nine storey. Figure B- 3, Figure B- 4, and Figure B- 5 show the reinforcement placement of first three storey, second three storey and third three storey, respectively. Confinement zones were used for first two storey. For confinement zone $\Phi 12$ was used with 150 mm interval at the end of the wall section and connections between web and flange. Minimum amount of lateral reinforcement was also used for the horizontal reinforcement of 45-meter height structural wall.

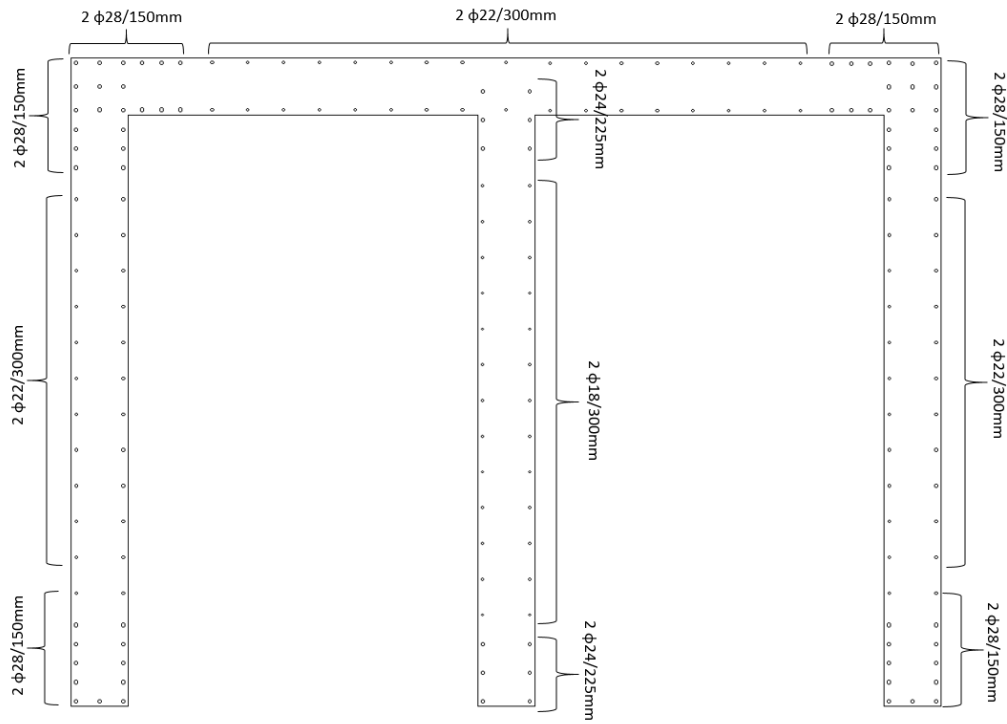


Figure B- 3 Longitudinal reinforcements of the first three storey

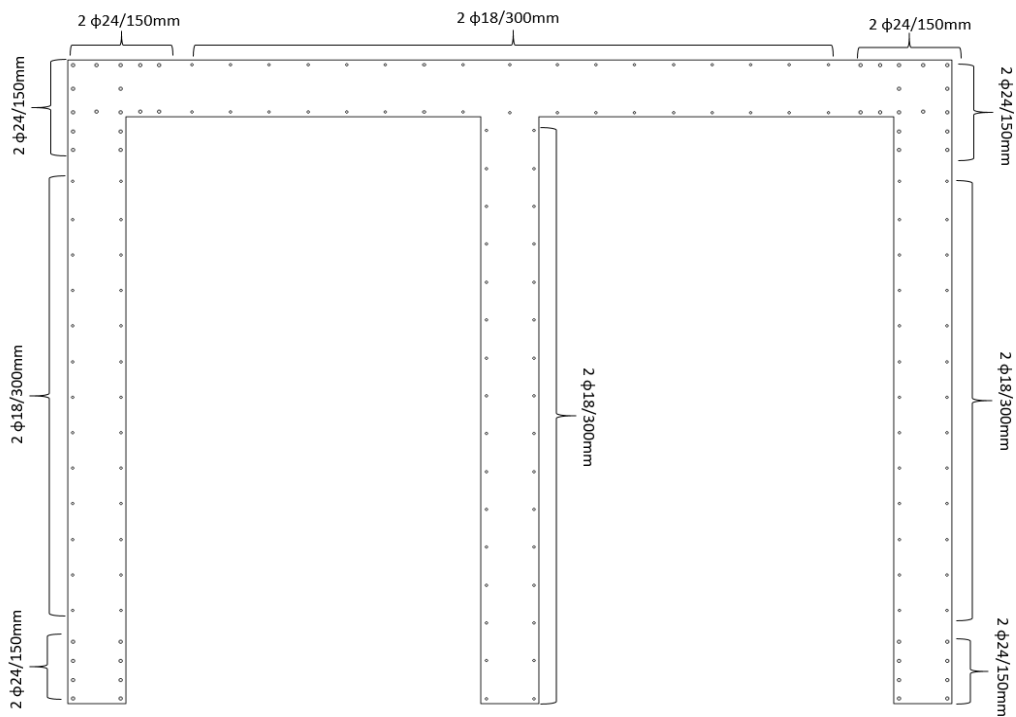


Figure B- 4 Longitudinal reinforcements of the second three storey

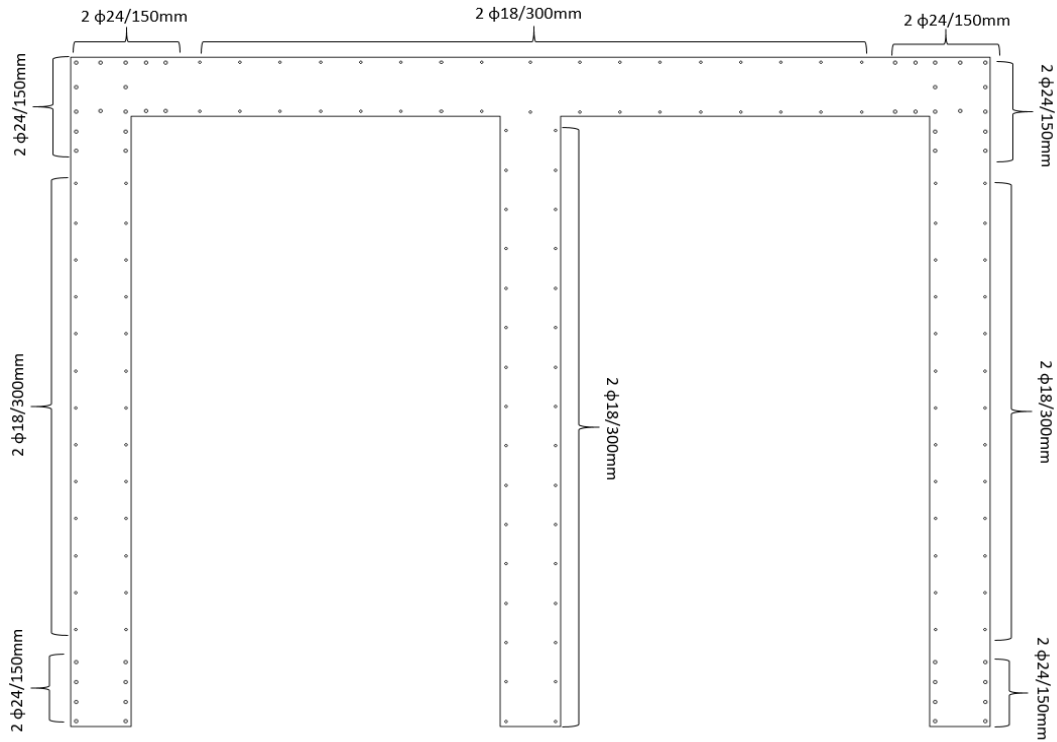


Figure B- 5 Longitudinal reinforcements of the third three storey

B.2 Properties of Ground Motions

Nonlinear time history analyses were performed for this study. Two different ground motions were used for time history analysis, since our aim was to compare the modeling approaches not to test the design. These ground motions are taken from Pacific Earthquake Engineering Research (PEER) strong motion database. Acceleration values of these ground motions are presented in Figure B- 6 and Figure B- 7. RSN989H1 ground motion was used for the analysis of tall buildings and RSN1618H1 ground motion was used for the analysis of short buildings. Peak ground accelerations of these ground motions are equal to 2.1g and 1.57g, respectively. Figure B- 8 shows the response spectrum of these ground motions. Magnitude of these ground motions are equal to 6.7 and 7.1, respectively.

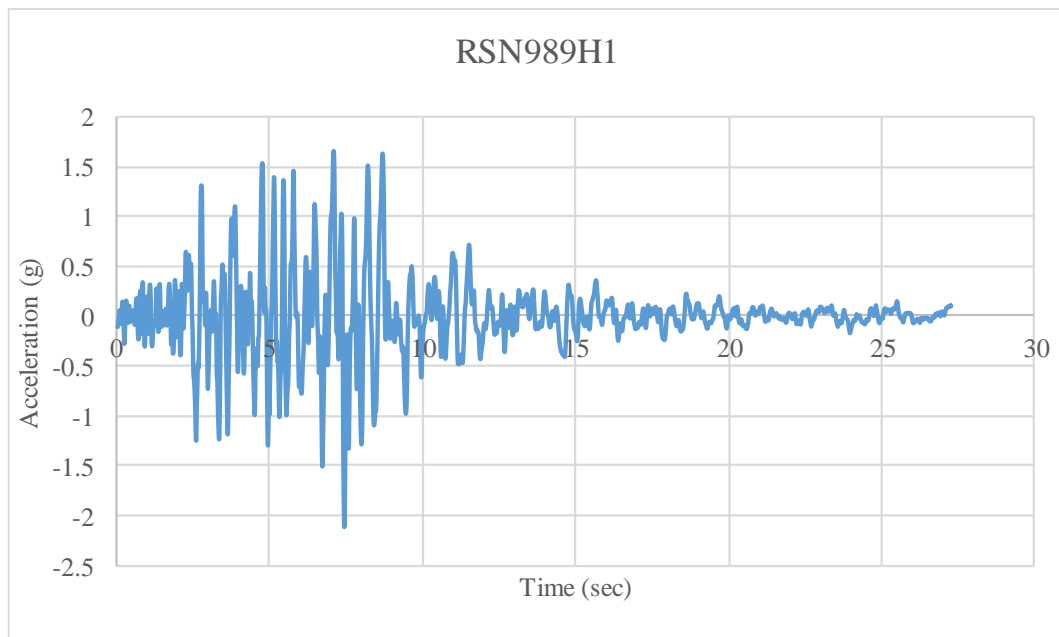


Figure B- 6 Acceleration versus time graph of RSN989H1

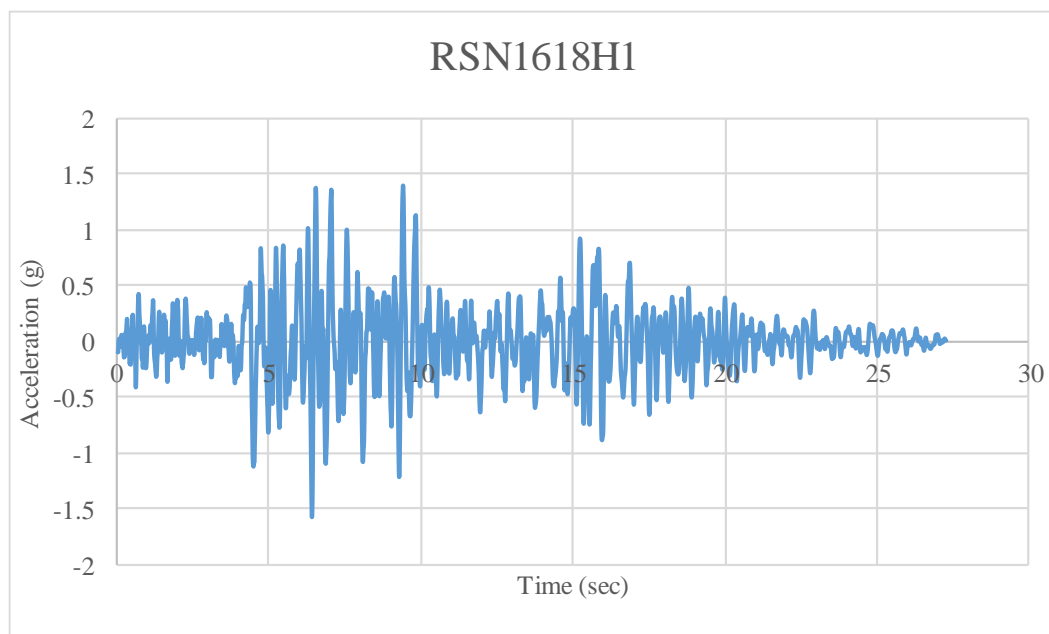


Figure B- 7 Acceleration versus time graph of RSN989H1

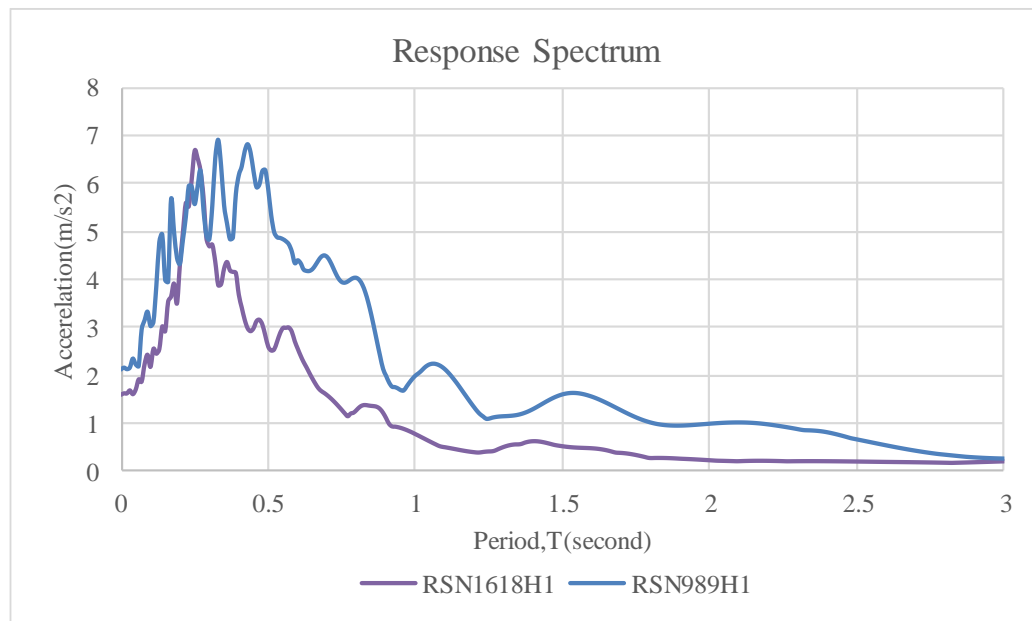


Figure B- 8 Response spectrum of ground motions